EXPERIMENTS IN VERY LOW-FREQUENCY RADIO PROPAGATION

Thesis by

Roger Morse Golden

In Partial Fulfillment of the Requirements

for the Degree of

Doctor of Philosophy

California Institute of Technology

Pasadena, California

1959

ACKNOWLEDGEMENT

I wish to thank Professor Robert V. Langmuir for his suggestions and advice in the conducting of the experimental work and in the preparing of this thesis. Professor Robert S. Macmillan is to be thanked for his work in inaugurating this research.

In the course of construction and operation of the experimental equipment, many people contributed significantly to the success of this work. In particular, I would like to thank: Mr. Robert Stratton and Mr. Noel Payne who aided in the construction of the receiving equipment; Mr. Art Hicks and his crew who were responsible for the safe transportation of the transmitting equipment to Shaver Lake; Mr. Harry Aubuchon, foreman of the Southern California Edison Company Line Crew, who assisted in the conducting of many tests; Mr. Harry R. Renoud, Head of the Engineering Department of Reedley Junior College, who made the facilities of the college available as a receiving site; Mrs. Adelheida Hohenlohe who prepared the illustrations; and finally (with an especial note of thanks) Mrs. Anne Graff who prepared the manuscript.

I am grateful to the Radio Corporation of America and to the Consolidated Electrodynamics Corporation for aid in the form of fellowships.

Gratitude is also expressed to the Air Force Office of Scientific Research for their financial support of this program.

Roger Morse Golden

ABSTRACT

In an effort to extend experimentally determined data on the characteristics of very low-frequency radio waves, a vlf transmitting station (8.4 kc) was established at Shaver Lake, California.

The establishment of this station permitted controlled experiments in long distance propagation, ionospheric vertical sounding measurements, and attempts at the generation of round trip gyroelectric-echoes.

The long distance measurements indicated that at vlf, the ground or surface wave radiated by the antenna, can be detected at great distances. The ionospheric vertical incidence measurements showed rapid fading of the received signal around local sunrise and sunset.

Propagation in the presence of the ionosphere is considered in the theoretical form of propagation in a homogeneous gyroelectric medium. The results of this analysis are tabulated in graphical form so that the dispersive qualities of the medium can be readily examined. With the aid of these results, an examination of the natural phenomena of whistlers is presented in order to determine the feasibility of generating gyroelectric-echoes. Reflection and transmission coefficients are presented for vertical incidence in order to ascertain the order of magnitude of such an echo. Experiments thus far performed have not yielded echoes but with modifications in the transmitting and receiving equipment, echoes may be detected.

A complete description of the experimental equipment used is given along with a proposal for a more sophisticated receiving system.

TABLE OF CONTENTS

I. INTRODUCTION

The most important two modes by which electromagnetic waves below 30 Mc propagate from transmitter to receiver are: 1) ground wave propagation, where the receiving and transmitting antennas are located close to the surface of the earth and the transmitted wave is vertically polarized; and 2) reflection of the transmitted wave (no restriction on polarization) from the ionosphere (sky wave).

One may recall that the earliest commercial radio stations operated at the lowest radio frequencies (20 - 30 kc) and many of the early experiments were performed at these frequencies. However, when it became apparent that more efficient operation could be obtained by moving to the higher frequencies, the low radio frequencies were almost entirely abandoned.

Experimental investigation of electromagnetic wave propagation at low frequencies has since been primarily limited by the transmitters and antennas available for such work. At present, these are mainly military transmitters operating at 15.5, 16.6, 18.6, and 19.8 kc. Because of this limitation, many of the properties of the ionosphere at very low frequencies must be deduced from atmospheric noise that occurs in this frequency spectrum (band number 4 - 3 - 30 kc).

Since there has been a sparsity of experimental vlf transmitters for performing controlled experiments below 16 kc, a vlf (8.4 kc) transmitting station was constructed to help fulfill this need. It is the principal purpose of this station (call letters KM2XIX) to conduct experiments concerning:

1. Reflection and refraction of vlf radio waves at the boundary of the ionosphere.

2. Long distance propagation.

3. Excitation of the whistler or magneto-ionic duct mode of propagation.

4. Phase stability of vlf radio waves.

Before considering the experimental aspects of vlf propagation, it will be necessary to review the so-called magneto-ionic theory. The final results of this theory will then be presented in a manner that permits ready correlation with the experimental data. First, however, a general review of ionospheric characteristics will be given along with the usual radio sounding techniques used to explore the ionosphere.

II. THE IONOSPHERE AND RADIO EXPLORATION TECHNIQUES

Review of Ionospheric Characteristics

Until the time of Marconi's success (1901) in sending electromagnetic waves between Cornwall and Newfoundland, the existence of an ionized layer of gas surrounding the earth was virtually unknown. (The only previous postulation of a conducting layer in the earth's upper atmosphere, was made by the British magnetician, Balfour Stewart (1). In an article on "Terrestrial Magnetism" for the Encyclopaedia Britannica in 1882, Stewart hypothesized that electrical currents in a conducting layer, high in the terrestrial atmosphere, might explain the well-known regular variations in the magnetic elements.)

Before Kennelly (2) and Heaviside (3) independently postulated the existence of a conducting layer in the upper atmosphere in 1902, many workers tried unsuccessfully to account for the great distance traveled by Marconi's signal by analyzing the diffraction of electromagnetic waves by a spherical earth.

The Kennelly-Heaviside postulation led to many new theories concerning the propagation of radio waves. These theories found a culmination in the Eccles-Larmor theory (4, 5) as the basic theory of radio propagation in the ionosphere (1924). This theory was later supplemented by the magneto-ionic theory (1927) developed by Appleton, Hartree, Goldstein and others (6, 7, 8, 9). This basic theory is reviewed and extended in section III.

It is now well known that the constituents of the earth's upper atmosphere are ionized under the influence of solar ultraviolet radiation. Ionization begins at a height of approximately 60 km and extends to the upper limits of the atmosphere. Beyond this limit, there exists the recently discovered Van Allen radiation belt. This belt may be partly responsible for the propagation of the natural phenomena of whistlers (described in section IV). For the present, however, discussion will be confined to the more familiar regions of the ionosphere.

Because of the variation of the constituents of the atmosphere with increasing height, the ionization in the ionosphere is stratified into a number of layers of maximum ionization density. These layers are known as: the D region (it is not certain whether this region is composed of definite ionized layers or whether it is a regularly stratified distribution of ionization), and the E, F1 and F2 layers. The relative electron density as a function of height above the earth for daytime and nighttime is shown schematically in figures II-1a and II-1b respectively.

Waynick (10) has formulated a composite table of equinox noon electron density-height distribution. This table was deduced by Houston on the basis of all available radio and rocket results. These characteristics are plotted in figure II-2. [For profiles above 160 km, see (11).]

Of the four regions or layers, the F2 and E are most likely to be observed. The F1 region, which is intermediate between E

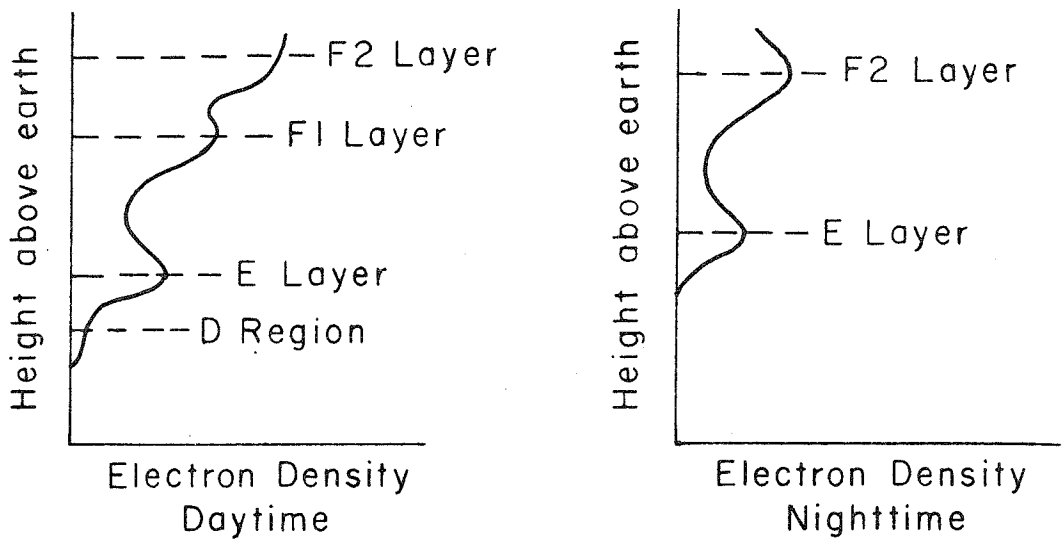

FIGURE II-1. SCHEMATIC DIAGRAMS ILLUSTRATING ELECTRON DENSITY-HEIGHT PROFILES OF THE IONOSPHERE.

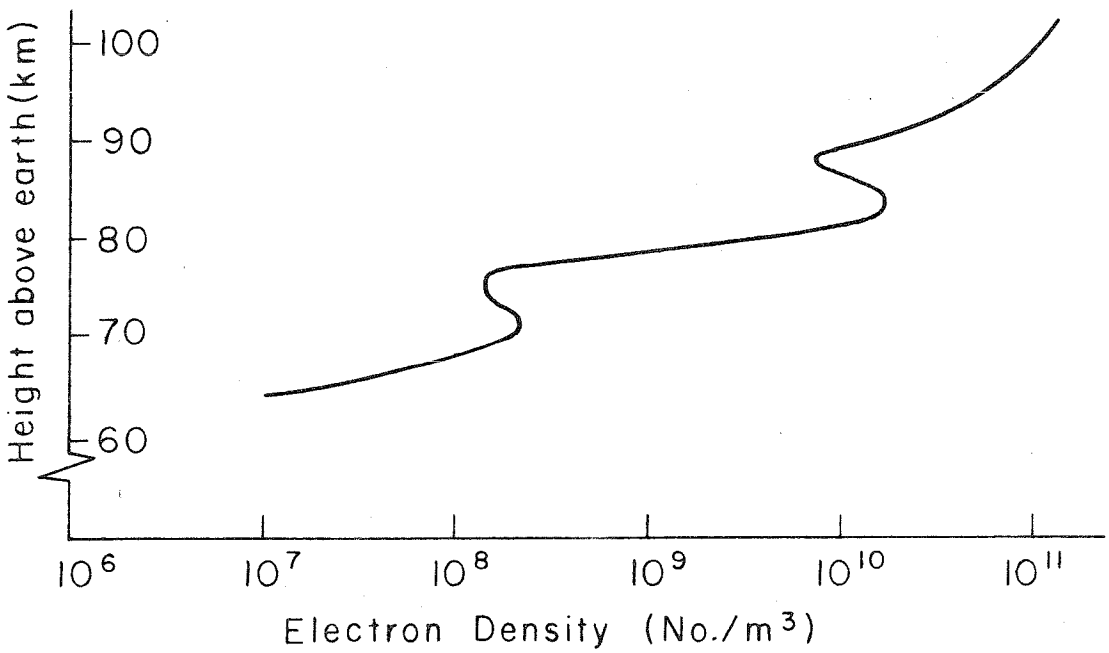

FIGURE II-2. EXPERIMENTAL ELECTRON DENSITY-HEIGHT PROFILE FOR EQUINOX NOON.

and F2 is observable only during the daylight hours, and usually merges with F2 after sunset to form a single F region. Region D has been considered primarily to be an absorbing region for waves of medium frequencies and is produced only during daylight hours.

The theoretical problem of how each atmospheric constituent forms an ionized layer under the influence of solar ultraviolet radiation has been discussed in detail by Chapman (12). The physics of this idealized process are as follows. The earth is assumed to be surrounded by a single gaseous element whose density decreases exponentially upwards (determined by combining the equation of state for this gas with the differential equation for the pressure of the gas when assumed to be in hydrostatic equilibrium). A beam of monochromatic radiation is assumed incident upon this atmosphere from the outside and is absorbed in producing ionization. However, the rate of absorption at any height is controlled by the density of the absorbing gas and the intensity of the incident radiation. As the radiation penetrates this idealized atmosphere, the intensity decreases and the density of the gas increases. These factors combine to produce a level of maximum ionization which is determined by the coefficient of absorption of the gas (for the radiation under consideration) and by the rate of change of the density of the gas with increasing height. Such a distinct region of ionization is called a Chapman region.

As observed experimentally and predicted theoretically by the above, the ionization density of the various regions follows a diurnal, seasonal and solar variation. Generally the intensity of ionization in

the E and F1 regions is proportional to a $\sqrt{\cos X}$ law, where X is the zenith angle of the sun.

To date, observations on the D region are rather sparse since electron density-height profiles, determined with the aid of rocket-borne instrumentation and by radio sounding techniques, have led to a value of 10^4 electrons per cubic centimeter which thus far is the minimum density that can be measured with confidence.

The variation of the ionization density in the F2 region is so erratic that it is difficult to make definite statements concerning it. The changes of ionization in this region are much greater than occur in the E and F1 regions; the diurnal variation has in general two maxima, one before and the other after midday; and finally, this region does not obey the simple Chapman law describing variation in height of a layer of given density with the zenith angle of the sun.

While the above four regions are readily observable characteristics of the ionosphere, another region may occasionally be observed which appears close to the height of the E region. Because of the irregularity in occurrence of this intense ionization, this region is designated as sporadic E. At least part of sporadic E can be attributed to ionization produced by meteoric impacts (13).

Radio Sounding of the Ionosphere

The greatest percentage of the data accumulated on the ionosphere has been obtained by the use of radio sounding techniques. These techniques permit the direct measurement of:

1. The transit time for a radio frequency pulse to travel from transmitter to receiver via reflections from the ionosphere (and hence the determination of the so-called equivalent height of the ionosphere - that height at which radio waves are apparently reflected).

2. The amplitude or intensity of the reflected signal.

3. The state of polarization of the reflected wave.

The usual methods used in radio sounding will now be briefly described.

Angle of incidence method (14). The equivalent height of the ionosphere is determined by measuring the angle of incidence of the received reflected wave at a known distance from the transmitter.

Change of wavelength method (15). This method also permits calculation of the equivalent height. Because the received signal is the vector resultant of the ground wave (or surface wave) and the sky wave, this resultant will vary between a relative maximum and minimum, depending on the relative phases of the two waves. Therefore, a controlled variation in the frequency of the transmitted wave causes the received signal to vary between a number of relative minima and maxima. From this information, the equivalent height may be deduced.

Hollingworth method (16). Again the equivalent height is deduced but this method is primarily applicable to waves of low and very low frequencies. As a variation in the change of wavelength method, the received signal is measured at different distances from the transmitter. Since the phases of the waves are dependent on the different

paths of propagation, the received signal varies through a number of relative maxima and minima. It is apparent that at higher frequencies, appreciable changes in phase are also produced as the equivalent height of the reflecting layer slowly varies. Hence this method must be restricted to vlf if any accuracy is to be expected.

Pulse method (17). A useful technique that permits measurement of the above three quantities is the pulse method. Short radio frequency pulses are transmitted and received at near vertical incidence with respect to the ionosphere. Measurement of the time of arrival of the pulses (or travel time) permits calculation of the equivalent height. At the same time it is possible to determine the reflection coefficients of the ionosphere and the state of polarization of the downcoming wave. The range of frequencies used in this method usually lies between .5 and 20 Mc.

Ground wave null method (18, 19). This method utilizes a horizontal transmitting antenna which has a ground wave radiation pattern as shown in figure II-3. By locating a receiver in a plane that is perpendicular to and bisects the antenna, it is possible to effectively eliminate the ground wave from the received signal. Hence the received signal primarily consists of the wave reflected from the ionosphere. This method permits measurement of the polarization of the received signal and the diurnal variations in the reflection coefficients for the different polarizations. For very low frequencies any change in the apparent equivalent height is small compared to a wavelength so that the Hollingworth method can be used in conjunction

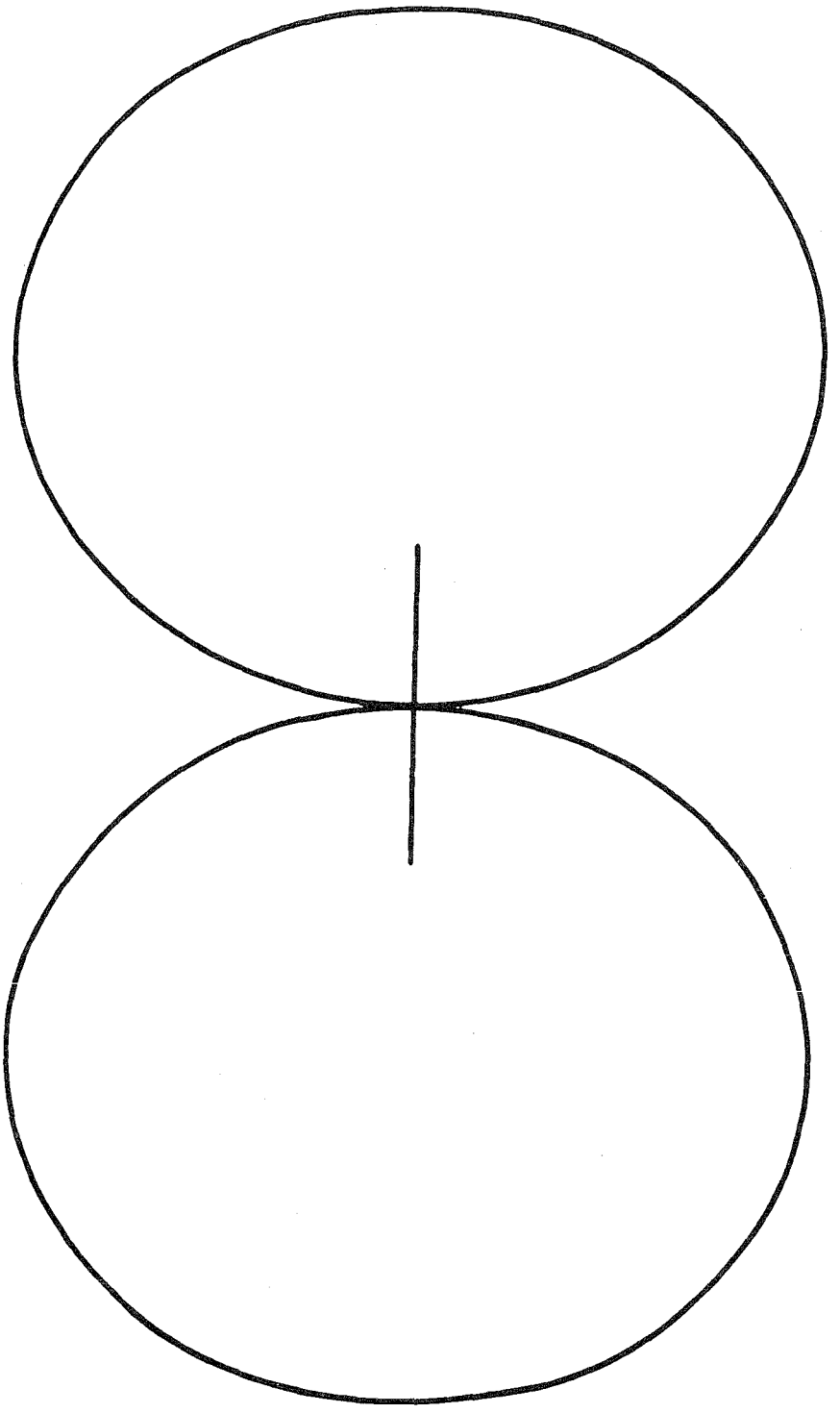

FIGURE II-3. RADIATION PATTERN OF A HORIZONTAL ANTENNA AT THE SURFACE OF THE EARTH.

with this method provided the receiver is moved along a radial path from the center of the antenna (in order that the relative strength of the ground wave remains constant with respect to the sky wave).

Although much information can be obtained from each of the above methods, it should be noted that the frequency range of the transmitted waves determines which ionospheric layers can be investigated. In general, the pulse method is useful for investigating the E, F1 and F2 layers but does not permit a direct study of the D region because of its lower degree of ionization. This region is most readily investigated by very low-frequency waves.

For theoretical considerations, the ionosphere will be assumed homogeneous and under the influence of a constant magnetic field (an approximation to the terrestrial magnetic field). This model will now be used for the development of the magneto-ionic theory.

III. PROPAGATION OF PLANE WAVES IN A GYROELECTRIC MEDIUM - THE MAGNETO-IONIC THEORY

As mentioned earlier, the present theory concerning propagation in an ionized medium is that of Eccles and Larmor which was later extended by Appleton, Hartree, Goldstein and others. However, the final results of this theory are difficult to present in a useful form. In what follows, the theory of propagation in a homogeneous ionized medium under the influence of a constant magnetic field is reviewed as put forth by Papas (20) and the results of this theory are presented in a series of curves which show the square of the index of refraction of the ionized medium as a function of the angular gyro-frequency ($\omega_g = eB/m$), plasma frequency ($\omega_p = \sqrt{Ne^2/m\varepsilon}$), and the angle between the constant magnetic field and the wave normal of the propagating plane waves. In the development of this theory, the capacitivity of the medium is no longer a scalar quantity but becomes an anti-symmetric tensor which causes the medium to behave in a manner similar to an optically active crystal. By determining the eigenvalues of this tensor, it is possible to show that a basis exists such that this tensor can be put into diagonal form and that the transformed fields corresponding to this form are electromagnetic waves that are usually elliptically polarized. Relations similar to the Fresnel and Indicial Ellipsoid are also given for the medium. Finally, dual relations between the ray surface and the wave surface are given.

The idealized ionosphere (see section II), will be assumed to consist of a stationary homogeneous ionized plasma (electrically neutral) in which there exists a constant and uniform magnetic field ($\underline{B}_o$). The permeability of this medium, is assumed equal to μ_v

the permeability of free space. The plasma is assumed to consist of free electrons and protons so that the quasi-elastic binding forces between oppositely-charged particles can be neglected. Consider a plane wave propagating in this medium in a direction that makes an arbitrary angle, ϕ, with the constant magnetic field. For convenience, assume that the constant magnetic field lies along the z-axis of the rectangular coordinate system shown in figure III-1.

The properties of this wave are determined by Maxwell's equations which are appropriate to the medium. These can be written explicitly once the contribution to convection current due to the motion of the electrons is computed. (The effects of the positively-charged particles will be neglected because of their much greater mass.) This convection current is $Ne\underline{v}$ where:

N = the number of particles/m^3

e = the charge on an electron (-1.60206×10^{19}C)

$\underline{v}$ = the velocity of an electron (meters per second)

Hence, it is only necessary to determine the velocity of the electrons. Neglecting the interaction of electrons between themselves other than collisions, the Lorentz force law on a single electron is:

$$\underline{F} = \underbrace{m\, d\underline{v}/dt}_{ma} + \underbrace{m\omega_c \underline{v}}_{\text{damping}} = \underbrace{e\underline{E} + e\,(\underline{v} \times \underline{H})}_{\text{force due to plane wave}} + \underbrace{e(\underline{v} \times \underline{B}_o)}_{\text{force due to constant magnetic field}} \quad \text{(III-1)}$$

(ω_c represents the collisional frequency of electrons and is essentially a damping constant.)

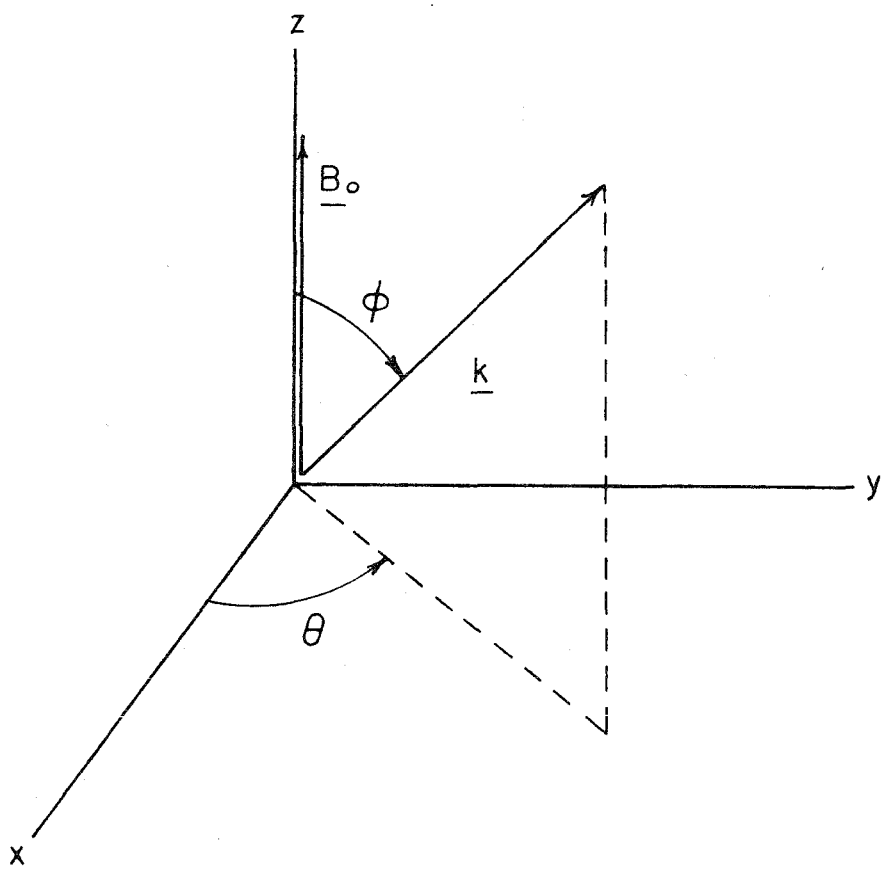

FIGURE III-1. COORDINATE SYSTEM FOR THE PROPAGATION OF PLANE WAVES IN A GYROELECTRIC MEDIUM.

For plane waves, the second term on the right is smaller than the first by a factor of $\underline{v}/c$ and therefore will be neglected. Assuming all time dependence as $e^{-i\omega t}$, equation III-1 may be written as:

$$-i\omega m\underline{v} + m\omega_c\underline{v} = e\underline{E} + e\underline{v} \times \underline{B}_o \tag{III-2}$$

After some vector manipulation (see appendix A) the velocity of an electron is found to be:

$$\underline{v} = \frac{\gamma^2 e\underline{E} + e^2\gamma(\underline{E} \times \underline{B}_o) + e^3(\underline{E} \cdot \underline{B}_o)\underline{B}_o}{\gamma(\gamma^2 + eB_o^2)} \tag{III-3}$$

where

$$\gamma = -i\omega m(1 + i\omega_c/\omega) \tag{III-3.1}$$

Maxwell's equations are therefore:

$$\nabla \times \underline{H} = Ne\underline{v} - i\omega\varepsilon\underline{E} = \underline{I} \tag{III-4}$$

$$\nabla \times \underline{E} = i\omega\mu_v\underline{H} \tag{III-5}$$

The total current density, $\underline{I}$, can now be related to the impressed electric field by writing equation III-4 in component form and substituting for $\underline{v}$ from equation III-3. Consequently,

$$\begin{bmatrix} I_x \\ I_y \\ I_z \end{bmatrix} = -i\omega \begin{bmatrix} \varepsilon_{xx} & -i\varepsilon_{xy} & 0 \\ i\varepsilon_{yx} & \varepsilon_{yy} & 0 \\ 0 & 0 & \varepsilon_{zz} \end{bmatrix} \begin{bmatrix} E_x \\ E_y \\ E_z \end{bmatrix} = \nabla \times \underline{H} = -i\omega[\varepsilon]\underline{E} \tag{III-6}$$

with

$$\varepsilon_{xx} = \varepsilon_{yy} = \varepsilon_v \left(1 - \frac{\omega_p^2 (1 + i\omega_c/\omega)}{\omega^2 (1 + i\omega_c/\omega)^2 - \omega_g^2} \right) \qquad \text{(III-6.1)}$$

$$\varepsilon_{xy} = \varepsilon_{yx} = \frac{\varepsilon_v \omega_p^2 \omega_g}{\omega \left[\omega^2 (1 + i\omega_c/\omega)^2 - \omega_g^2 \right]} \qquad \text{(III-6.2)}$$

$$\varepsilon_{zz} = \varepsilon_v \left(1 - \frac{\omega_p^2}{\omega^2 (1 + i\omega_c/\omega)^2} \right) \qquad \text{(III-6.3)}$$

Taking the curl of equation III-3 and substituting equation III-4 gives:

$$\underline{\nabla} \times \underline{\nabla} \times \underline{E} = \omega^2 \mu_v [\varepsilon] \underline{E} \qquad \text{(III-7)}$$

Propagation of these plane waves can now be represented as:

$$\underline{E} = \underline{E}_o e^{i(\underline{k} \cdot \underline{r} - \omega t)} \qquad \text{(III-8)}$$

The vector propagation constant is $\underline{k}$ and is related to the unit wave normal, $\underline{n}$, of the wave, by the relation:

$$\underline{k} = \underline{n}\, \omega/u \qquad \text{(III-9)}$$

(u is the phase velocity of the wave). Upon substitution of equation III-8 into equation III-7, the characteristic field equation for the medium becomes:

$$\underline{E} - \underline{n}(\underline{n} \cdot \underline{E}) = \left(\frac{1}{M^2} \right) \frac{[\varepsilon]}{\varepsilon_v} \underline{E} \qquad \text{(III-10)}$$

with $M = c/u$, the phase index of refraction of the medium.

Writing this in component form and, without loss of generality, letting $\theta = \pi/2$, yields the following relation:

$$\begin{bmatrix} 1 - \frac{1}{M^2}\frac{\varepsilon_{xx}}{\varepsilon_v} & \frac{i}{M^2}\frac{\varepsilon_{xy}}{\varepsilon_v} & 0 \\ -\frac{i}{M^2}\frac{\varepsilon_{yx}}{\varepsilon_v} & \cos^2\phi - \frac{1}{M^2}\frac{\varepsilon_{yy}}{\varepsilon_v} & -\cos\phi\sin\phi \\ 0 & -\cos\phi\sin\phi & \sin^2\phi - \frac{1}{M^2}\frac{\varepsilon_{zz}}{\varepsilon_v} \end{bmatrix} \begin{bmatrix} E_{ox} \\ E_{oy} \\ E_{oz} \end{bmatrix} = 0 \qquad \text{(III-11)}$$

For a non-trivial solution, the determinant of the first matrix must equal zero.

Setting the determinant equal to zero requires:

$$-\tan^2\phi = \frac{\left(\frac{1}{M^2} - \frac{1}{\varepsilon_1}\right)\left(\frac{1}{M^2} - \frac{1}{\varepsilon_2}\right)}{\left(\frac{1}{M^2} - \frac{1}{\varepsilon_3}\right)\left(\frac{1}{M^2} - \frac{1}{2}\left(\frac{1}{\varepsilon_1} + \frac{1}{\varepsilon_2}\right)\right)} \quad * \qquad \text{(III-12)}$$

where

$$\varepsilon_1 = \frac{\varepsilon_{xx} - \varepsilon_{xy}}{\varepsilon_v} = 1 - \frac{\omega_p^2}{\omega(\omega - \omega_g + i\omega_c)} \qquad \text{(III-12.1)}$$

$$\varepsilon_2 = \frac{\varepsilon_{xx} + \varepsilon_{xy}}{\varepsilon_v} = 1 - \frac{\omega_p^2}{\omega(\omega + \omega_g + i\omega_c)} \qquad \text{(III-12.2)}$$

---

* An equivalence between this equation and the Appleton-Hartree equation is given in appendix E.

$$\varepsilon_3 = \frac{\varepsilon_{zz}}{\varepsilon_v} = 1 - \frac{\omega_p^2}{\omega(\omega + i\omega_c)} \qquad \text{(III-12.3)}$$

Inspection of equation III-12 shows the anisotropic properties of the medium since M^2 is dependent on $\tan \phi$. Solving this equation for M^2 yields the square of the phase index of refraction of the medium as a function of the variables, ω_g, ω_p, ω_c, and ϕ. For a medium in which the collisional frequency, ω_c, is negligible, M^2 is a real number. (This is shown in appendix A.) Curves of M^2 as a function of ω/ω_g, ω_p/ω_g and ϕ are presented in figures III-2a through III-2f and have been plotted for this case.

The gyro-frequency, appropriate to the maximum terrestrial magnetic field in the area in which experimental observations have been made, is approximately 1.5 Mc. This number was calculated using a value of .52 gauss for the magnetic field which is inclined at an angle of 30° with the vertical. The plasma frequency is calculated to be of the order of 900 kc assuming a value of 10^{10} electrons per cubic meter for the E layer of the ionosphere. Hence the range of parameters presented is appropriate to low and very low-frequency propagation.

The transition from longitudinal propagation ($\phi = 0^\circ$) to transverse propagation ($\phi = 90^\circ$) is readily noted from the curves. For M^2 negative, the propagation constant becomes imaginary and the wave is absorbed or attenuated by the medium, the attenuation being $8.68(\omega/c)\,|M|$ db per wavelength.

The group index of refraction, M_g, can now be computed from the phase index of refraction since $M_g = M + \omega dM/d\omega$, (see appendix C, equation C-5). The group velocity (c/M_g) determines the arrival of a

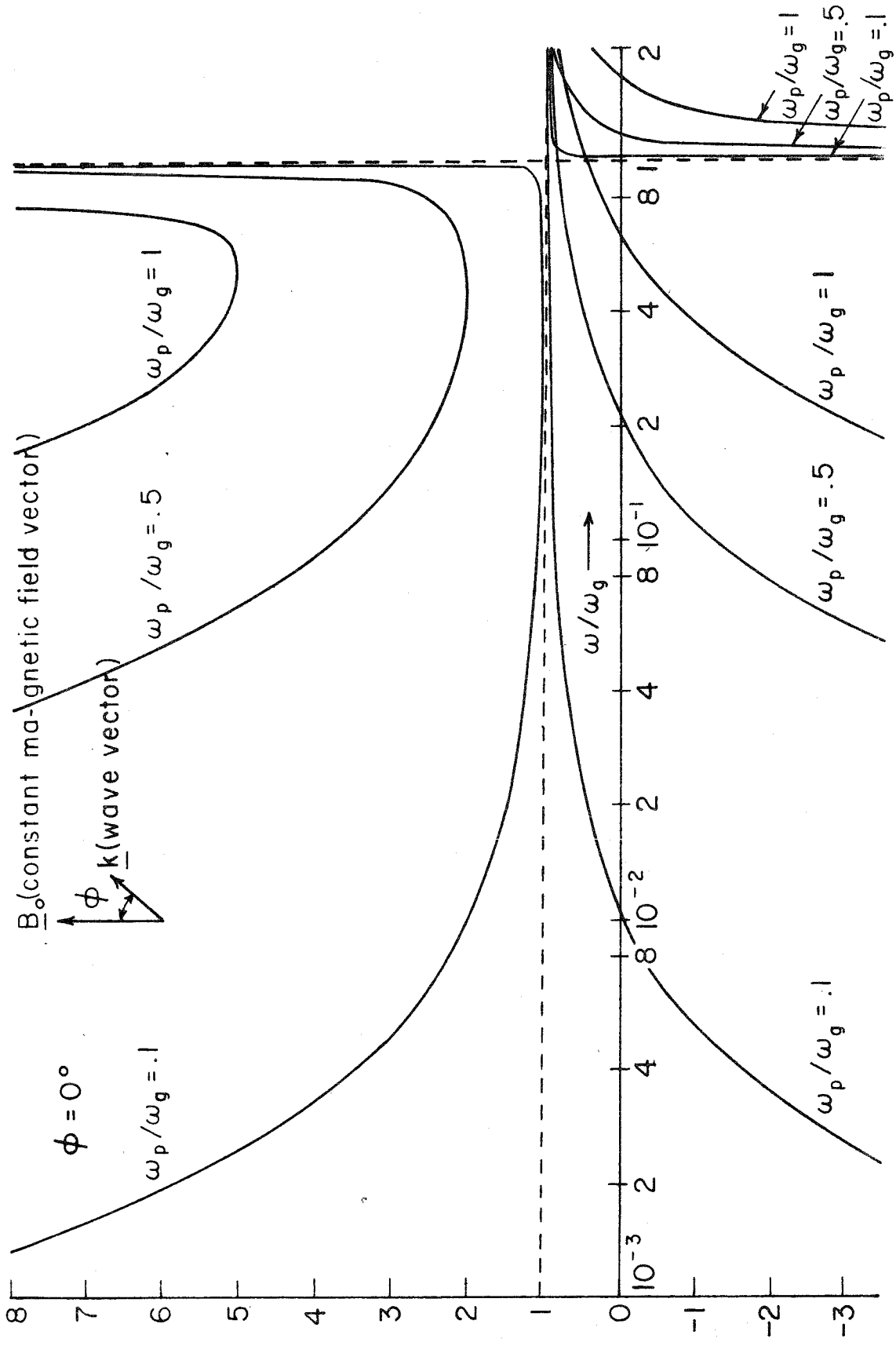

FIGURE III-2a. PHASE INDEX OF REFRACTION AS A FUNCTION OF GYRO- AND PLASMA FREQUENCY FOR A CONSTANT DIRECTION OF PROPAGATION.

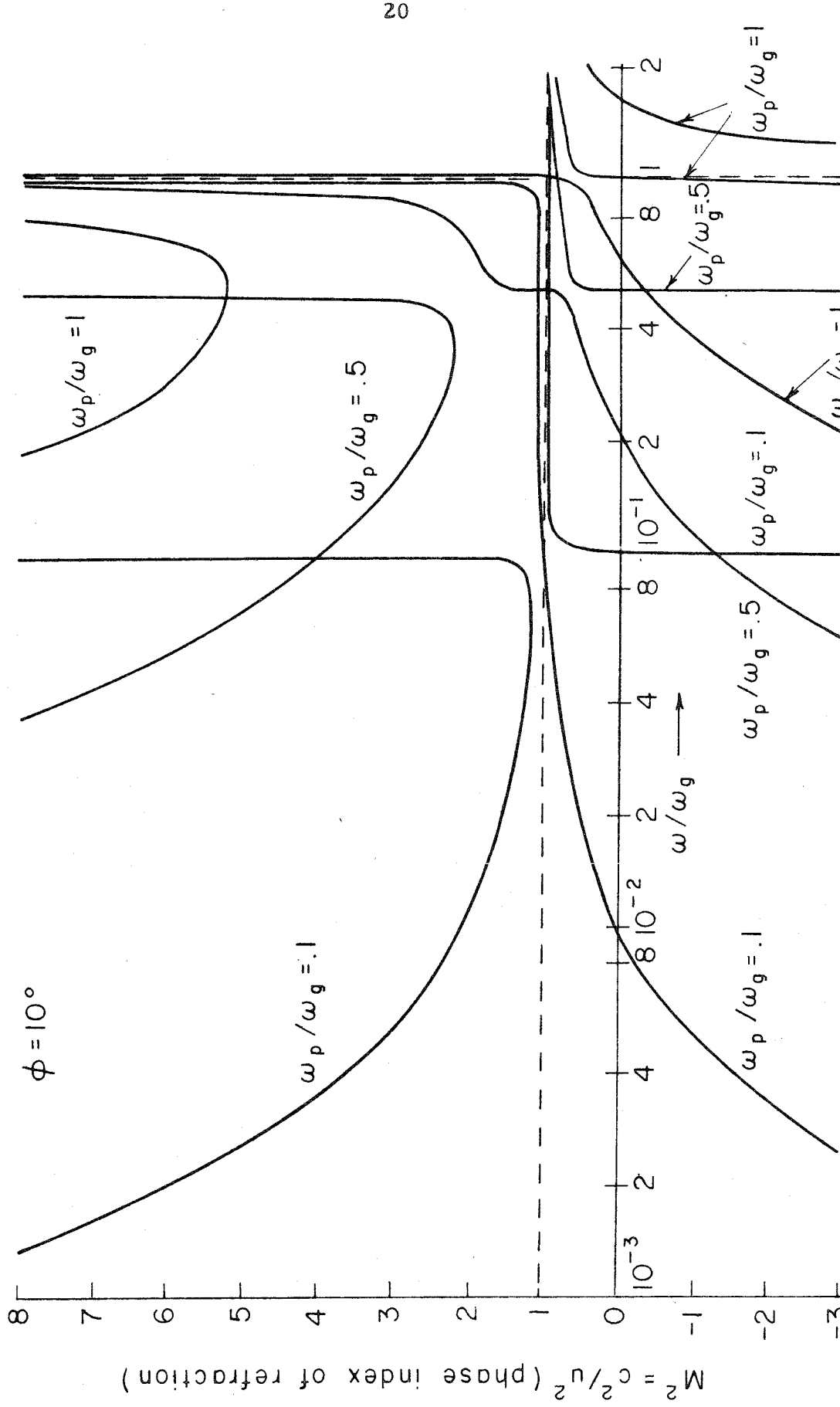

FIGURE III-2b. PHASE INDEX OF REFRACTION AS A FUNCTION OF GYRO- AND PLASMA FREQUENCY FOR A CONSTANT DIRECTION OF PROPAGATION.

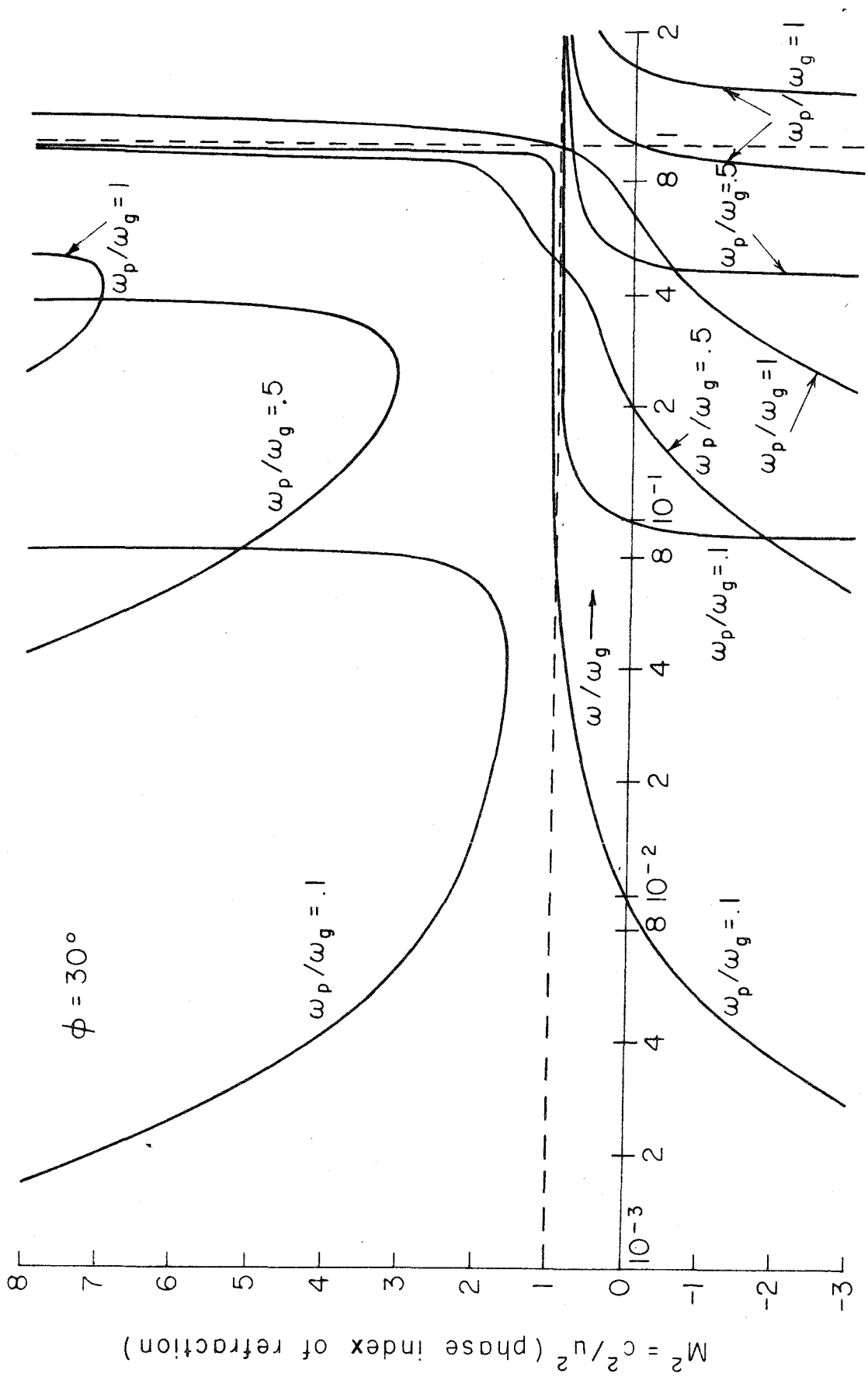

FIGURE III-c. PHASE INDEX OF REFRACTION AS A FUNCTION OF GYRO- AND PLASMA FREQUENCY FOR A CONSTANT DIRECTION OF PROPAGATION.

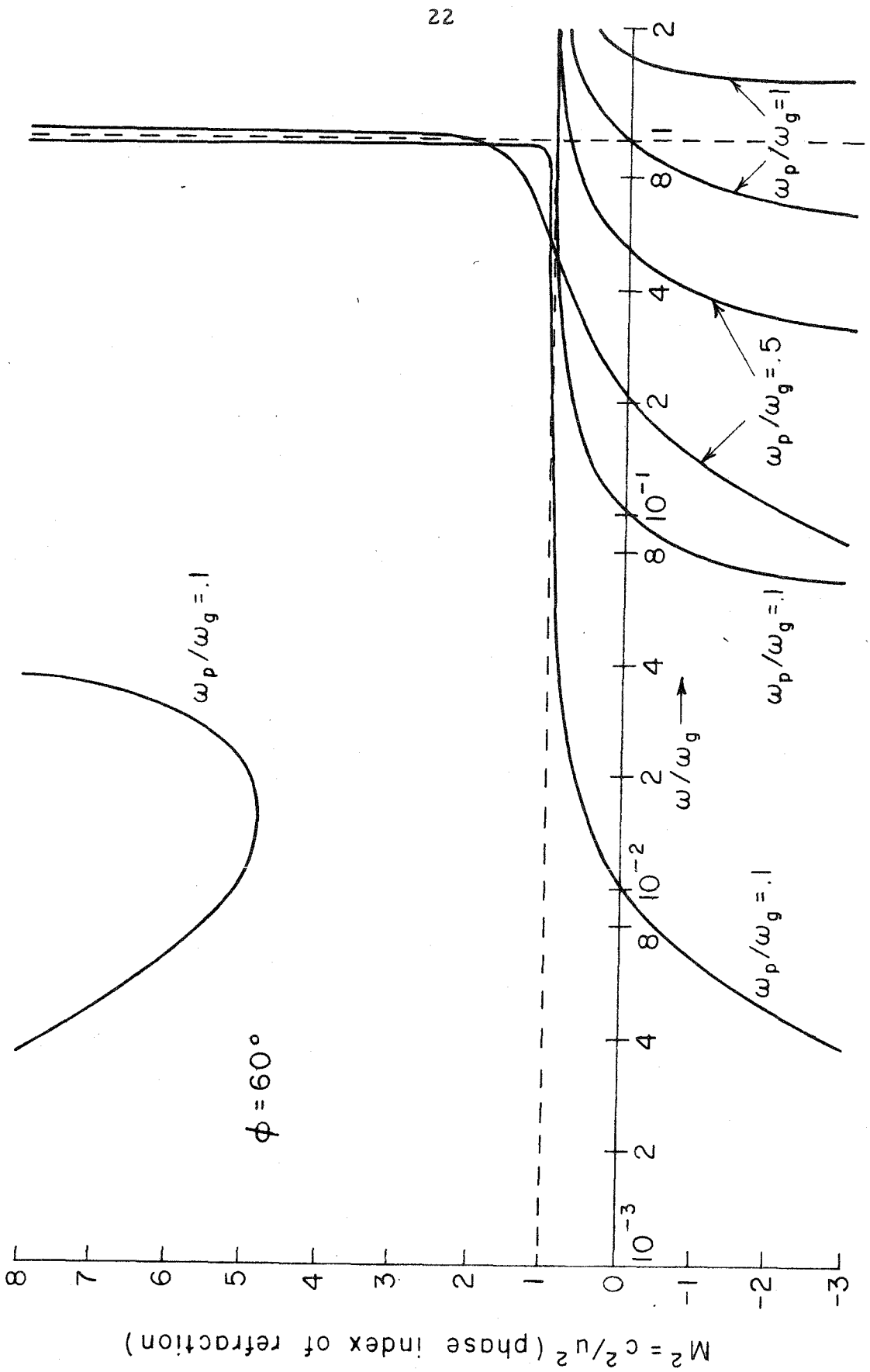

FIGURE III-2d. PHASE INDEX OF REFRACTION AS A FUNCTION OF GYRO- AND PLASMA FREQUENCY FOR A CONSTANT DIRECTION OF PROPAGATION.

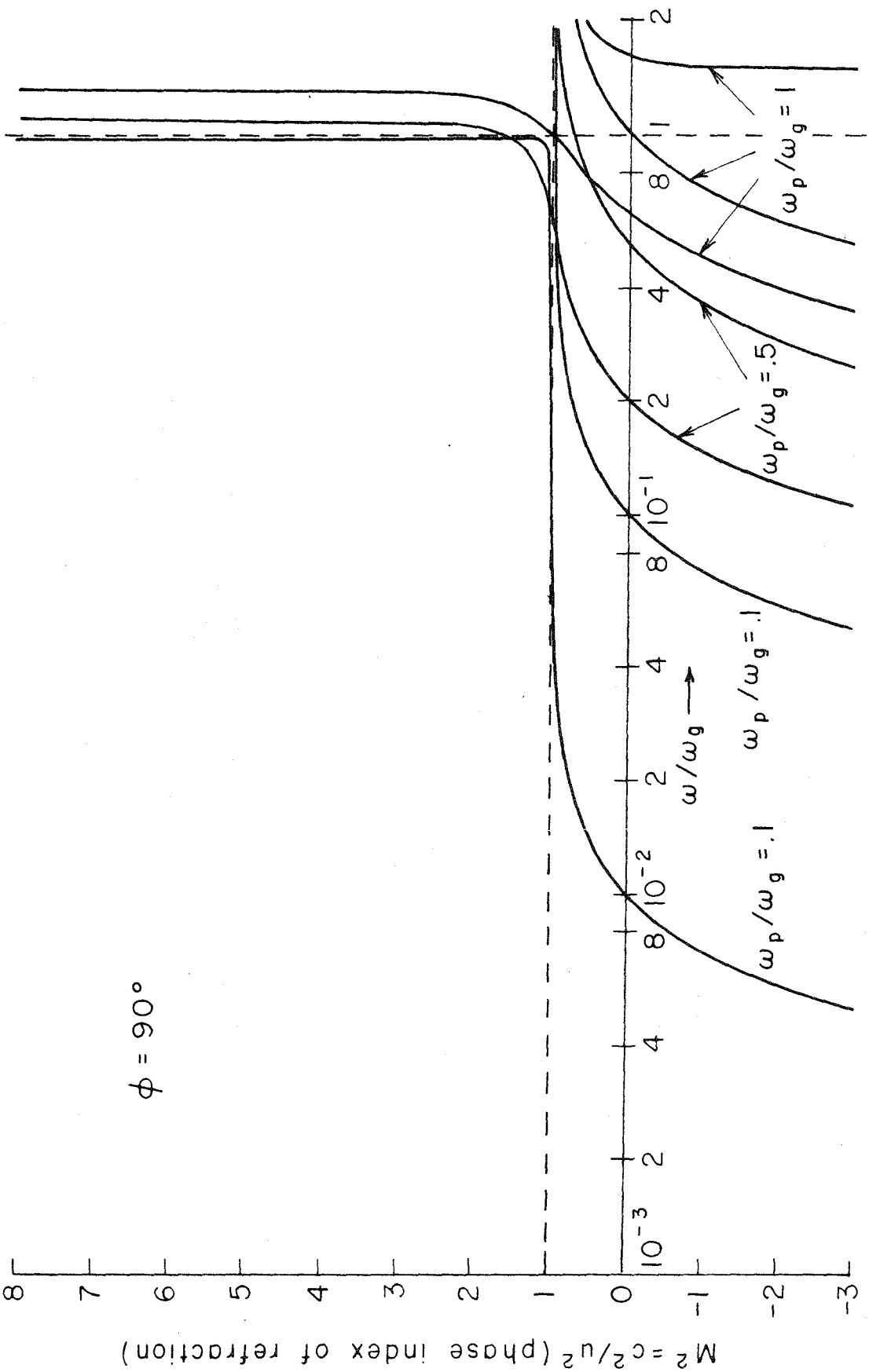

FIGURE III-2e. PHASE INDEX OF REFRACTION AS A FUNCTION OF GYRO- AND PLASMA FREQUENCY FOR A CONSTANT DIRECTION OF PROPAGATION.

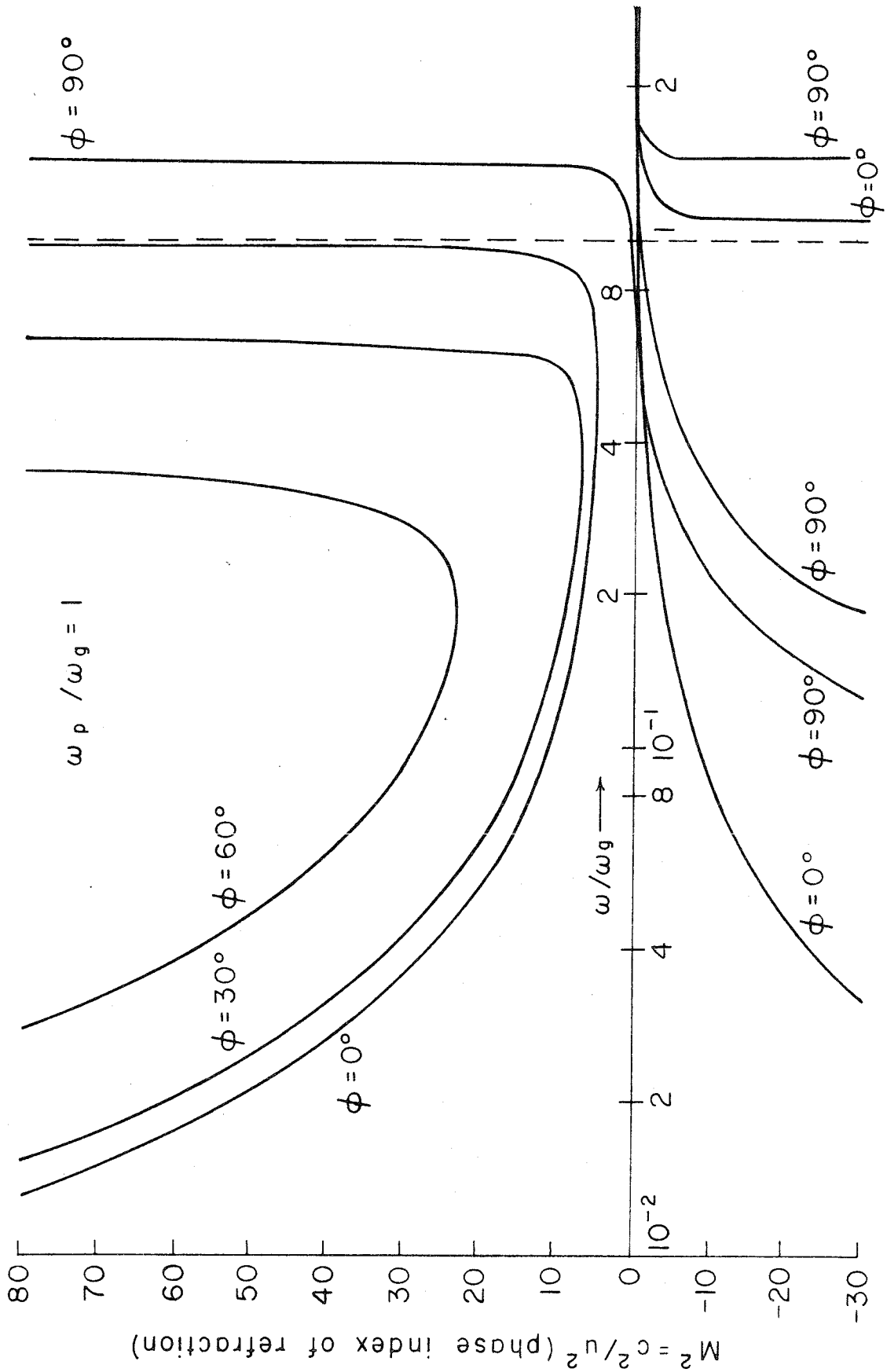

FIGURE III-2f. PHASE INDEX OF REFRACTION AS A FUNCTION OF GYRO- AND PLASMA FREQUENCY FOR A CONSTANT DIRECTION OF PROPAGATION.

bounded wave train at any point in the medium, whereas the phase index (or phase velocity) refers only to the propagation of the phase of a wave. [A discussion of the various velocities of propagation is given in (21) and (22).] Curves for longitudinal propagation ($\phi = 0$ and $M^2 = \varepsilon_1$) are given in figures III-3a and III-3b and were computed using equation C-7, appendix C.

Since the phase index of refraction of the medium is determined by setting the determinant of the matrix equal to zero, it is not possible to solve for the value of the components of the electric field but only for their ratio (the initial or boundary conditions determine the absolute value of the electric field vector). However, it is useful to consider the ratio of the components of the field as this yields information concerning the state of polarization of the waves.

The coordinate system used for the above calculation does not readily lend itself to computing the state of polarization of the waves. Hence the following change of coordinates will be made: a new coordinate system will be determined by rotating the old system through an angle $\pi/2 - \phi$ about the x axis as shown in figure III-4. The rotation matrix for this transformation is:

$$\begin{bmatrix} x' \\ y' \\ z' \end{bmatrix} = \begin{bmatrix} 1 & 0 & 0 \\ 0 & \sin\phi & \cos\phi \\ 0 & -\cos\phi & \sin\phi \end{bmatrix} \begin{bmatrix} x \\ y \\ z \end{bmatrix} \qquad \text{(III-13)}$$

In this system, the wave front is transverse to the y' axis and is traveling in the y' direction. The polarization, P , can now be defined as:

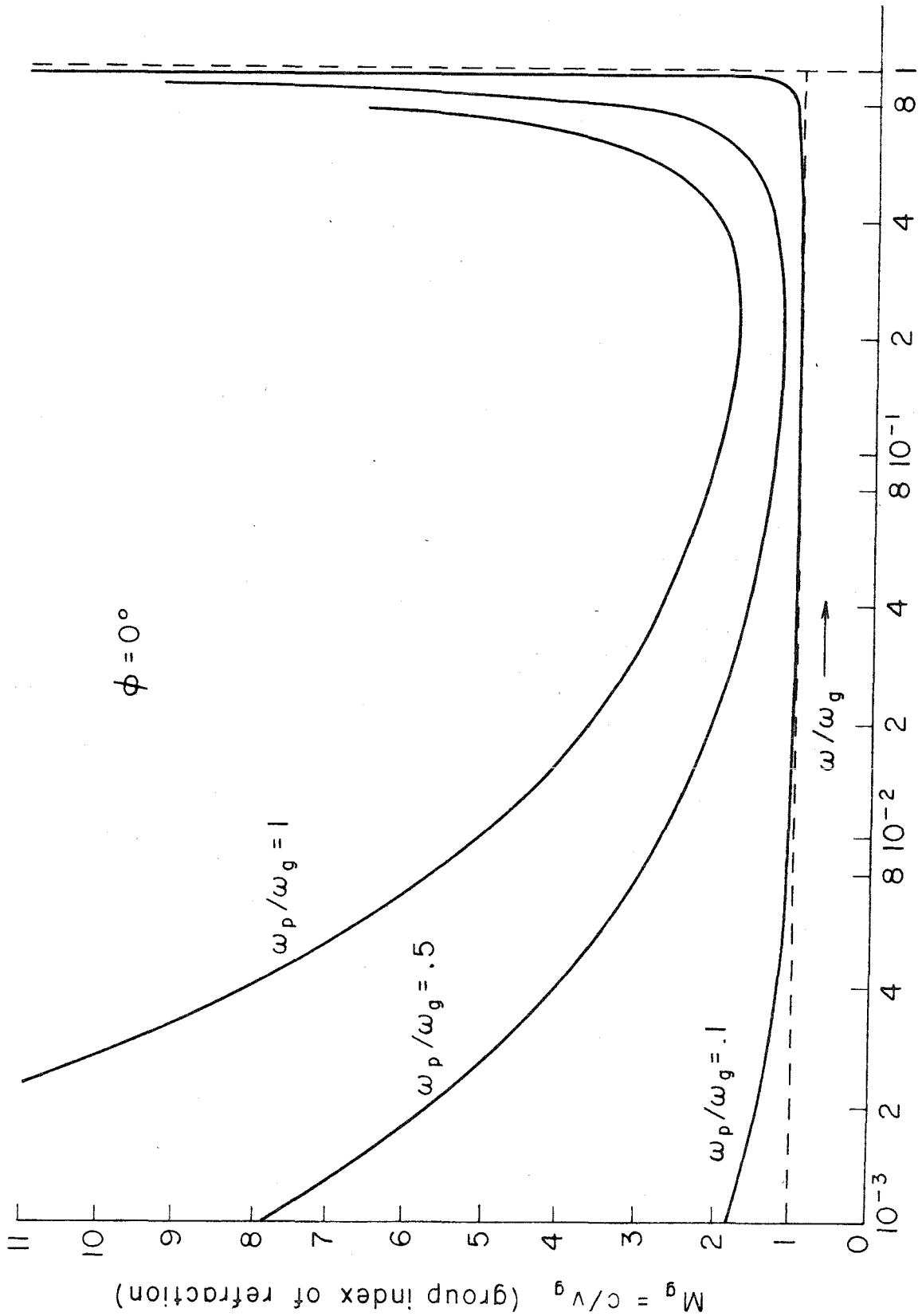

FIGURE III-3a. GROUP INDEX OF REFRACTION AS A FUNCTION OF GYRO- AND PLASMA FREQUENCY FOR A CONSTANT DIRECTION OF PROPAGATION.

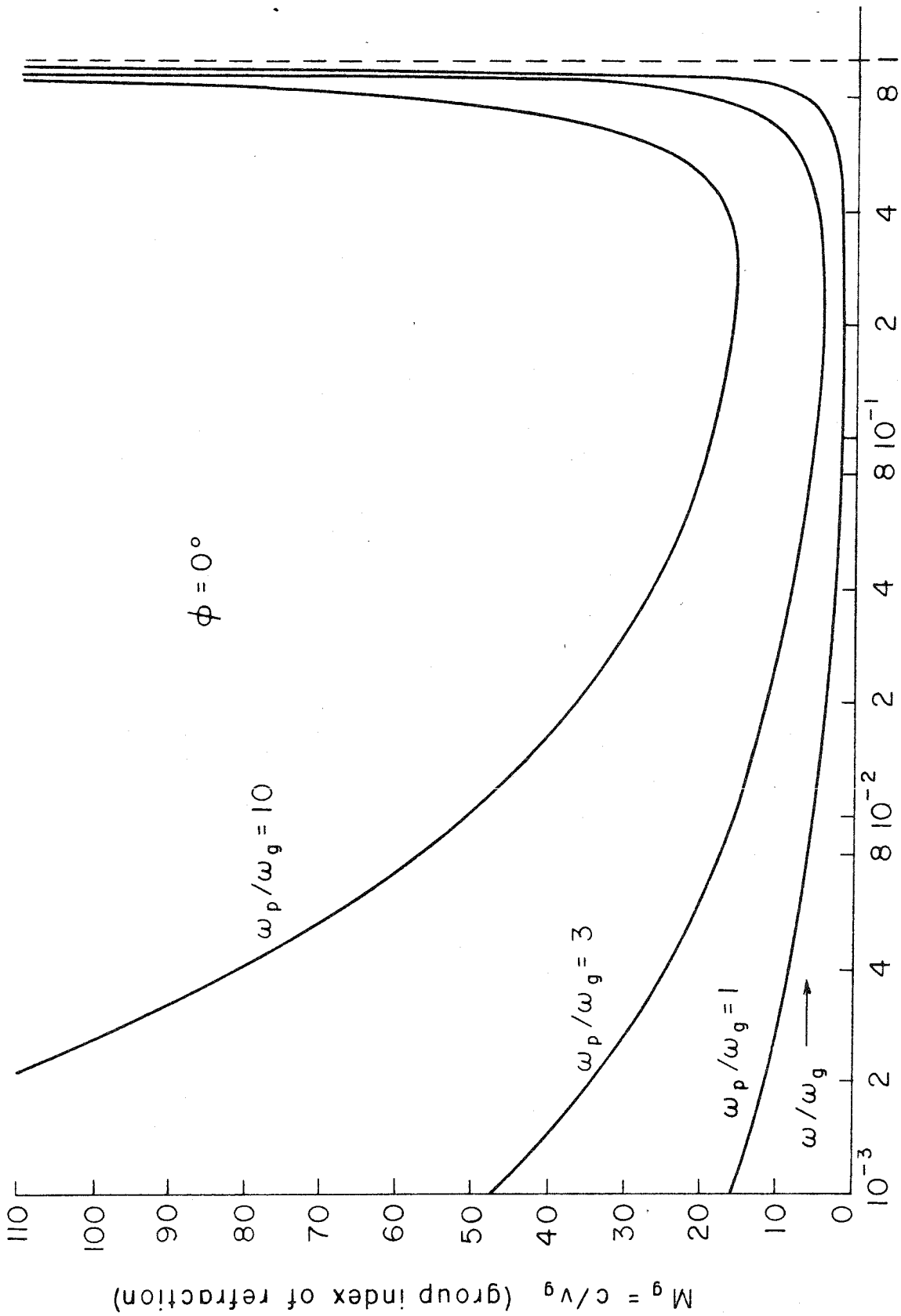

FIGURE III-3b. GROUP INDEX OF REFRACTION AS A FUNCTION OF GYRO- AND PLASMA FREQUENCY FOR A CONSTANT DIRECTION OF PROPAGATION.

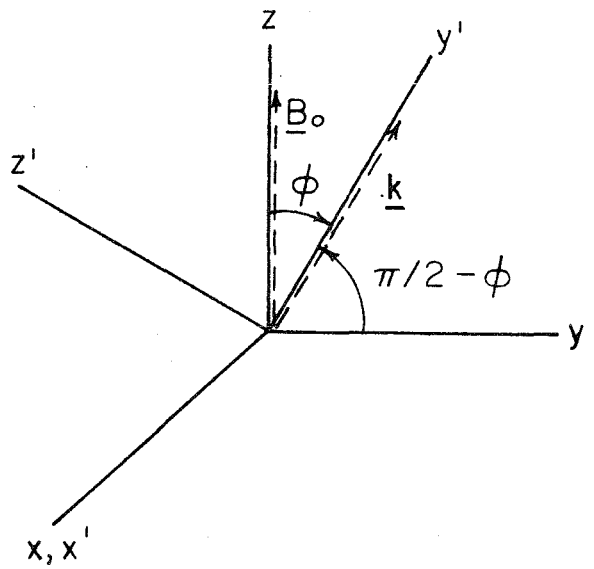

FIGURE III-4. CHANGE OF COORDINATE SYSTEM FOR DETERMINING THE STATE OF POLARIZATION OF PLANE WAVES IN A GYROELECTRIC MEDIUM.

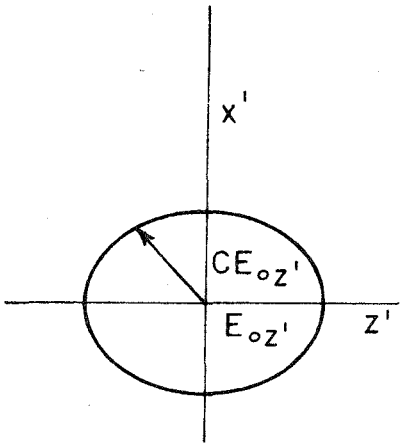

Lossless medium
(Size of ellipse is constant for all y')

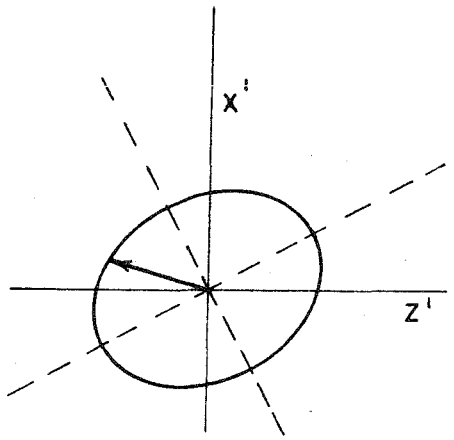

Lossy medium
(Size of ellipse decreases for increasing y')

FIGURE III-5. LOCUS OF ELECTRIC FIELD VECTOR IN A HOMOGENEOUS GYROELECTRIC MEDIUM (DIRECTION OF PROPAGATION IS OUT OF THE PAGE).

$$P = E_{x'}/E_{z'} \quad * \tag{III-14}$$

In terms of the old coordinate system this becomes

$$P = \frac{E_{ox}}{(E_{oz} \sin \phi - E_{oy} \cos \phi)} \tag{III-14.1}$$

Solving for this ratio (see appendix A) gives for the polarization:

$$P = i \frac{(\varepsilon_2 - \varepsilon_1)}{\varepsilon_3} \frac{\left[\tan^2 \phi (M^2 - \varepsilon_3) - \varepsilon_3\right]}{\sqrt{1 + \tan^2 \phi}\left[\varepsilon_1 + \varepsilon_2 - 2M^2\right]} \tag{III-15}$$

The electric field can therefore be represented in terms of the z' component as:

$$\underline{E} = E_{oz'}(\underline{e}_{z'} + iC\underline{e}_{x'})\, e^{i(\underline{k} \cdot \underline{r} - \omega t)} \tag{III-16}$$

where

$$C = \frac{(\varepsilon_2 - \varepsilon_1)}{\varepsilon_3} \frac{\left[\tan^2 \phi (M^2 - \varepsilon_3) - \varepsilon_3\right]}{\sqrt{1 + \tan^2 \phi}\left[\varepsilon_1 + \varepsilon_2 - 2M^2\right]} \tag{III-16.1}$$

For the lossless case, C is a real number so that the waves are elliptically polarized. The locus of $\underline{E}$ in the x', y', z' coordinate system is an ellipse whose semi-axes are $E_{oz'}$ and $CE_{oz'}$ as shown in figure III-5a. For the general case that M^2 is complex (collisional term included), C is also complex, and therefore the major and minor axes of the ellipse are rotated about the y' axis as shown in figure III-5b. For the lossy case, M^2 is complex and therefore the wave is

---

* See appendix E for equivalence to Appleton-Hartree formulation.

attenuated as it propagates, all components (for a given M) being attenuated at the same rate.

Returning now to the capacitivity tensor, it will be shown that a basis can be determined in which the capacitivity tensor is diagonal with diagonal elements equal to $\varepsilon_1\varepsilon_v$, $\varepsilon_2\varepsilon_v$, $\varepsilon_3\varepsilon_v$.

From equation III-6 the capacitivity tensor was found to be

$$\begin{bmatrix} \varepsilon_{xx} & -i\varepsilon_{xy} & 0 \\ i\varepsilon_{yx} & \varepsilon_{yy} & 0 \\ 0 & 0 & \varepsilon_{zz} \end{bmatrix}$$

The electric displacement, $\underline{D}$, is related to the electric field $\underline{E}$ by $[D] = [\varepsilon][E]$. It is desired to find a new basis such that $[\varepsilon]$ is diagonal and hence $\underline{D}$ and $\underline{E}$ in the new basis are collinear. The following similarity transform will accomplish this desired result, namely:

$$\begin{aligned} [D'] &= [A^{-1}][D] , & [A] &= \text{eigenvectors of } [\varepsilon] \\ [E'] &= [A^{-1}][E] , & [A^{-1}] &= \text{inverse of } [A] \\ [\varepsilon'] &= [A^{-1}][\varepsilon][A] = [\Lambda] , & [\Lambda] &= \text{eigenvalues of } [\varepsilon] \end{aligned} \qquad \text{(III-17)}$$

Proceeding in the usual manner to find the eigenvalues results in:

$$\det \begin{bmatrix} \varepsilon_{xx} - \lambda & -i\varepsilon_{xy} & 0 \\ i\varepsilon_{yx} & \varepsilon_{yy} - \lambda & 0 \\ 0 & 0 & \varepsilon_{zz} - \lambda \end{bmatrix} = 0 \qquad \text{(III-18)}$$

Solving for λ yields the three values:

$$\lambda_1 = \varepsilon_{xx} - \varepsilon_{xy} = \varepsilon_1 \varepsilon_v$$

$$\lambda_2 = \varepsilon_{xx} + \varepsilon_{xy} = \varepsilon_2 \varepsilon_v \qquad \text{(III-19)}$$

$$\lambda_3 = \varepsilon_{zz} = \varepsilon_3 \varepsilon_v$$

The corresponding eigenvectors are respectively:

$$\begin{bmatrix} C_1 \\ -iC_1 \\ 0 \end{bmatrix} \quad \begin{bmatrix} C_2 \\ iC_2 \\ 0 \end{bmatrix} \quad \begin{bmatrix} 0 \\ 0 \\ C_3 \end{bmatrix}$$

As C_1, C_2, and C_3, are arbitrary, these will be chosen equal to 1/2, 1/2 and 1 respectively. Therefore, the transform matrix, $\left[A^{-1}\right]$, becomes:

$$\begin{bmatrix} 1 & i & 0 \\ 1 & -i & 0 \\ 0 & 0 & 1 \end{bmatrix} = \left[A^{-1}\right] \qquad \text{(III-20)}$$

In this new basis, $\underline{D}$ and $\underline{E}$ become:

$$\left[D'\right] = \begin{bmatrix} D_x + iD_y \\ D_x - iD_y \\ D_z \end{bmatrix} \quad , \quad \left[E'\right] = \begin{bmatrix} E_x + iE_y \\ E_x - iE_y \\ E_z \end{bmatrix} \qquad \text{(III-21)}$$

which shows that the capacitivity is a scalar quantity for waves that are elliptically polarized.

Considering next the electric energy density, $W_e = 1/2\,(\underline{E} \cdot \underline{D})$, then,

$$W_e = 1/2\,(\varepsilon_{xx} E_x^2 + \varepsilon_{yy} E_y^2 + \varepsilon_{zz} E_z^2) \qquad \text{(III-22)}$$

The off-diagonal terms of the capacitivity tensor do not contribute to this quantity. It is now possible to construct a characteristic tensor surface which has the character of Fresnel's ellipsoid in optics. This surface assumes the form:

$$\frac{(\varepsilon_1 + \varepsilon_2)}{2} x^2 + \frac{(\varepsilon_1 + \varepsilon_2)}{2} y^2 + \varepsilon_3 z^2 = \frac{2W_e}{\varepsilon_v} = \text{a constant} \qquad \text{(III-23)}$$

Unfortunately the lengths of the principal axes of this ellipsoid cannot be directly identified as the reciprocals of the principal indices of refraction. The indices of refraction along the x and y axes, (transverse to the constant magnetic field), are equal and assume the values

$$\sqrt{\varepsilon_3} \quad \text{or} \quad \sqrt{\frac{1}{\frac{1}{2}\left(\frac{1}{\varepsilon_1} + \frac{1}{\varepsilon_2}\right)}}$$

Along the z axis, (parallel to the constant magnetic field), M assumes the values $\sqrt{\varepsilon_1}$ or $\sqrt{\varepsilon_2}$.

The principal axes are therefore related to the phase indices of refraction in the following manner: the x and y axes of the ellipsoid are equal to the reciprocal of the root mean square value, $\left[\frac{1}{2}(M_1^2 + M_2^2)\right]^{-1/2}$, of the phase index of waves propagating parallel to $\underline{B}_o$. The z axis is equal to the reciprocal of only one of the values of the phase index, for waves propagating transverse to $\underline{B}_o$.

If the electric energy density is computed from $\left[E\right] = \left[\varepsilon^{-1}\right]\left[D\right]$ where,

$$\left[\varepsilon^{-1}\right] = \frac{1}{\varepsilon_v}\begin{bmatrix} \frac{1}{2}(1/\varepsilon_1 + 1/\varepsilon_2) & -\frac{i}{2}(1/\varepsilon_2 - 1/\varepsilon_1) & 0 \\ \frac{i}{2}(1/\varepsilon_2 - 1/\varepsilon_1) & \frac{1}{2}(1/\varepsilon_1 + 1/\varepsilon_2) & 0 \\ 0 & 0 & 1/\varepsilon_3 \end{bmatrix} \tag{III-24}$$

then the corresponding tensor surface becomes

$$1/2(1/\varepsilon_1 + 1/\varepsilon_2)x^2 + 1/2(1/\varepsilon_1 + 1/\varepsilon_2)y^2 + 1/\varepsilon_3 z^2 = 2W_e\varepsilon_v \text{, a constant} \tag{III-25}$$

For this surface, it is seen that the lengths of the principal axes give both values of the phase index of refraction for waves propagating transverse to $\underline{B}_o$. This surface can be identified with the index ellipsoid of optics.

Briefly reiterating the above shows that the characteristics of plane electromagnetic waves propagating in a gyroelectric medium, can be represented by the following equations:

1. The vector propagation constant, $\underline{k}$, is related to the various field quantities by:

$$\underline{k} = \omega\mu_v \frac{(\underline{D} \times \underline{H})}{(\underline{D} \cdot \underline{E})} \text{ , } \quad \underline{k} \cdot \underline{D} = \underline{k} \cdot \underline{H} = \underline{D} \cdot \underline{H} = 0$$

$$\text{and} \quad \underline{k} \cdot \underline{E} \neq 0$$

2. The governing field equation is:

$$\underline{E} - \underline{n}(\underline{n} \cdot \underline{E}) = \mu_v u^2 \underline{D}$$

3. The vectors $\underline{D}$, $\underline{E}$, $\underline{n}$ are coplanar, i.e.,

$$\underline{n} \cdot (\underline{D} \times \underline{E}) = 0$$

4. The phase refractive index is given by:

$$M = c/u$$

5. The electric field and electric displacement are related by,

$$\left[D\right] = \left[\varepsilon\right]\left[E\right]$$

and

$$\left[\varepsilon\right] = \varepsilon_v \begin{bmatrix} \left(\frac{\varepsilon_1 + \varepsilon_2}{2}\right) & -i\left(\frac{\varepsilon_2 - \varepsilon_1}{2}\right) & 0 \\ i\left(\frac{\varepsilon_2 - \varepsilon_1}{2}\right) & \left(\frac{\varepsilon_1 + \varepsilon_2}{2}\right) & 0 \\ 0 & 0 & \varepsilon_3 \end{bmatrix}$$

A dual set of relations involving the quantities $\underline{E}$, $\underline{D}$, $\underline{s}$ (the unit Poynting vector) and $\underline{v}$, (the ray velocity) are readily constructed, (see appendix B). These dual relations are presented below:

1. The ray vector or Poynting vector is given by:

$$\underline{S} = \underline{E} \times \underline{H} \quad , \quad \underline{S} \cdot \underline{E} = \underline{S} \cdot \underline{H} = \underline{E} \cdot \underline{H} = 0$$

$$\text{and} \quad \underline{S} \cdot \underline{D} \neq 0$$

2. The governing field equation is:

$$\underline{D} - (\underline{s} \cdot \underline{D})\underline{s} = \frac{1}{\mu_v v^2} \underline{E}$$

3. The vectors, $\underline{D}$, $\underline{E}$, $\underline{s}$, are coplanar:

$$\underline{s} \cdot (\underline{D} \times \underline{E}) = 0$$

4. The ray velocity is related to the phase velocity by:

$$\underline{v} = \underline{u} \left[1 - \frac{(\underline{n} \cdot \underline{E})^2}{E^2} \right]^{-1/2}$$

5. The ray refractive index is given by:

$$M' = c/v = M \left[1 - \frac{(\underline{n} \cdot \underline{E})^2}{E^2} \right]^{1/2}$$

6. The electric displacement and electric field are related by:

$$[E] = [\varepsilon^{-1}][D]$$

$$[\varepsilon^{-1}] = \frac{1}{\varepsilon_v} \begin{bmatrix} \frac{1}{2}\left(\frac{1}{\varepsilon_1} + \frac{1}{\varepsilon_2}\right) & -\frac{i}{2}\left(\frac{1}{\varepsilon_2} - \frac{1}{\varepsilon_1}\right) & 0 \\ \frac{i}{2}\left(\frac{1}{\varepsilon_2} - \frac{1}{\varepsilon_1}\right) & \frac{1}{2}\left(\frac{1}{\varepsilon_1} + \frac{1}{\varepsilon_2}\right) & 0 \\ 0 & 0 & 1/\varepsilon_3 \end{bmatrix}$$

With the above theory as a basis, it is now possible to discuss some of the features of observed natural and experimental electromagnetic phenomena at vlf.

IV. NATURAL PHENOMENA AT VERY LOW FREQUENCIES

About 1930, a naturally occurring electromagnetic phenomenon was reported by Barkhausen (23), which he [and Eckersley independently (24)] deduced to be due to the dispersion of a short electromagnetic pulse or "click" in the ionosphere. In 1953, Storey (25) showed conclusively that the short pulse of electromagnetic energy had its origins in a lightning discharge and then gave a detailed analysis of the mechanism by which such a pulse propagates.

From the magneto-ionic theory presented, it is seen that the ionosphere is a highly dispersive medium for waves of frequencies small compared to the corresponding gyro- and plasma frequencies of the medium. Hence, when a large pulse of short duration propagates through such a medium, the higher frequency components generally travel faster, so that the duration of the pulse is dispersed or spread out in time. The resulting wave is then one of descending frequency - a gliding tone or so-called whistler (generally in the frequency range between 15 kc and 400 cycles).

In appendix C, a simple derivation is given for the relation between the time of arrival of the highest tone of the whistler and its corresponding frequency. This is:

$$T = D/\sqrt{f} \qquad \text{(IV-1)}$$

where

T is the arrival time of the frequency f

D is the dispersion

Typical values for D are between 50 and 150 for a frequency of 10 kc.

Storey has also shown that many whistlers have their origin in the hemisphere opposite to the one in which they are observed and hence must be under the influence of some guiding mechanism. This mechanism is the earth's magnetic field since waves propagating along a field line tend to travel fastest and suffer the least dispersion. Because of the great distance covered by the magnetic field lines, the original pulse can propagate far out into space and back again along the field lines to their termination in the opposite hemisphere. At this point the pulse may undergo reflection and return to its point of origin, again being dispersed through the ionosphere.

It is practically impossible to determine the length of the path traveled by such a pulse for the dispersion depends on the electron density and the magnetic field strength along the path, which are unknown quantities. Storey has made a rough calculation for the minimum distance traveled by whistlers by assuming the electron density to be equal to that of the densest layer in the ionosphere and assuming a constant magnetic field strength. He arrives at a number that is approximately 15,000 miles [this assumes an average dispersion of 120 $(\text{sec})^{-1/2}$]. It is only with the recent discovery of the high energy radiation belts surrounding the earth that Storey's calculation becomes amenable, for until now, there had been much doubt as to the validity of his assumption regarding ionization density.

Another type of whistler has received considerable attention (26); namely, the nose whistler in which there are present waves of both ascending and descending frequency, joining at the nose frequency. This type of whistler can be explained in terms of the M_g curves

(see figures III-3a and 3b) as follows. For all frequencies less than the gyro-frequency, it is seen that the group velocity, inversely proportional to M_g, will reach a maximum and then decrease. Therefore a pulse that contains frequency components on either side of this maximum will be dispersed such that the frequency corresponding to the maximum group velocity arrives first and is then followed by higher and lower frequencies according (approximately) to the above dispersion law (the law holds primarily for the case that $\omega << \omega_g << \omega_p$). The frequency at which the group velocity reaches a maximum (M_g a minimum) is the nose frequency.

One of the important qualities of whistlers is that they yield information concerning some of the properties of the outer ionosphere in the presence of the earth's magnetic field. The past I.G.Y. program included a vast network of whistler monitoring stations which was jointly under the direction of Helliwell and Morgan. The aspects of this program are discussed in (27).

Since whistlers are due to the dispersion of the field of a lightning stroke, a calculation was made (28) to determine the resulting fields when the field of an idealized lightning stroke (figure IV-1) is slightly dispersed. The results of this calculation are shown in figure IV-2. It is seen that while the duration of the idealized lightning stroke field is only about 100 micro-seconds, the duration of the dispersed fields is considerably longer.

The fact that whistlers are a random natural occurrence means that they do not lend themselves to controlled experiments and therefore have a limited use. With this fact in mind, it was proposed that

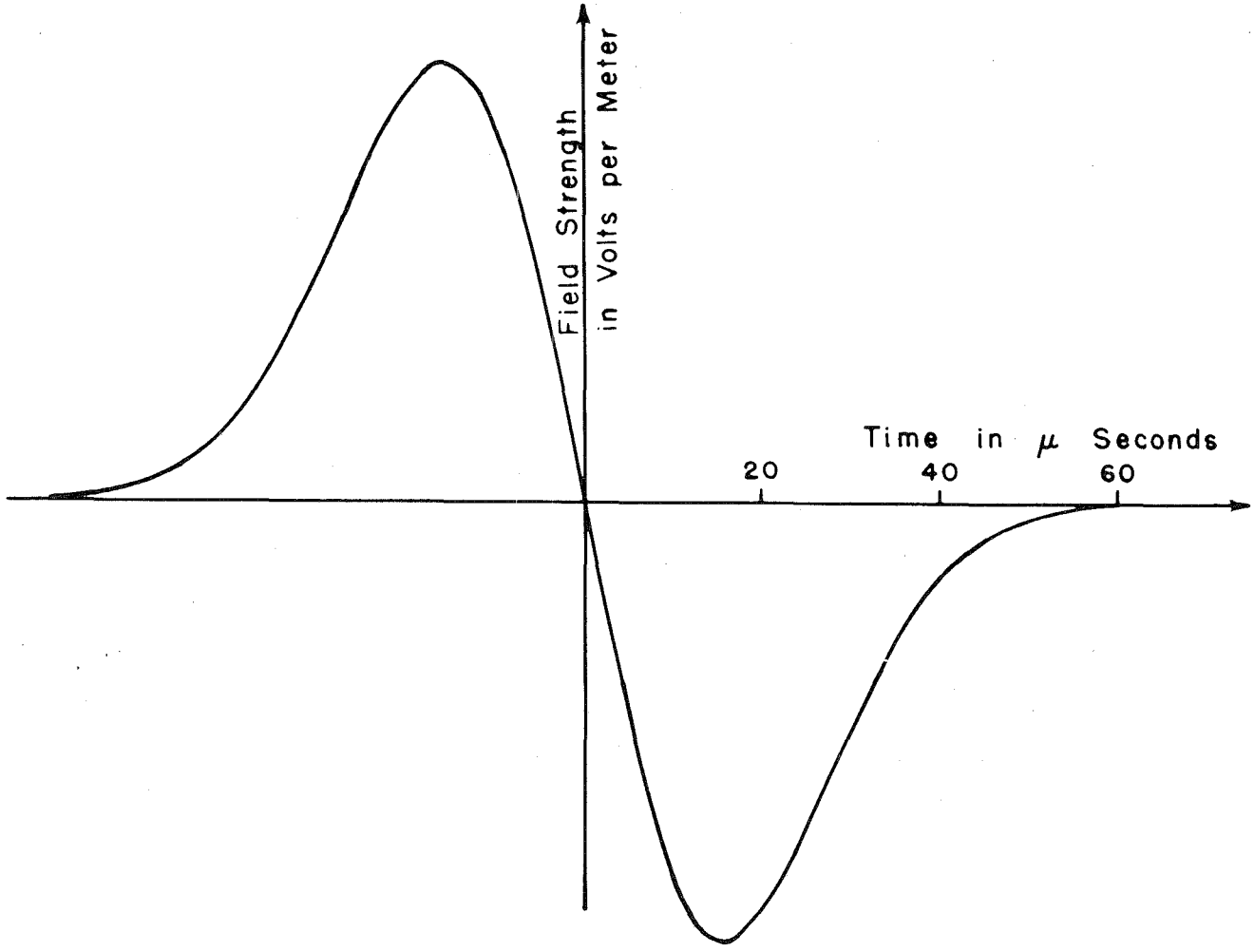

FIGURE IV-1. ASSUMED FORM FOR THE FIELD OF AN IDEALIZED LIGHTNING STROKE.

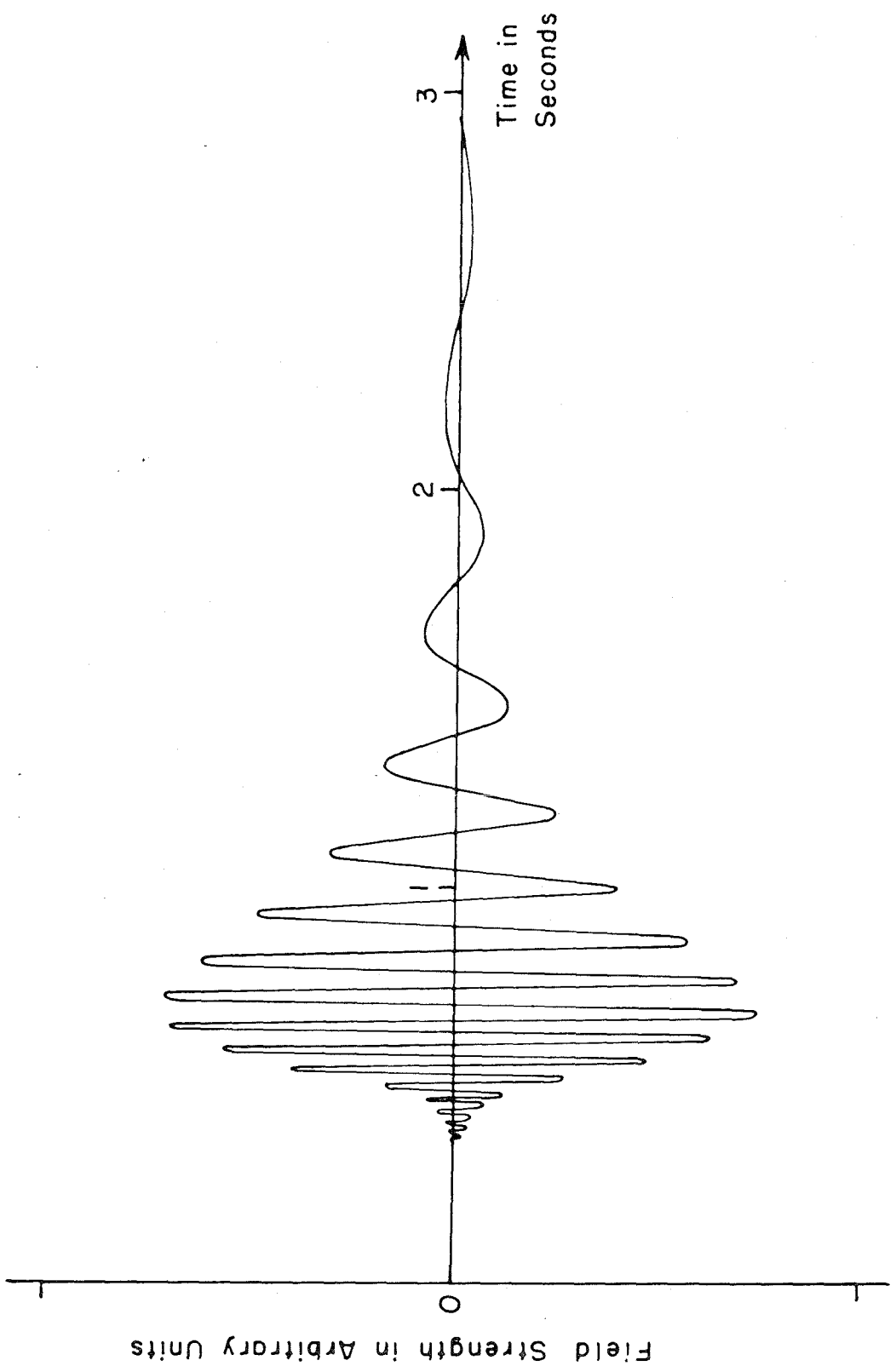

FIGURE IV-2. DISPERSED FIELDS OF AN IDEALIZED LIGHTNING STROKE.

"artificial whistlers" might possibly be generated and thereby provide a means of obtaining a controlled experiment.

Rather than generate a pulse of energy content comparable to that of a lightning stroke, it was planned to use a unique radio transmitting system to radiate short radio frequency pulses of sufficient energy such that it would be possible to excite the whistler mode of propagation [called magneto-ionic duct propagation by Helliwell (29)]. Because a pulse that propagates in this mode is essentially confined to a single frequency (the effects of sidebands due to off-on modulation can in general be neglected) the echo or reflected pulse would also be confined to this frequency. Hence the term gyroelectric-echo (or echo) will hereafter be used to describe waves of a single frequency that propagate via this mode, while the term whistler will be reserved to describe gliding tones which originate from lightning strokes.

The power requirements of the transmitting system used to generate gyroelectric-echoes (see section VII) were determined by employing the results of the above dispersion calculation (28). This yielded the power requirements of the system as a function of excitation frequency. For a horizontal antenna of 50 ohms input resistance located over a ground of 500 ohm-meters, the resulting power requirements are shown in figure IV-3. (Figure IV-3 is <u>essentially</u> the relative power spectrum of the whistler shown in figure IV-2.)

During the construction phase of the transmitting station, Helliwell and Geherels (29) were able to detect echoes of transmitted radio signals from NSS (radiated power of 50 kw at 15.5 kc) at Cape Horn, South America (the approximate magnetic conjugate of NSS). The echoes

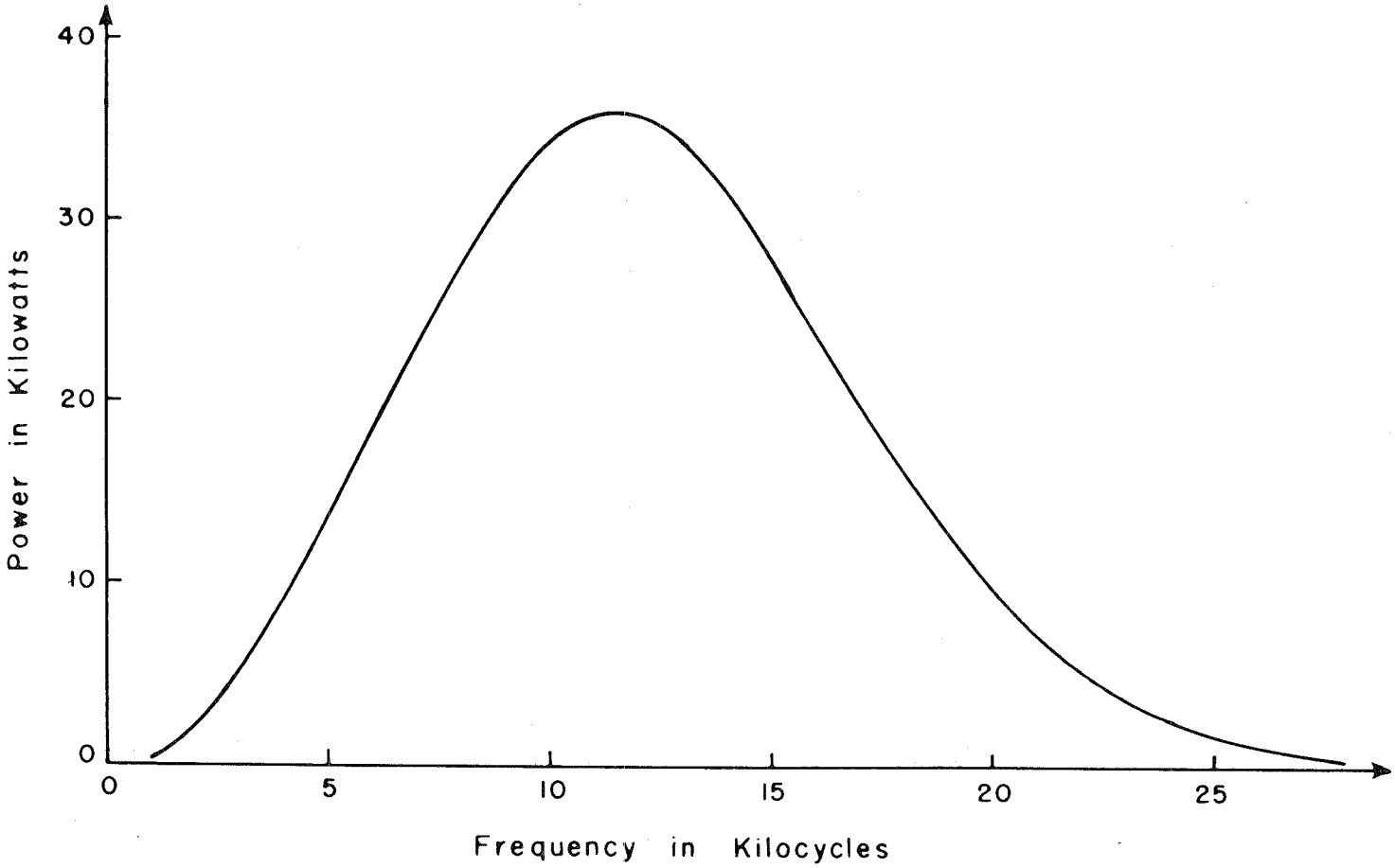

FIGURE IV-3. POWER REQUIREMENTS FOR GENERATING GYROELECTRIC-ECHOES USING A HALF-WAVE HORIZONTAL ANTENNA.

detected were usually 10 to 30 db below the direct signal (150 micro-volts per meter) with delays up to nearly one second. These results lent further encouragement to the possibility of generating echoes at lower frequencies.

There appeared no reason why an echo thus generated could not be reflected from the magnetic conjugate of its source of energy and return to the vicinity of its source as often observed for whistlers. However, it is evident that such a "round trip" echo would be subject to at least twice the attenuation as the "one way" echo since it must travel over a path length that is twice as long. Consequently, a round trip echo from NSS might be attenuated between 20 and 60 db below the signal recorded at Cape Horn. (This indicates that the received signal strength would probably lie between 15 and .15 micro-volts per meter.)

If, on the other hand, the medium is assumed to be lossless, * then the change in signal strength would primarily be due to a reflection-transmission loss at the boundary of the ionosphere. These of course are the extreme cases and it is more likely that a combination of the two factors determine the final amplitude of the echo.

The theoretical problem of reflection and transmission at a gyro-electric boundary will now be considered in order to determine the relative losses encountered at such a boundary and to obtain an estimate of the field strength of the round trip echo.

---

* Here lossless means that the effects of collision between electrons can be neglected (see section III).

V. REFLECTION AND TRANSMISSION COEFFICIENTS AT A GYROELECTRIC BOUNDARY

The theoretical problem of reflection and transmission at the surface of a sharply bounded ionosphere has been presented in a number of ways (30, 31, 32, 33) with graphical results presented over a limited range of variable parameters. The complexity of this computation lies in the fact that the index of refraction of such a medium is in general a function of the angle of incidence of the impinging wave. This problem along with the computation of the reflection and transmission coefficients will now be discussed.

The ionosphere will again be represented by a homogeneous lossless gyroelectric medium which now occupies the positive z half space, while the negative z half space is a vacuum. A constant magnetic field, $\underline{B}_o$, makes an angle β with the vertical. The angle of incidence of an impinging plane wave is θ_i. The wave normals of the incident, reflected, and refracted waves are given by $\underline{n}_i$, $\underline{n}_r$, and $\underline{n}_1$, $\underline{n}_2$, respectively. The geometry used is shown in figure V-1.

In general, there will be two waves present in the gyroelectric medium because of its anisotropic properties. The reflected wave will usually consist of an elliptically polarized wave even though the incident wave may be linearly polarized either parallel or perpendicular to the plane of incidence. The boundary conditions at $z = 0$ require that,

$$\theta_i = \theta_r \qquad (V-1)$$

and,

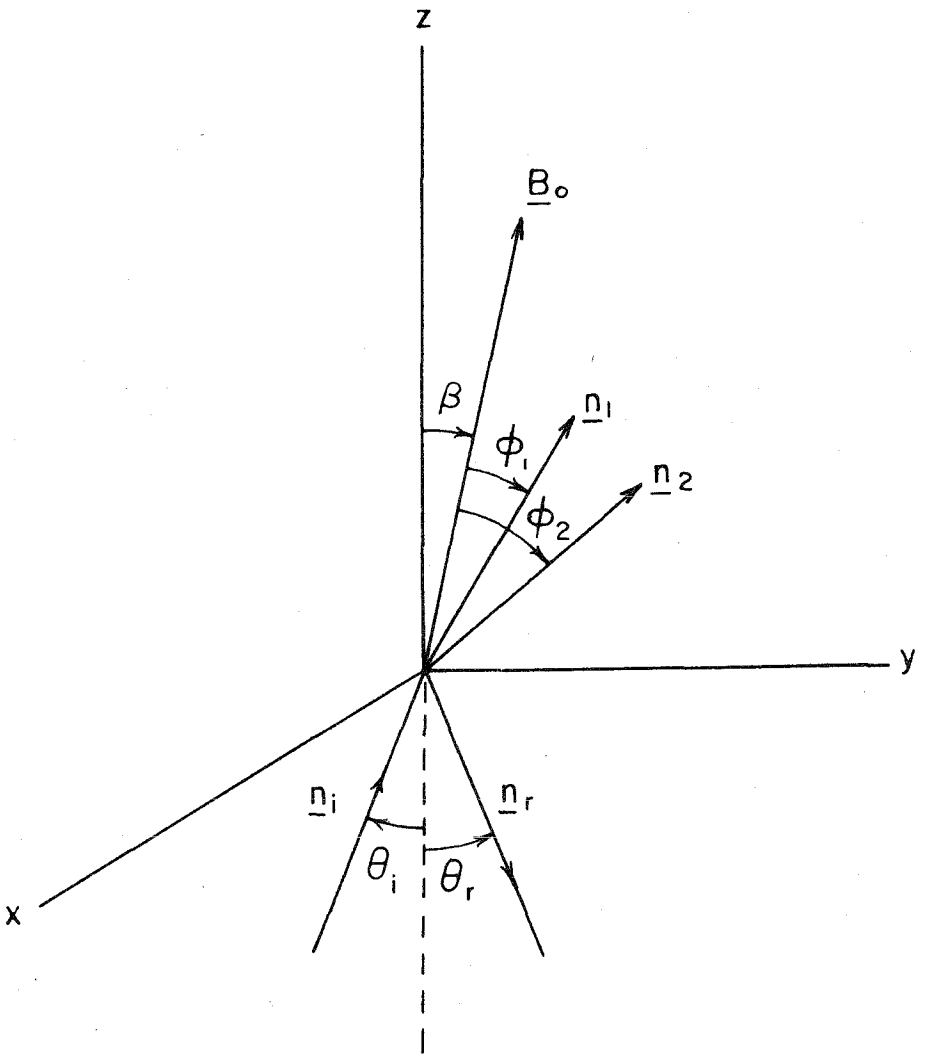

FIGURE V-1. COORDINATE SYSTEM SHOWING THE RELATION BETWEEN INCIDENT, REFLECTED, AND REFRACTED PLANE WAVES AT A GYROELECTRIC BOUNDARY.

$$\sin\theta_i = M_1(\phi_1)\sin(\beta+\phi_1) = M_2(\phi_2)\sin(\beta+\phi_2) \qquad (V\text{-}2)$$

where $M_1(\phi_1)$ and $M_2(\phi_2)$ are the indices of refraction as determined by equation III-12.

For angles of incidence other than $\theta_i = 0$, M_1 and M_2 must be real and greater than or equal to 1 if propagation is to take place in the gyroelectric medium. If, however, $\theta = 0$, then $\beta = -\phi$ so that the values of M are determined from equation III-12 directly, the results of which have been presented in figures III-2a through III-2f. For this case, all values of M are permitted but propagation takes place only for $M > 0$.

Assuming that M can be determined for any θ (by combining equations III-12 and V-2), it only remains to consider the nature of the polarization of the incident electric field. Since any plane wave can be resolved into two components, one in which the electric vector lies in the plane of incidence (waves of the electric type) and one in which the magnetic vector lies in the plane of incidence (waves of the magnetic type), these two cases will be considered separately.

Incident Waves of the Magnetic Type

The incident electric field is represented by,

$$\underline{E} = \underline{e}_x E_m e^{i(\underline{k}_o \cdot \underline{r} - \omega t)} \qquad (V\text{-}3)$$

$$\underline{H} = \sqrt{\frac{\epsilon_v}{\mu_v}}\, E_m \left[\underline{e}_y \cos\theta_i - \underline{e}_z \sin\theta_i\right] e^{i(\underline{k}_o \cdot \underline{r} - \omega t)} \qquad (V\text{-}3.1)$$

with

$$\underline{k}_o \cdot \underline{r} = (\omega/c) \left|y\right| \sin \theta_i + (\omega/c) \left|z\right| \cos \theta_i \qquad \text{(V-3.2)}$$

Because of the properties of the gyroelectric medium, the reflected fields (see above) generally consist of magnetic-type and electric-type waves, and are represented respectively by the subscripts mm and me . These are,

$$\underline{E}_{mm} = \underline{e}_x R_{mm} E_m e^{i(\underline{k}_{or} \cdot \underline{r} - \omega t)} \qquad \text{(V-4)}$$

$$\underline{H}_{mm} = \sqrt{\frac{\varepsilon_v}{\mu_v}} R_{mm} E_m \left[- \underline{e}_y \cos \theta_r - \underline{e}_z \sin \theta_r \right] e^{i(\underline{k}_{or} \cdot \underline{r} - \omega t)} \qquad \text{(V-4.1)}$$

and,

$$\underline{E}_{me} = R_{me} E_m \left[\underline{e}_y \cos \theta_r + \underline{e}_z \sin \theta_r \right] e^{i(\underline{k}_{or} \cdot \underline{r} - \omega t)} \qquad \text{(V-5)}$$

$$\underline{H}_{me} = \sqrt{\frac{\varepsilon_v}{\mu_v}} \left[\underline{e}_x R_{me} E_m \right] e^{i(\underline{k}_{or} \cdot \underline{r} - \omega t)} \qquad \text{(V-5.1)}$$

with

$$\underline{k}_{or} \cdot \underline{r} = (\omega/c) \left|y\right| \sin \theta_r - (\omega/c) \left|z\right| \cos \theta_r \qquad \text{(V-5.2)}$$

(R_{mm} and R_{me} are the reflection coefficients of the reflected wave and are sometimes given as $\perp R_\perp$ and $\parallel R_\parallel$ respectively.)

The refracted fields propagate in the $\underline{n}_1$ and $\underline{n}_2$ directions and are given by,

$$\underline{E}_{1,2} = \left[\underline{e}_x E_{x_{1,2}} + \underline{e}_y E_{y_{1,2}} + \underline{e}_z E_{z_{1,2}} \right] e^{i(\underline{k}_{1,2} \cdot \underline{r} - \omega t)} \qquad \text{(V-6)}$$

and

$$\underline{H}_{1,2} = \sqrt{\frac{\varepsilon_v}{\mu_v}}\, M_{1,2}\Big\{ \underline{e}_x\Big[E_{z_{1,2}} \sin(\beta+\phi_{1,2}) - E_{y_{1,2}} \cos(\beta+\phi_{1,2})\Big] + \underline{e}_y\Big[E_{x_{1,2}} \cos(\beta+\phi_{1,2})\Big] + \underline{e}_z\Big[-E_{x_{1,2}} \sin(\beta+\phi_{1,2})\Big]\Big\} e^{i(\underline{k}_{1,2}\cdot\underline{r}-\omega t)} \tag{V-6.1}$$

with,

$$\underline{k}_{1,2}\cdot\underline{r} = (\omega/c)\, y\, M_{1,2} \sin(\beta+\phi_{1,2}) + (\omega/c)\, z\, M_{1,2} \cos(\beta+\phi_{1,2}) \tag{V-6.2}$$

Two of the above components (E_x, E_y, or E_y, E_z, etc.) can now be expressed in terms of the third by utilizing equation III-11. However, equation III-11 refers to a coordinate system with $\underline{B}_o$ along the z axis and therefore the components in this system must be referred to the above coordinate system. This is readily accomplished by the following transformation,

$$\begin{bmatrix} E_{ox} \\ E_{oy} \\ E_{oz} \end{bmatrix} = \begin{bmatrix} 1 & 0 & 0 \\ 0 & \cos\beta & -\sin\beta \\ 0 & \sin\beta & \cos\beta \end{bmatrix} \begin{bmatrix} E_x \\ E_y \\ E_z \end{bmatrix} \tag{V-7}$$

Substituting the right hand side of this equation for the second matrix in equation III-11, and combining terms, gives the following relation,

$$\begin{bmatrix} 1 - \left(\frac{\varepsilon_1+\varepsilon_2}{2M^2}\right) & i\cos\beta\left(\frac{\varepsilon_2-\varepsilon_1}{2M^2}\right) & -i\sin\beta\left(\frac{\varepsilon_2-\varepsilon_1}{2M^2}\right) \\ -i\left(\frac{\varepsilon_2-\varepsilon_1}{2M^2}\right) & \cos\beta\left[\cos^2\phi - \left(\frac{\varepsilon_1+\varepsilon_2}{2M^2}\right)\right] - \cos\phi\sin\phi\sin\beta & -\sin\beta\left[\cos^2\phi - \left(\frac{\varepsilon_2+\varepsilon_1}{2M^2}\right)\right] - \cos\phi\sin\phi\sin\beta \\ 0 & \sin\beta\left(\sin^2\phi - \frac{\varepsilon_3}{M^2}\right) - \sin\phi\cos\phi\cos\beta & \sin\beta\sin\phi\cos\phi + \cos\beta\left(\sin^2\phi - \frac{\varepsilon_3}{M^2}\right) \end{bmatrix} \begin{bmatrix} E_x \\ E_y \\ E_z \end{bmatrix} = 0 \qquad (V\text{-}8)$$

Equation V-8 now permits the determination of E_y/E_x and E_z/E_x. These ratios are,

$$E_y/E_x = i r_{yx},\ r_{yx} = \frac{\left[2M^2 - (\varepsilon_1+\varepsilon_2)\right]}{(\varepsilon_2-\varepsilon_1)(M^2\sin^2\phi - \varepsilon_3)}\left[M^2\sin\phi\sin(\beta+\phi) - \varepsilon_3\cos\beta\right] \qquad (V\text{-}9)$$

and,

$$E_z/E_x = i r_{zx},\ r_{zx} = \frac{\left[2M^2 - (\varepsilon_1+\varepsilon_2)\right]}{(\varepsilon_2-\varepsilon_1)(M^2\sin^2\phi - \varepsilon_3)}\left[M^2\sin\phi\cos(\beta+\phi) + \varepsilon_3\sin\beta\right] \qquad (V\text{-}10)$$

After substituting these values in equations V-6 and V-6.1, and letting,

$$E_{x_{1,2}} = T_{m_{1,2}} E_m \qquad (V\text{-}11)$$

the boundary conditions at $z = 0$ for the continuity of tangential $\underline{E}$ and $\underline{H}$ reduce to the following set of simultaneous equations:

$$E_x: \quad 1 + R_{mm} = T_{m_1} + T_{m_2} \tag{V-12}$$

$$E_y: \quad R_{me} \cos\theta_r = i r_{yx_1} T_{m_1} + i r_{yx_2} T_{m_2} \tag{V-12.1}$$

$$H_x: \quad R_{me} = i M_1 T_{m_1}\left[r_{zx_1}\sin(\beta+\phi_1) - r_{yx_1}\cos(\beta+\phi_1)\right]$$

$$+ \; i M_2 T_{m_2}\left[r_{zx_2}\sin(\beta+\phi_2) - r_{yx_2}\cos(\beta+\phi_2)\right] \tag{V-12.2}$$

$$H_y: \quad \cos\theta_i - R_{mm}\cos\theta_r = M_1 T_{m_1}\cos(\beta+\phi_1) + M_2 T_{m_2}\cos(\beta+\phi_2) \tag{V-12.3}$$

Recognizing that,

$$r_{zx}\sin(\beta+\phi) - r_{yx}\cos(\beta+\phi) = \frac{2M^2 - (\varepsilon_1 - \varepsilon_2)}{(\varepsilon_2 - \varepsilon_1)(M^2\sin^2\phi - \varepsilon_3)}(\varepsilon_3\cos\phi) \equiv \rho(M,\phi) \tag{V-13}$$

permits combining the above equations into the following representation:

$$\begin{bmatrix} -1 & 0 & 1 & 1 \\ 0 & -\cos\theta_r & i r_{yx_1} & i r_{yx_2} \\ 0 & -1 & i M_1 \rho_1 & i M_2 \rho_2 \\ \cos\theta_r & 0 & M_1\cos(\beta+\phi_1) & M_2\cos(\beta+\phi_2) \end{bmatrix} \begin{bmatrix} R_{mm} \\ R_{me} \\ T_{m_1} \\ T_{m_2} \end{bmatrix} = \begin{bmatrix} 1 \\ 0 \\ 0 \\ \cos\theta_i \end{bmatrix} \tag{V-14}$$

The complexity of the above equations lies in the manner in which the coefficients vary as a function of the angle of incidence.

A corresponding equation can be derived for waves of the electric type. Using the expressions for the fields given in appendix D, the simultaneous equations resulting from the matching of tangential $\underline{E}$ and $\underline{H}$ are,

$$\begin{bmatrix} -1 & 0 & i M_1 \rho_1 & i M_2 \rho_2 \\ 0 & \cos\theta & M_1 \cos(\beta+\phi_1) & M_2 \cos(\beta+\phi_2) \\ 0 & -1 & 1 & 1 \\ \cos\theta & 0 & -i\, r_{yx_1} & -i\, r_{yx_2} \end{bmatrix} \begin{bmatrix} R_{ee} \\ R_{em} \\ T_{e_1} \\ T_{e_2} \end{bmatrix} = \begin{bmatrix} 1 \\ 0 \\ 0 \\ \cos\theta \end{bmatrix} \qquad \text{(V-15)}$$

For the present, attention will be confined to waves of the magnetic type since these most nearly approximate the fields radiated by a horizontal antenna. Considering the case of vertical incidence only permits calculation of the reflection and transmission coefficients more readily. From this calculation, it is possible to predict the amplitude of the electric field that propagates in the gyroelectric medium.

When $\theta_i = \theta_r = 0$, equation V-14 reduces to,

$$\begin{bmatrix} -1 & 0 & 1 & 1 \\ 0 & -1 & i\, r_{yx_1} & i\, r_{yx_2} \\ 0 & -1 & -i M_1 r_{yx_1} & -i M_2 r_{yx_2} \\ 1 & 0 & M_1 & M_2 \end{bmatrix} \begin{bmatrix} R_{mm} \\ R_{me} \\ T_{m_1} \\ T_{m_2} \end{bmatrix} = \begin{bmatrix} 1 \\ 0 \\ 0 \\ 1 \end{bmatrix} \qquad \text{(V-16)}$$

and

$$r_{yx} = \frac{\left[(\varepsilon_1 + \varepsilon_2) - 2M^2\right]}{(\varepsilon_2 - \varepsilon_1)} \frac{(\varepsilon_3 \cos\beta)}{(M^2 \sin^2\beta - \varepsilon_3)} \qquad \text{(V-16.1)}$$

Since $\beta = -\phi$ for the above case, the values of M^2 can be taken from figures III-2a through III-2f. A further degree of simplification is obtained if it is now assumed that $\beta = 0$. For this case, M^2 assumes the values ε_1 and ε_2. (This is the only case that $M^2 < 1$ is an acceptable solution.)

The reflection and transmission coefficients now can be written explicitly and are,

$$R_{mm} = \frac{1 - M_1 M_2}{(1 + M_1)(1 + M_2)} \qquad \text{(V-17)}$$

$$R_{me} = \frac{i\ (M_1 - M_2)}{(1 + M_1)(1 + M_2)} \qquad \text{(V-17.1)}$$

$$T_{m_1} = \frac{1}{(1 + M_1)} \qquad \text{(V-17.2)}$$

$$T_{m_2} = \frac{1}{(1 + M_2)} \qquad \text{(V-17.3)}$$

with,

$$M_1 = \sqrt{\varepsilon_1} \quad , \quad M_2 = \sqrt{\varepsilon_2} \qquad \text{(V-17.4)}$$

The first three of these coefficients have been evaluated as a function of the gyro- and plasma frequencies of the medium and are presented in figures V-2, V-3 and V-4. Since M_2 is imaginary for

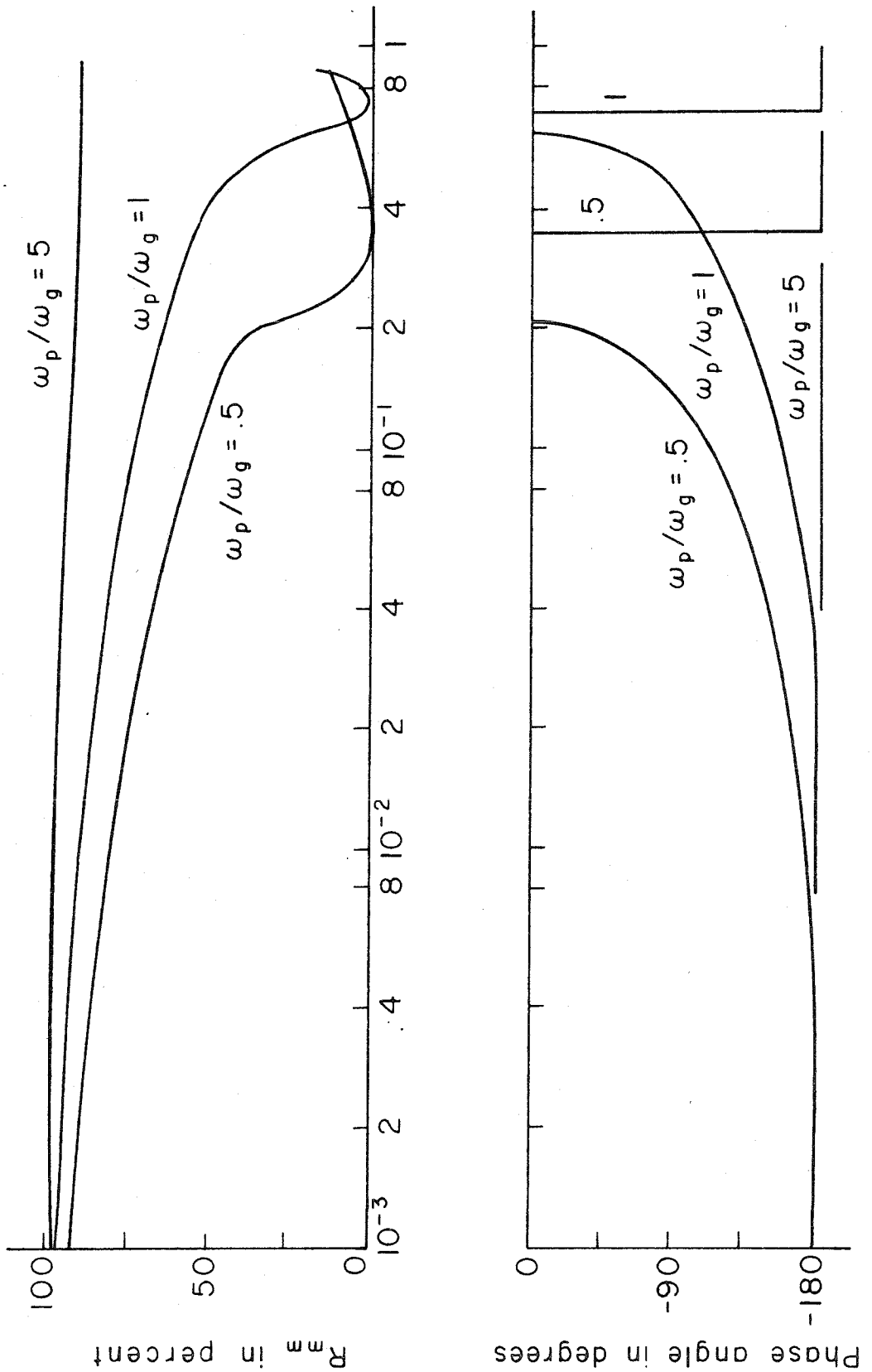

FIGURE V-2. COMPLEX REFLECTION COEFFICIENT AT A VACUUM-TO-GYROELECTRIC BOUNDARY (R_{mm}) AS A FUNCTION OF GYRO- AND PLASMA FREQUENCY.

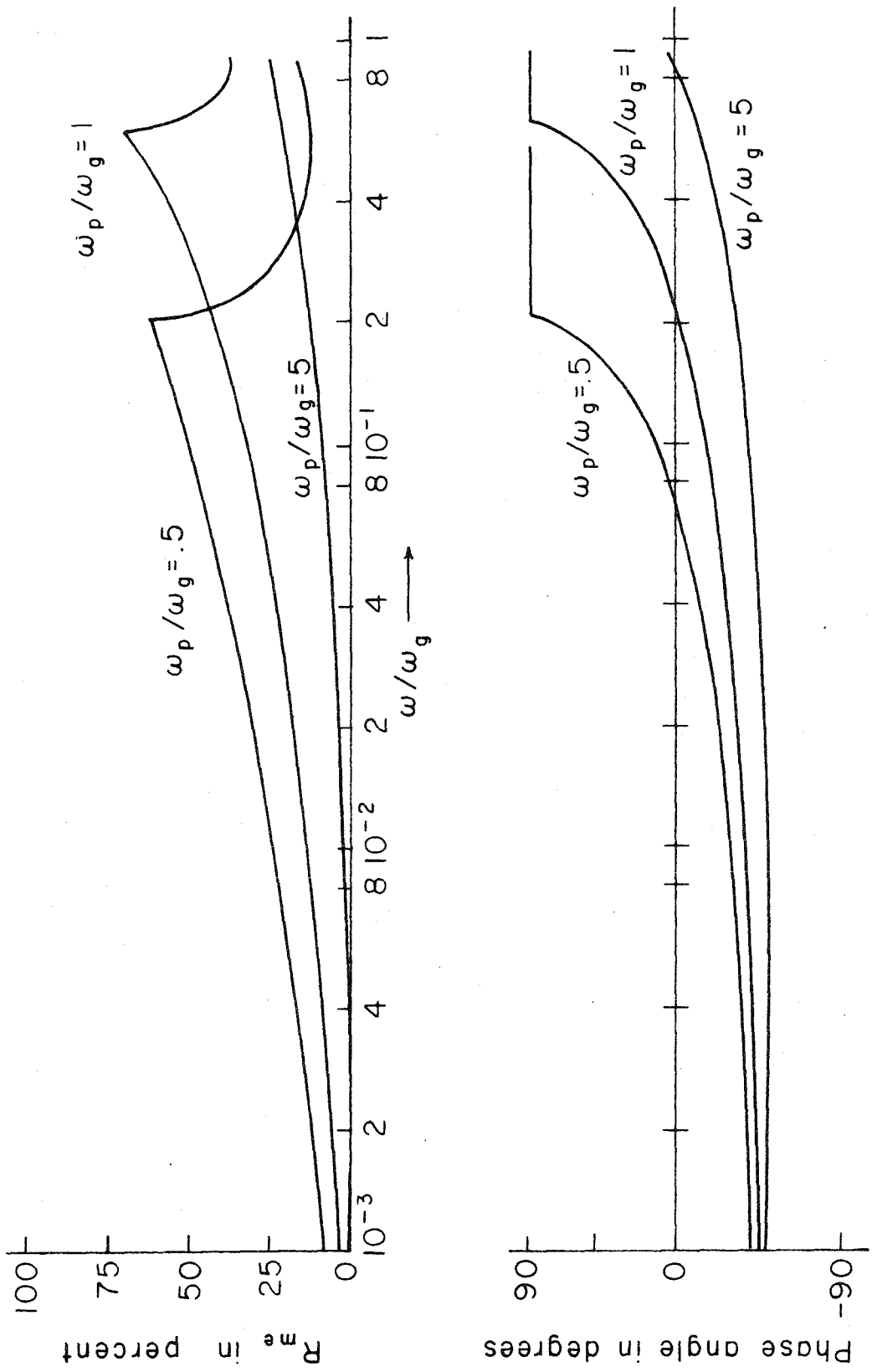

FIGURE V-3. COMPLEX REFLECTION COEFFICIENT AT A VACUUM-TO-GYROELECTRIC BOUNDARY (R_{me}) AS A FUNCTION OF GYRO- AND PLASMA FREQUENCY.

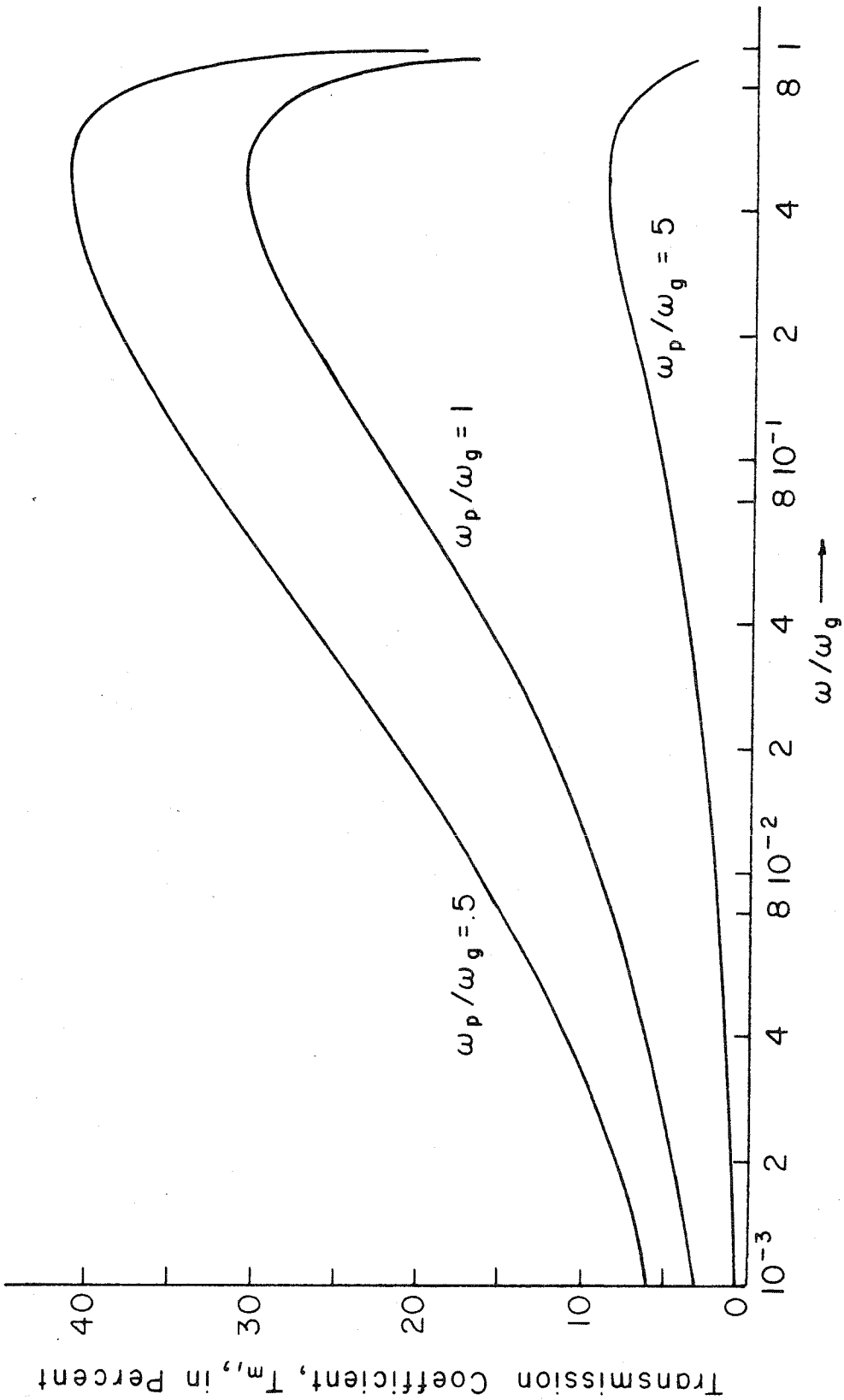

FIGURE V-4. TRANSMISSION COEFFICIENT AT A VACUUM-TO-GYROELECTRIC BOUNDARY (T_{m_1}) AS A FUNCTION OF GYRO- AND PLASMA FREQUENCY.

$\omega < -.5\,\omega_g + \sqrt{(.5\omega_g)^2 + \omega_p^2}$ (which generally covers the vlf range), values for T_{m_2} have not been presented. (This is the range in which only one of the two modes can propagate in the gyroelectric medium.) The transmitted wave corresponding to T_{m_1} is the wave responsible for exciting gyroelectric-echoes.

It therefore remains to determine the reflection and transmission coefficients of the wave corresponding to M_1 at the magnetic conjugate of its source. This is the inverse problem of the above, namely, transmission from a gyroelectric medium into a vacuum.

The incident, reflected and transmitted fields at this boundary are given respectively by,

$$\underline{E}_i = T_{m_1} E_m \left[\underline{e}_x - i\underline{e}_y\right] e^{i(k_1 z - \omega t)} \qquad \text{(V-18)}$$

$$\underline{H}_i = \sqrt{\frac{\varepsilon_v}{\mu_v}}\, M_1\, T_{m_1} E_m \left[i\underline{e}_x + \underline{e}_y\right] e^{i(k_1 z - \omega t)} \qquad \text{(V-18.1)}$$

$$\underline{E}_r = R_1 T_{m_1} E_m \left[\underline{e}_x - i\underline{e}_y\right] e^{-i(k_1 z + \omega t)} + R_2 T_{m_1} E_m \left[\underline{e}_x + i\underline{e}_y\right] e^{-i(k_2 z + \omega t)} \qquad \text{(V-18.2)}$$

$$\underline{H}_r = \sqrt{\frac{\varepsilon_v}{\mu_v}}\, M_1 R_1 T_{m_1} E_m \left[-i\underline{e}_x - \underline{e}_y\right] e^{-i(k_1 z + \omega t)} + \sqrt{\frac{\varepsilon_v}{\mu_v}}\, M_2 R_2 T_{m_1} E_m \left[i\underline{e}_x - \underline{e}_y\right] e^{-i(k_2 z + \omega t)} \qquad \text{(V-18.3)}$$

$$\underline{E}_t = T_{m_1} E_m \left[T_{x_1}\underline{e}_x + T_{y_1}\underline{e}_y\right] e^{i(k_o z - \omega t)} \qquad \text{(V-18.4)}$$

$$\underline{H}_t = \sqrt{\frac{\varepsilon_v}{\mu_v}}\, T_{m_1} E_m \left[-T_{y_1}\underline{e}_x + T_{x_1}\underline{e}_y\right] e^{i(k_o z - \omega t)} \qquad \text{(V-18.5)}$$

Matching tangential $\underline{E}$ and $\underline{H}$ at the surface requires,

$$\begin{bmatrix} 1 & 1 & -1 & 0 \\ i & -i & 0 & 1 \\ iM_1 & -iM_2 & 0 & -1 \\ M_1 & M_2 & 1 & 0 \end{bmatrix} \begin{bmatrix} R_1 \\ R_2 \\ T_{x_1} \\ T_{y_1} \end{bmatrix} = \begin{bmatrix} -1 \\ -i \\ iM_1 \\ M_1 \end{bmatrix} \qquad \text{(V-19)}$$

The solutions to equation V-19 are,

$$R_1 = \frac{M_1 - 1}{M_1 + 1} \qquad \text{(V-20)}$$

$$R_2 = 0 \qquad \text{(V-20.1)}$$

$$T_{x_1} = \frac{2M_1}{1 + M_1} \qquad \text{(V-20.2)}$$

$$T_{y_1} = -i\, T_{x_1} \qquad \text{(V-20.3)}$$

(If the incident wave had been appropriate to M_2, then values for R and T above are obtained by interchanging the subscripts 1 and 2 and writing $-i$ for i.) The values for these coefficients as a function of the gyro- and plasma frequencies of the medium are presented in figure V-5.

If the original wave train is considered to be of sufficient duration such that the effects of multiple reflections and transmissions can be neglected, then the one way echo, received at the magnetic conjugate point, would be of amplitude $T_{m_1} T_{x_1}$ times the amplitude of the transmitted pulse and would be a wave that is circularly polarized. This

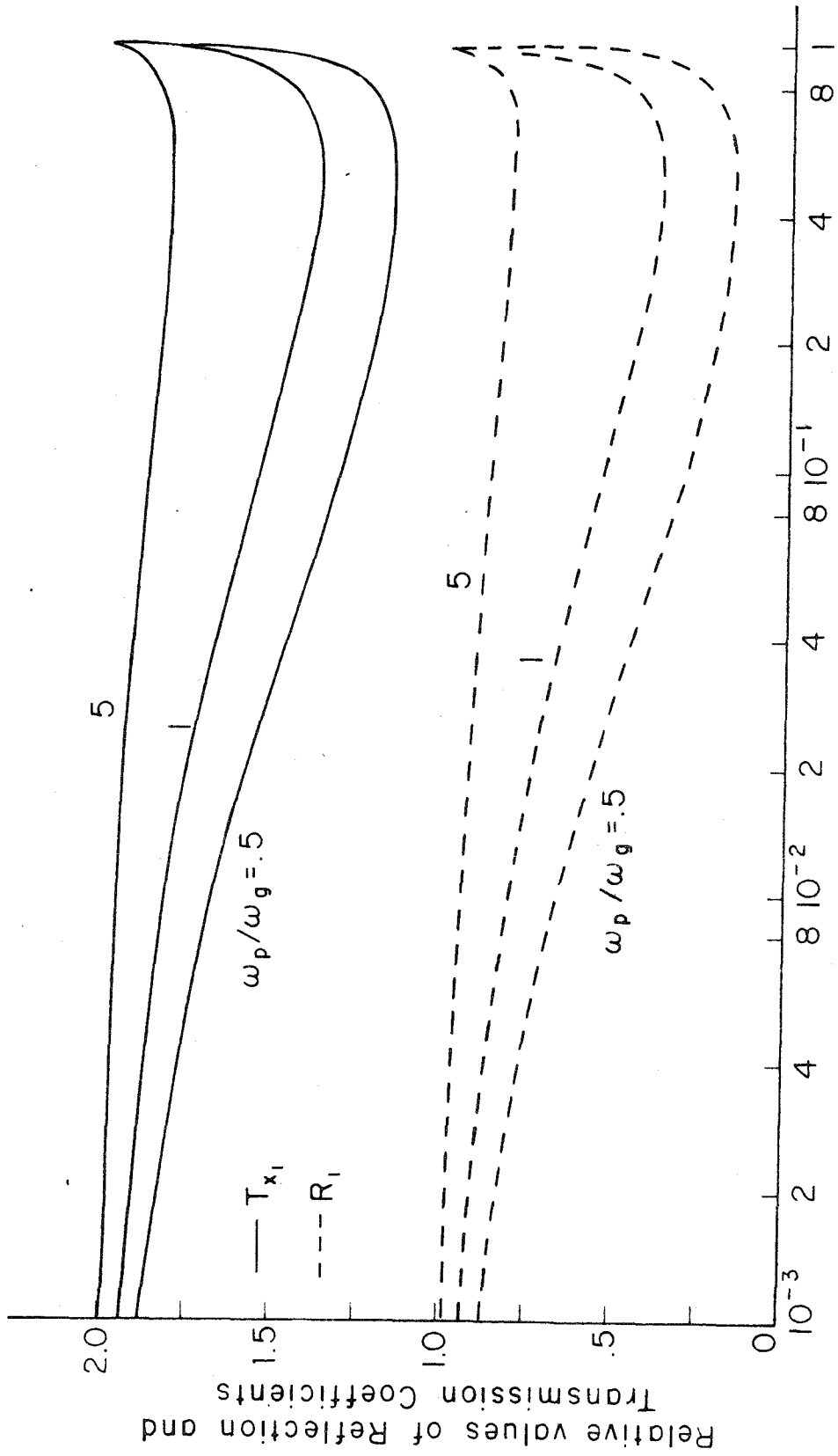

FIGURE V-5. REFLECTION AND TRANSMISSION COEFFICIENTS AT A GYROELECTRIC-TO-VACUUM BOUNDARY AS A FUNCTION OF GYRO- AND PLASMA FREQUENCY

product is shown in figure V-6, for ω_p/ω_g equal to one. It is seen from this figure that the amplitude of the electric field is approximately 0.20 (-14 db) of the initial amplitude at 15.5 kc and 0.15 (-16.5 db) of the initial amplitude at 8.4 kc, for a gyro-frequency of 1 Mc. This indicates that the reflection-transmission loss is probably greater than the path loss (in section IV it was stated that the echoes from NSS were 10 to 30 db below the direct received signal).

Figure V-6 also shows the relative value of a round trip echo due to reflection at a gyroelectric-to-vacuum boundary ($R_1 T_{m_1} T_{x_1}$). This product shows that the amplitude of the electric field is about 0.15 (-16.5 db) of the initial amplitude at 15.5 kc and 0.12 (-18.4 db) at 8.4 kc. The product $(T_{m_1} T_{x_1})^2$ is also plotted in order to estimate the amplitude of an echo that might be generated by reflection from the earth instead of the ionosphere.

The above results indicate that a round trip echo is most likely created by reflection from the earth. These results also indicate that a round trip echo is attenuated between 20 and 50 db as predicted in section IV.

The results of experimental attempts to excite gyroelectric-echoes along with data taken at near vertical incidence in the ground wave minimum will now be considered.

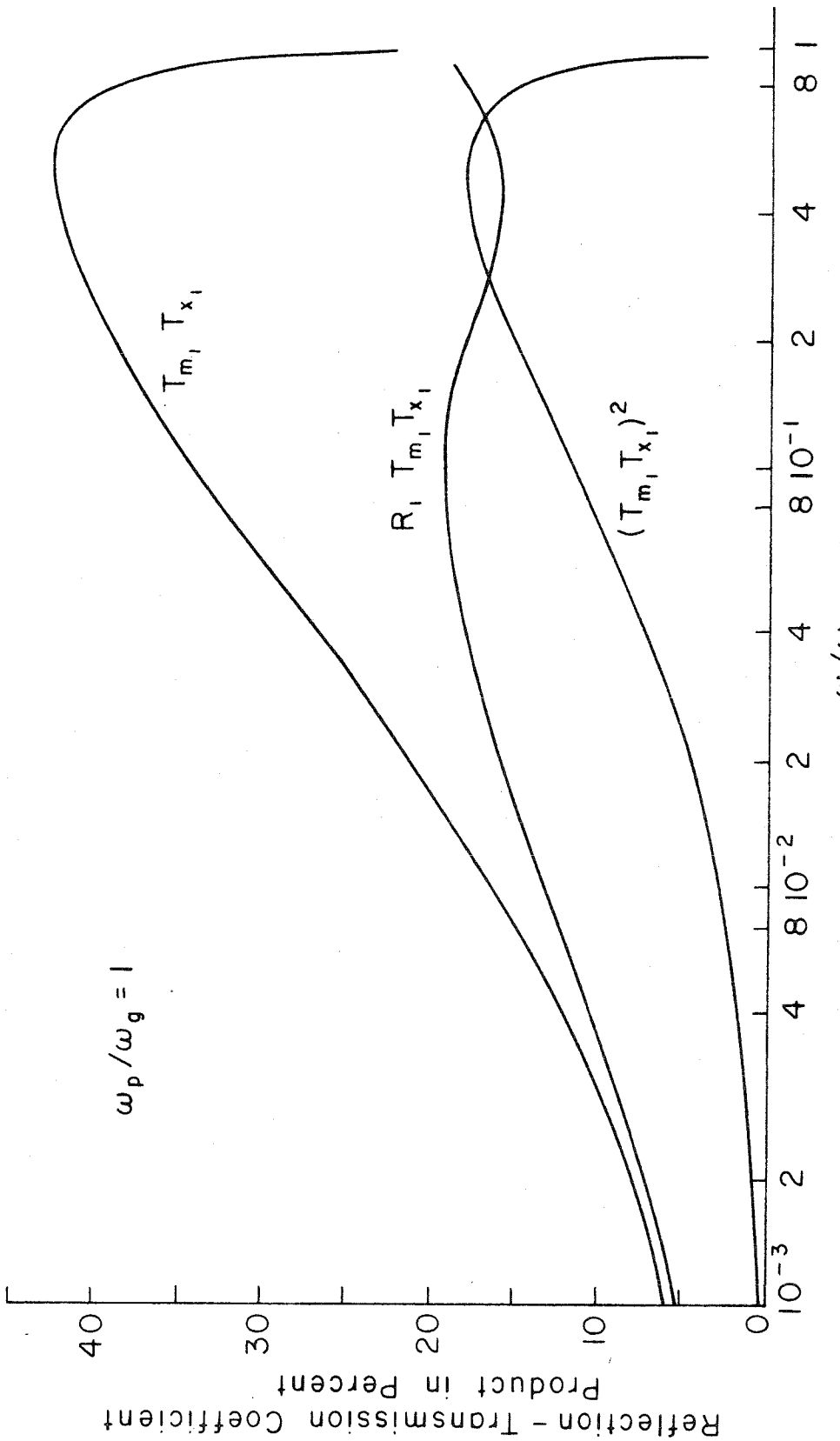

FIGURE V-6. REFLECTION-TRANSMISSION COEFFICIENT PRODUCT AS A FUNCTION OF GYRO- AND PLASMA FREQUENCY.

VI. EXPERIMENTAL OBSERVATIONS

With the completion of the 8.4 kc transmitting and receiving equipment (see section VII), a number of vertical incidence, long distance, and echo experiments were conducted. (A functional block diagram of the experimental system is shown in figure VI-1.) Initial experiments were conducted using a low power transmitter (200 watts) to determine the effectiveness of the tuned circuits in the power line and the sensitivity of the receiver. From these measurements, it was found that certain minor modifications in the receiver were necessary. Once these were made, tests using the 20 kw transmitter were conducted at a straight line distance of approximately 25 miles from the center of the antenna.

These tests were conducted primarily to locate the ground wave minimum of the transmitting antenna. However, because of the strong signal received over a wide range of azimuthal angle (measured with respect to the antenna), a true minimum could not be determined. This strong signal can be attributed to the fact that the ionosphere may be regarded as a good reflector for waves of very low frequencies (especially at vertical and near vertical incidence). Hence the received signal is the resultant of a strong, elliptically polarized sky wave, and a vertically polarized ground wave.

With the conclusion of these tests, permission was obtained from Reedley Junior College, Reedley, California, to locate the receiving equipment on the college campus. This site had the advantage of being far from roads and power lines and located approximately in the perpendicular bisector plane of the antenna. A detailed map showing the

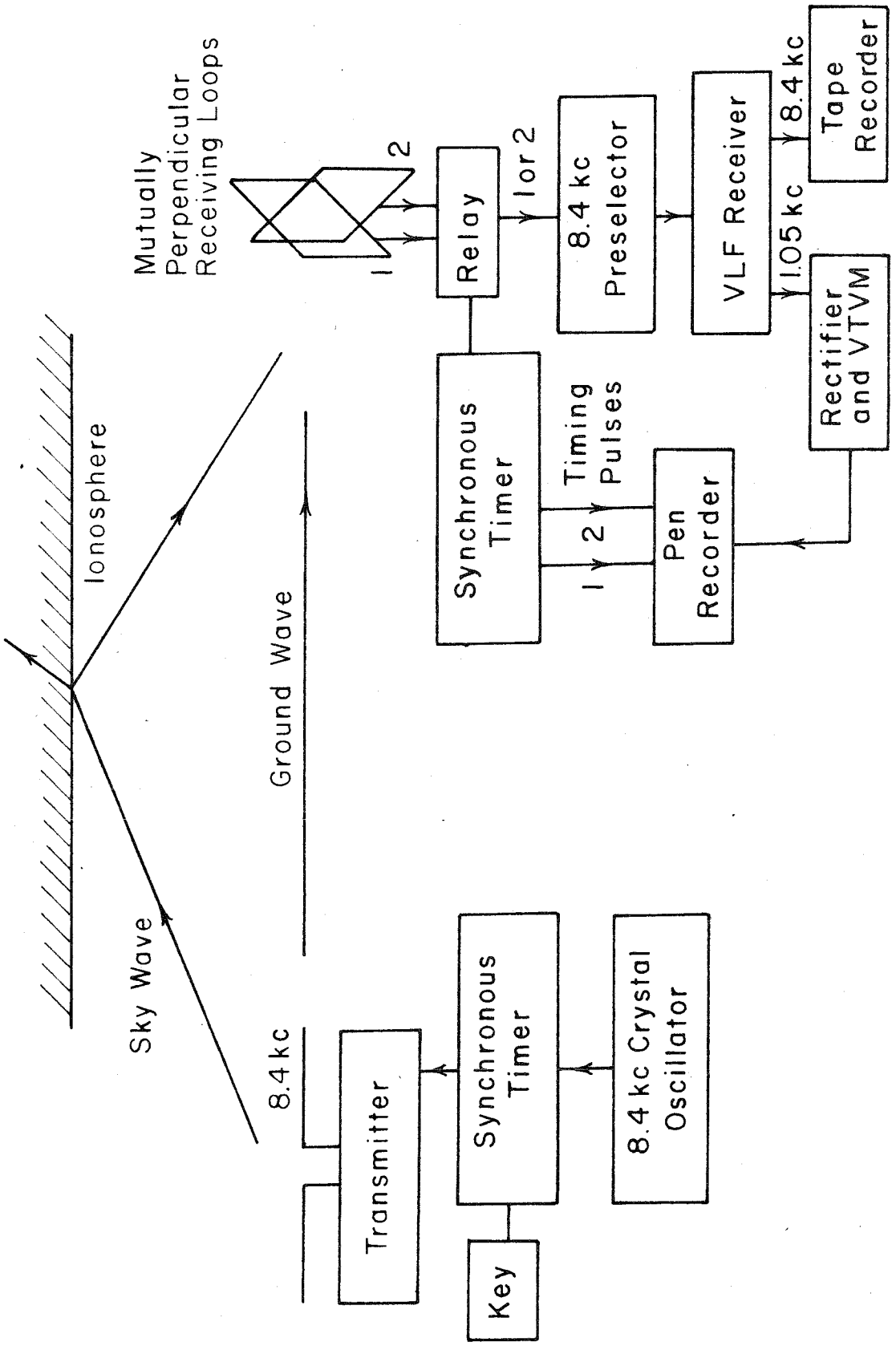

FIGURE VI-1. FUNCTIONAL BLOCK DIAGRAM OF 8.4 KC TRANSMITTING-RECEIVING SYSTEM.

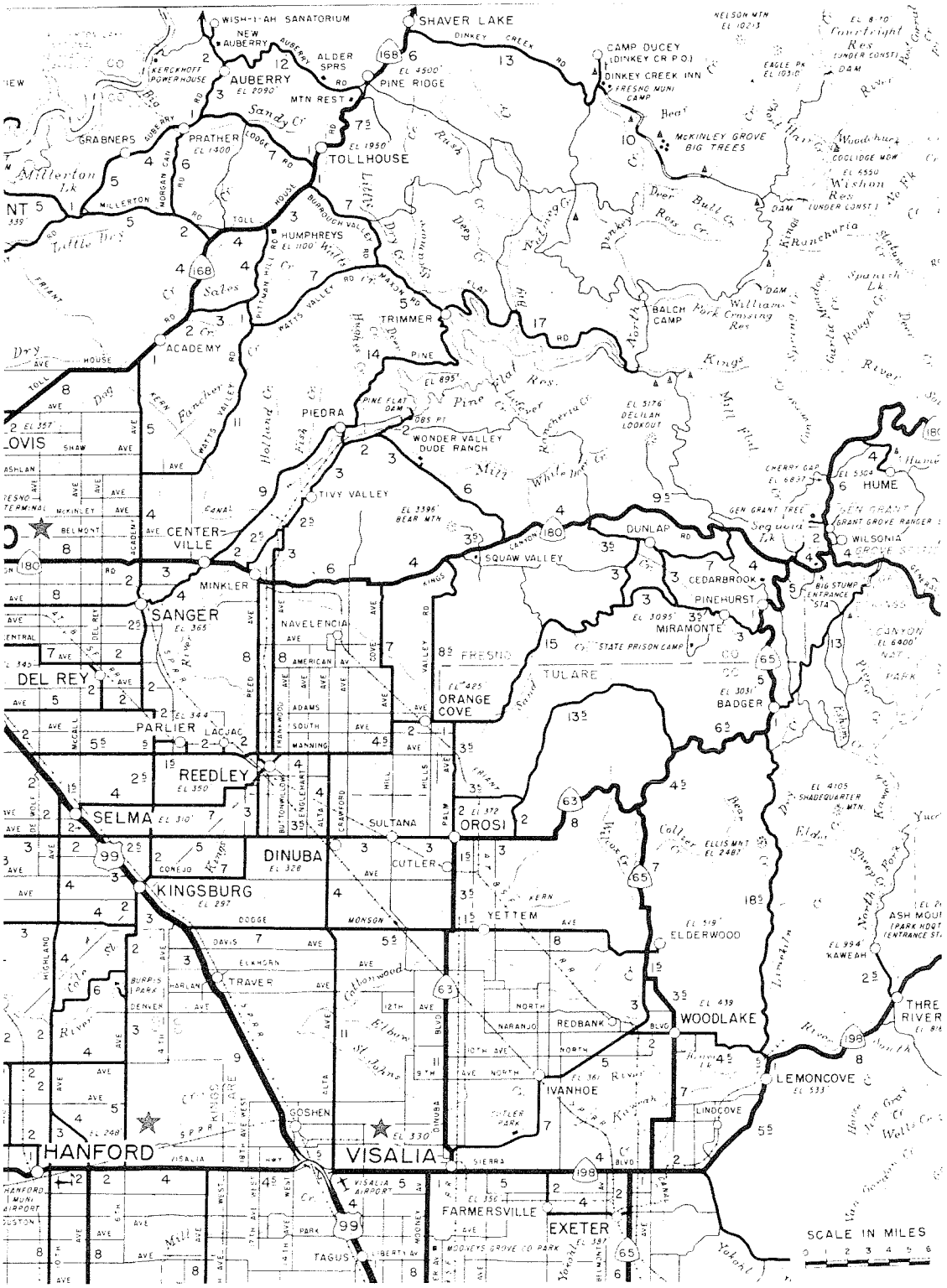

FIGURE VI-2. MAP OF SHAVER LAKE - REEDLEY AREA.

relative locations of the receiving site at Reedley and the transmitting site at Shaver Lake, is shown in figure VI-2.

The establishment of this location permitted the taking of vertical incidence amplitude records. (Assuming an average height of 80 km for the ionosphere, the angle of incidence appropriate to Reedley is 15°.) Two of these records are shown in figures VI-3a, 3b and VI-4a, 4b. Figure VI-5 is a representative portion of the record taken on 7 March 1959. In each case the records show a rapid decrease in amplitude beginning a half-hour before local sunrise and lasting until an hour after sunrise. This may be explained in terms of the formation of the lower regions of the ionosphere (D layer) and stratification of the F layer. As these layers begin forming, the ionosphere goes through a transition state during which time it becomes highly absorbing. Once this transition has been completed, the lower regions once again act as a reflector and the received signal increases in amplitude.

During the day the amplitude is subject to a slowly varying change with an occasional dip which may be due to a sudden ionospheric disturbance or sporadic E layer formation. From fifty to thirty minutes before local sunset, the records again indicate fading which is probably the inverse of the effect that takes place at sunrise.

After the evening transition was completed, the received signal was subject to more rapid variations in amplitude with an average value twice that of the daytime value. This erratic behavior of the received signal can be attributed to the fact that the nighttime signal is reflected

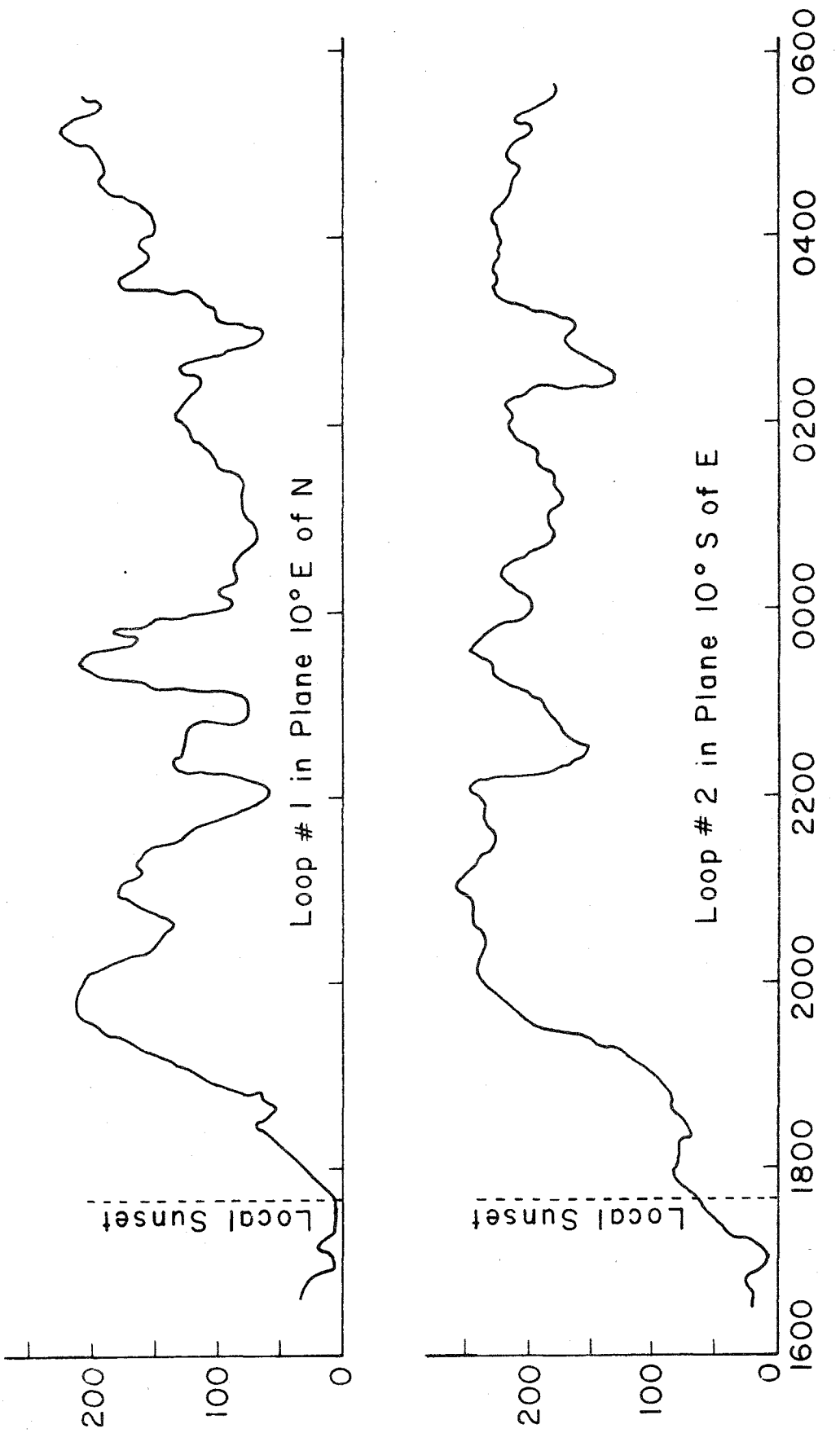

FIGURE VI-3a. AMPLITUDE OF 8.4 KC SIGNAL RECORDED AT REEDLEY, CALIFORNIA 20 - 21 FEBRUARY 1959 FROM TWO MUTUALLY PERPENDICULAR RECEIVING LOOPS.

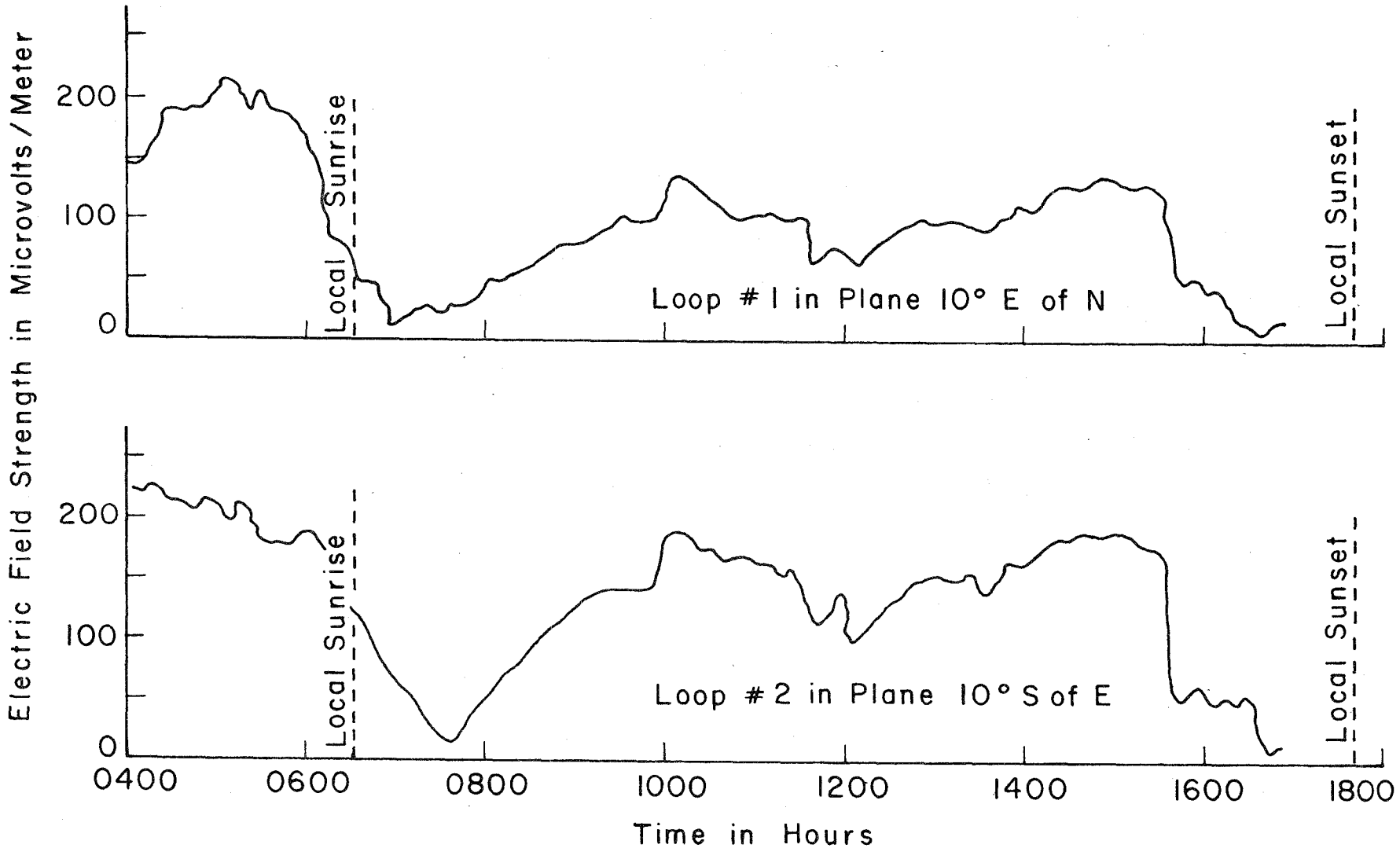

FIGURE VI-3b. AMPLITUDE OF 8.4 KC SIGNAL RECORDED AT REEDLEY, CALIFORNIA 20 - 21 FEBRUARY 1959 FROM TWO MUTUALLY PERPENDICULAR RECEIVING LOOPS.

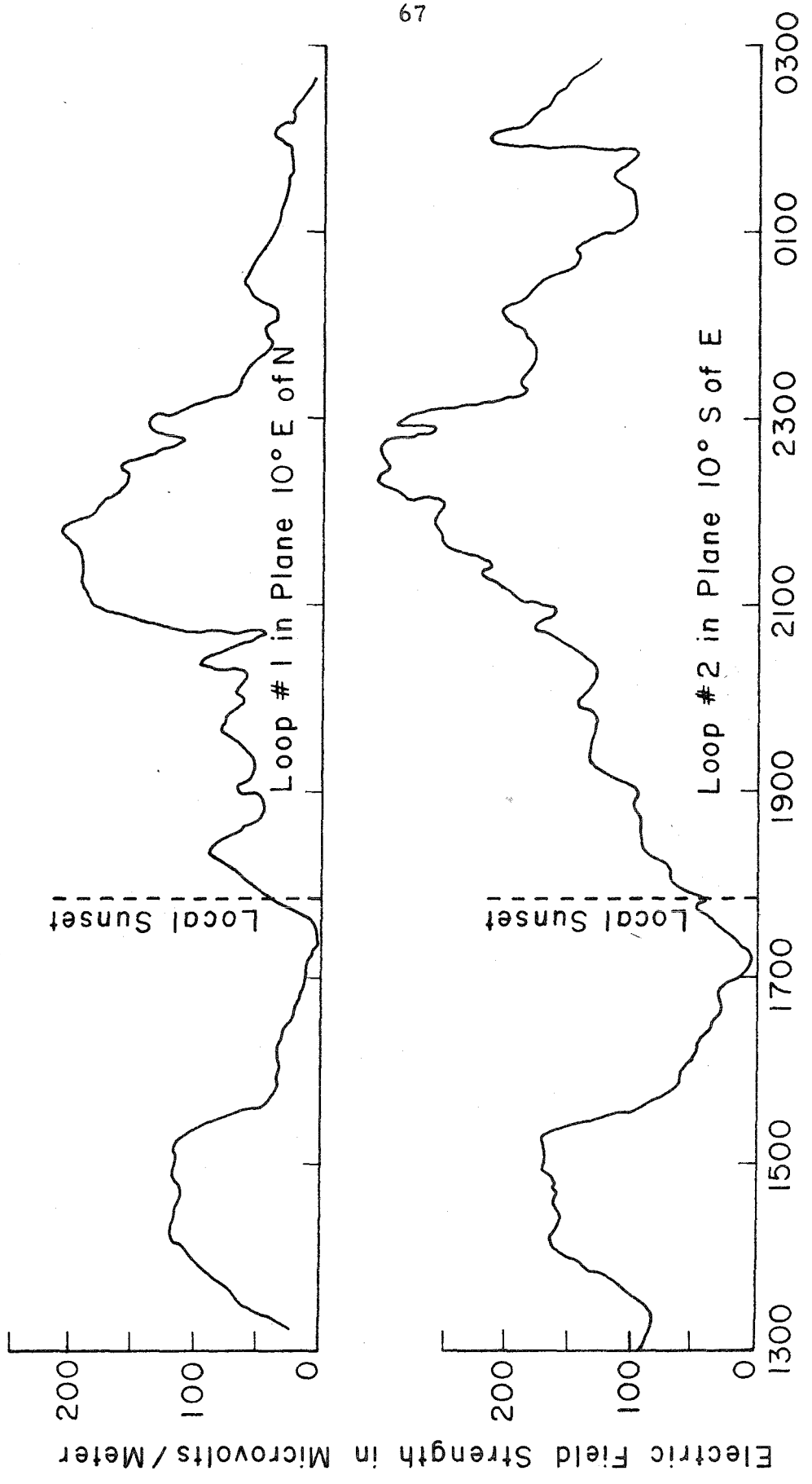

FIGURE VI-4a. AMPLITUDE OF 8.4 KC SIGNAL RECORDED AT REEDLEY, CALIFORNIA
6 - 7 MARCH 1959 FROM TWO MUTUALLY PERPENDICULAR RECEIVING LOOPS.

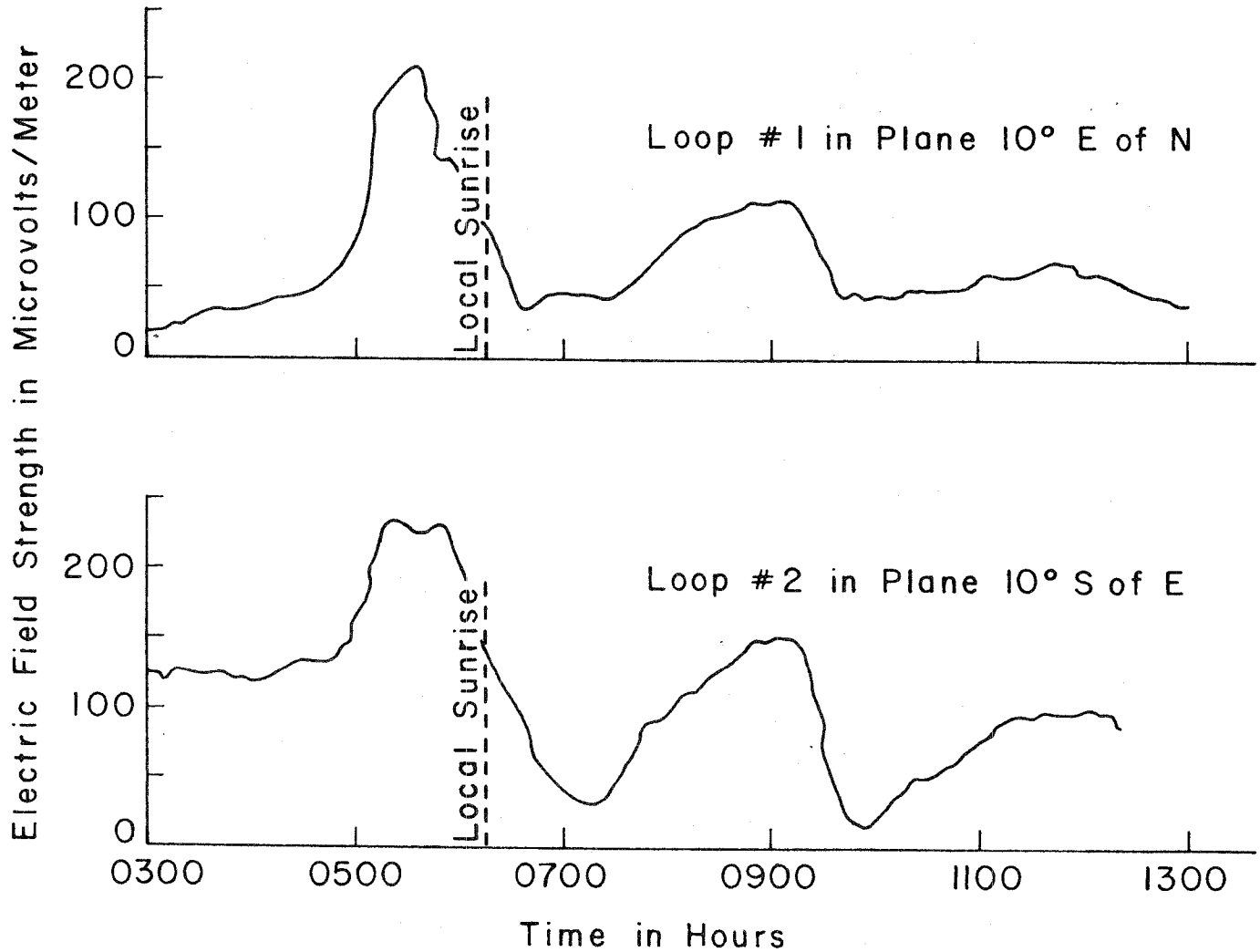

FIGURE VI-4b. AMPLITUDE OF 8.4 KC SIGNAL RECORDED AT REEDLEY, CALIFORNIA 6 - 7 MARCH 1959 FROM TWO MUTUALLY PERPENDICULAR RECEIVING LOOPS.

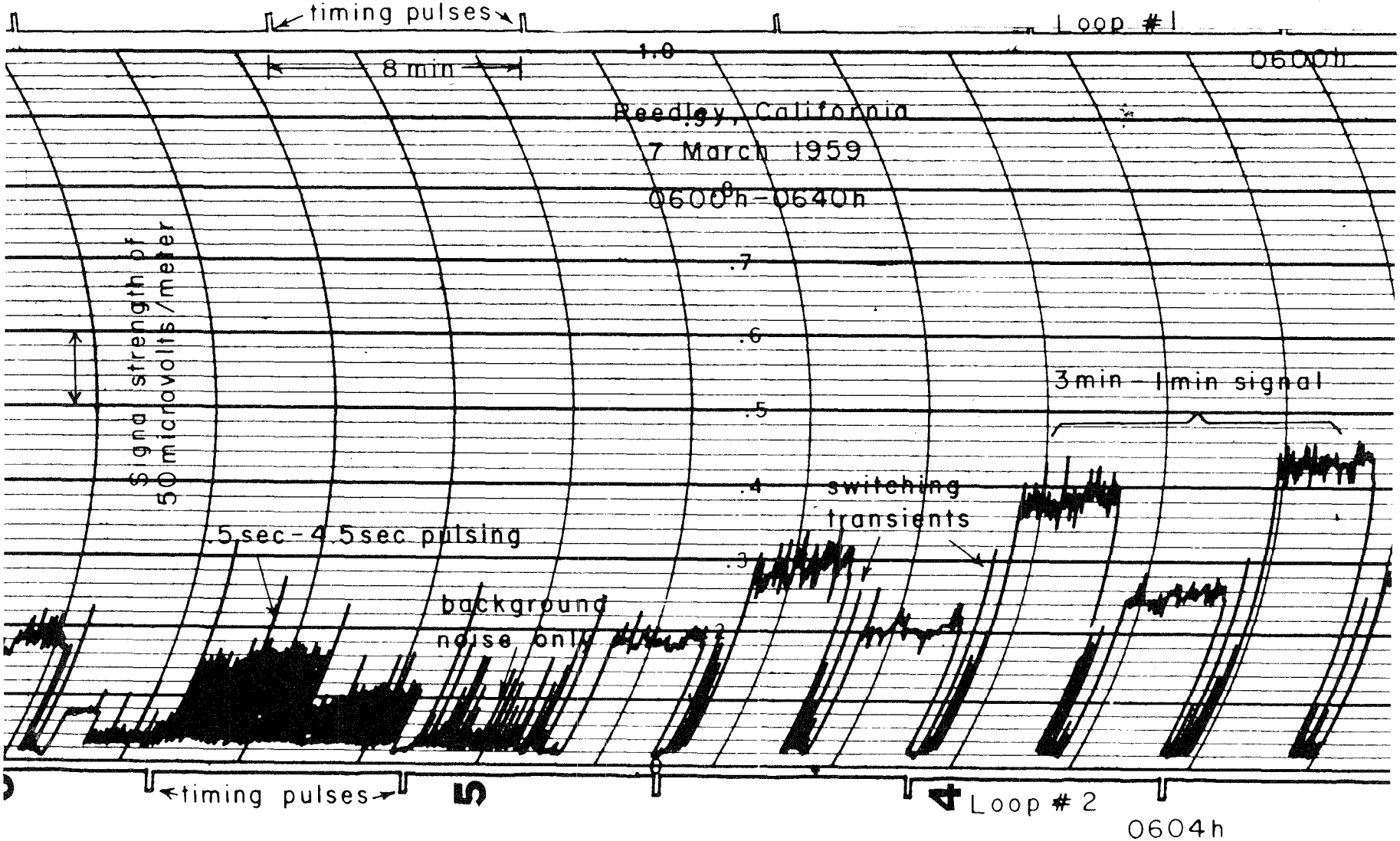

FIGURE VI-5. REPRESENTATIVE PORTION OF AMPLITUDE DATA RECORDED 7 MARCH 1959 REEDLEY, CALIFORNIA 0600 h - 0640 h .

primarily from the F region and therefore subject to the same erratic fluctuations that the F region undergoes at night (see section II).

An attempt to receive the 8.4 kc signal at Solvang, California (also in the ground wave minimum), was only partially successful. The presence of an extremely high level noise signal for several hours prevented the recording of amplitude data. However, it was possible to record the signal for a period of eight hours and this record is shown in figure VI-6. This data shows that the received signal reached its peak amplitude at 0200 h at a level which is approximately one-tenth of the peak levels recorded at Reedley. Evidence of morning and evening fading cannot be readily deduced from this record. The reason that the observed amplitude was so small might be attributed to the large angle of incidence (61°) required for a single reflection and also the fact that sunspot activity was very high during this period, thereby creating strong ionospheric disturbances.

Another record taken at Pasadena, figures VI-7a and 7b (azimuthal angle of 55° with respect to the antenna and appropriate angle of incidence of 65°), shows the presence of a strong ground or surface wave during the day, the amplitude of which remains relatively constant. Reference to figure III-3 shows that the theoretical amplitude of the ground wave at this angle is indeed of appreciable magnitude.

By orienting the loops in mutually perpendicular vertical planes, it was possible to receive the sky wave of the magnetic type (see section V) on one loop (loop No. 2) while receiving a combination of the ground wave and the sky wave of the electric type on the other loop (loop No. 1). Hence figures VI-7a and 7b show an increase in

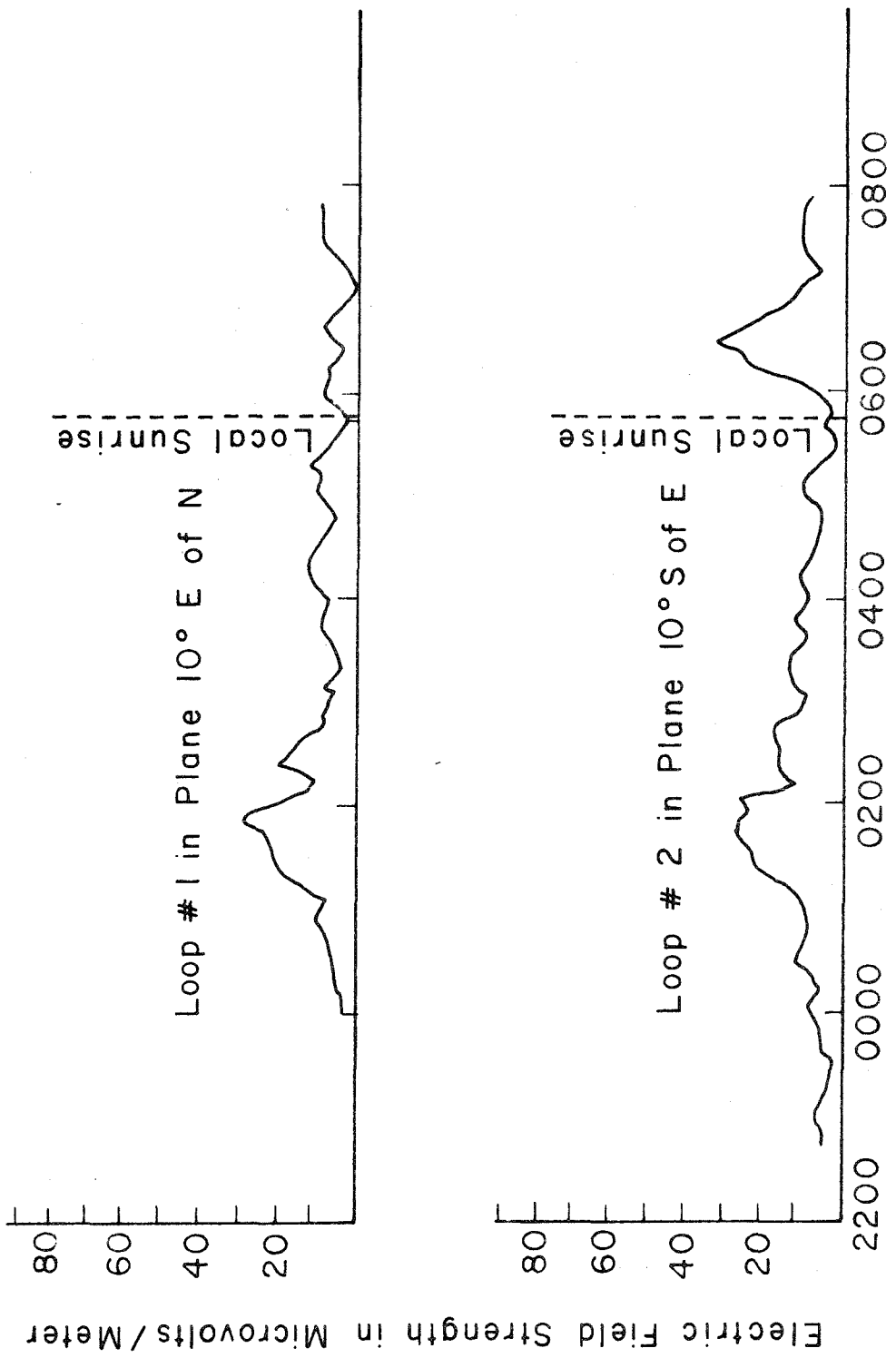

FIGURE VI-6. AMPLITUDE OF 8.4 KC SIGNAL RECORDED AT SOLVANG, CALIFORNIA 27 - 28 MARCH 1959 FROM TWO MUTUALLY PERPENDICULAR RECEIVING LOOPS.

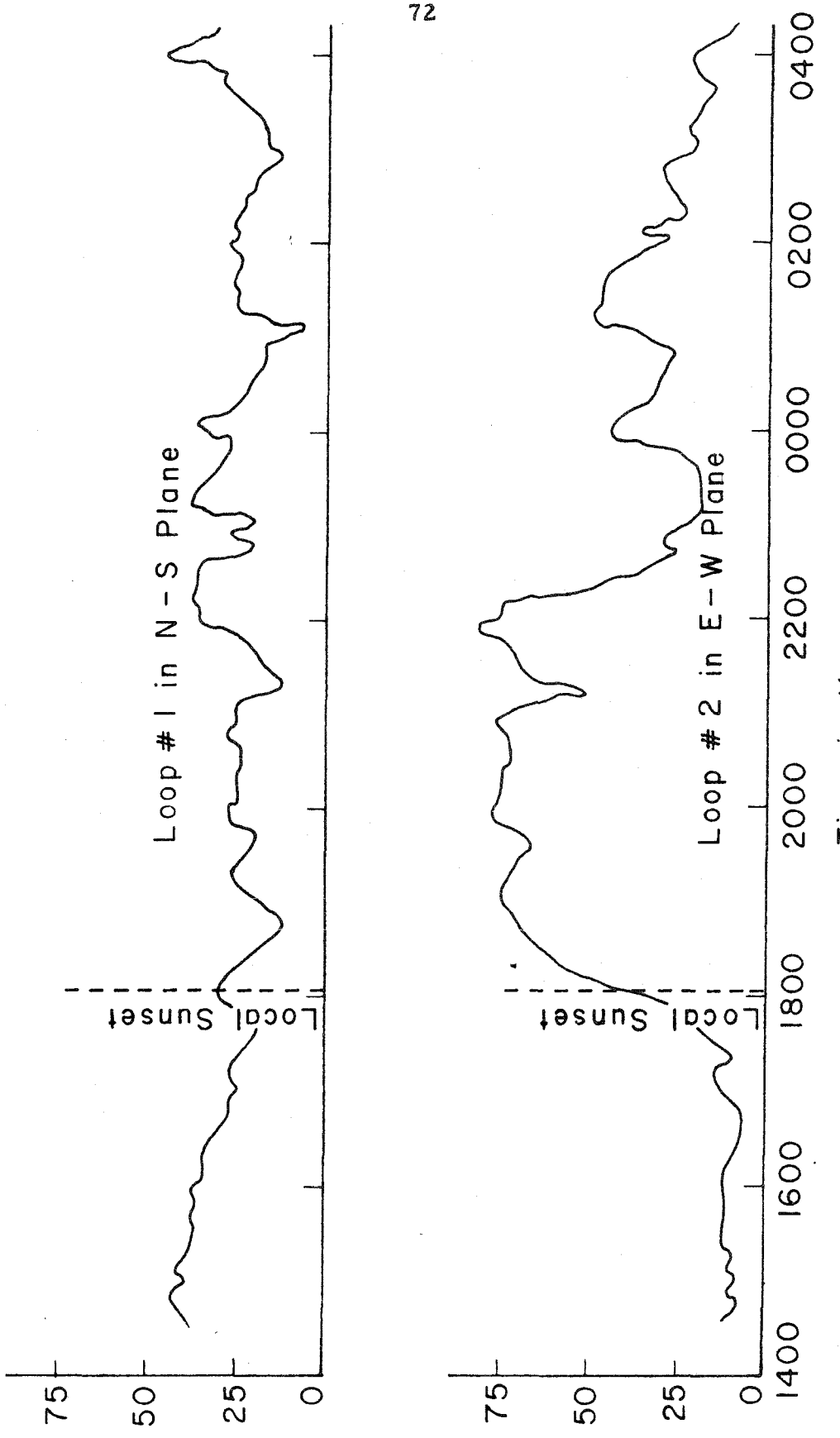

FIGURE VI-7a. AMPLITUDE OF 8.4 KC SIGNAL RECORDED AT PASADENA, CALIFORNIA
20 - 21 MARCH 1959 FROM TWO MUTUALLY PERPENDICULAR RECEIVING LOOPS.

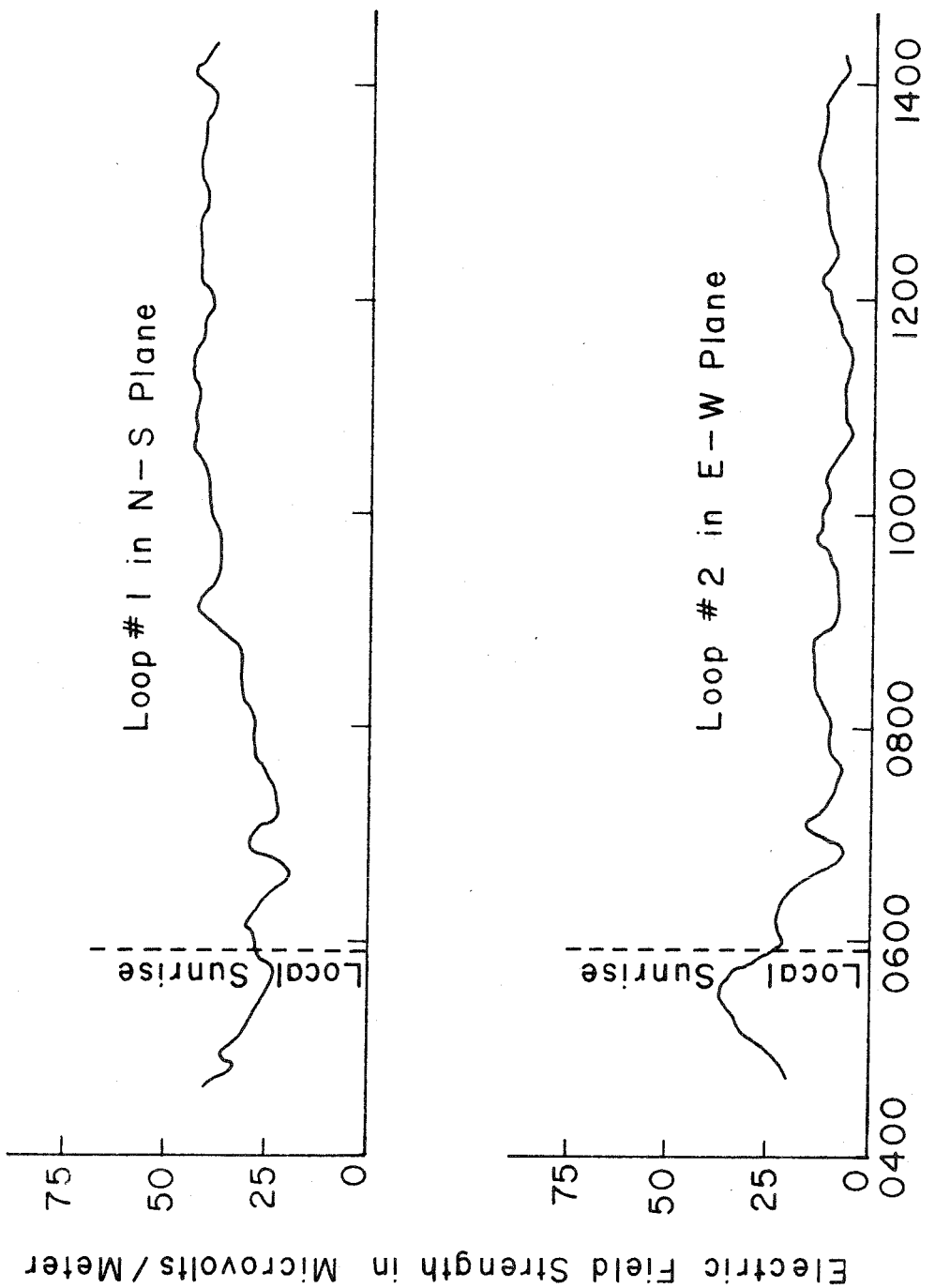

FIGURE VI-7b. AMPLITUDE OF 8.4 KC SIGNAL RECORDED AT PASADENA, CALIFORNIA 20 - 21 MARCH 1959 FROM TWO MUTUALLY PERPENDICULAR RECEIVING LOOPS.

the magnetic type sky wave during several hours of the evening along with appreciable interference taking place between the sky wave of the electric type and the ground wave field. (This effect is the well-known increase in long distance communication that is due to the better reflection properties of the nighttime ionosphere.)

During the time of the Pasadena measurements, J. A. Pierce of the Cruft Laboratory, Harvard University, was able to detect the 8.4 kc signal at Cambridge which is at a distance of approximately 4,200 km from the transmitter. His success in detecting this signal offers a good deal of support for the use of vlf as a reliable long distance communication link and possibly as a world-wide frequency standard.

The Stanford Radio Propagation Laboratory was also able to detect the 8.4 kc signal at this time, using a standard whistler receiver.

Besides the amplitude measurements taken at Reedley, Pasadena, and Solvang, California, (figure VI-8 shows the relative locations of these sites with respect to the antenna) attempts were made to generate gyroelectric echoes during a ten minute period of each hour. (The transmitter was automatically keyed as described in section VII.) A continuous tape recording of the output of the receiver was made at this time.

Thus far, examination of the tape recordings has failed to show the existence of a recognizable echo. This is most likely due to the fact that the full power capabilities of the transmitter could not be realized. (Figure IV-3 predicts a power requirement of 30 kw at 8.4 kc while the actual operating value was only 6 kw.) However, it

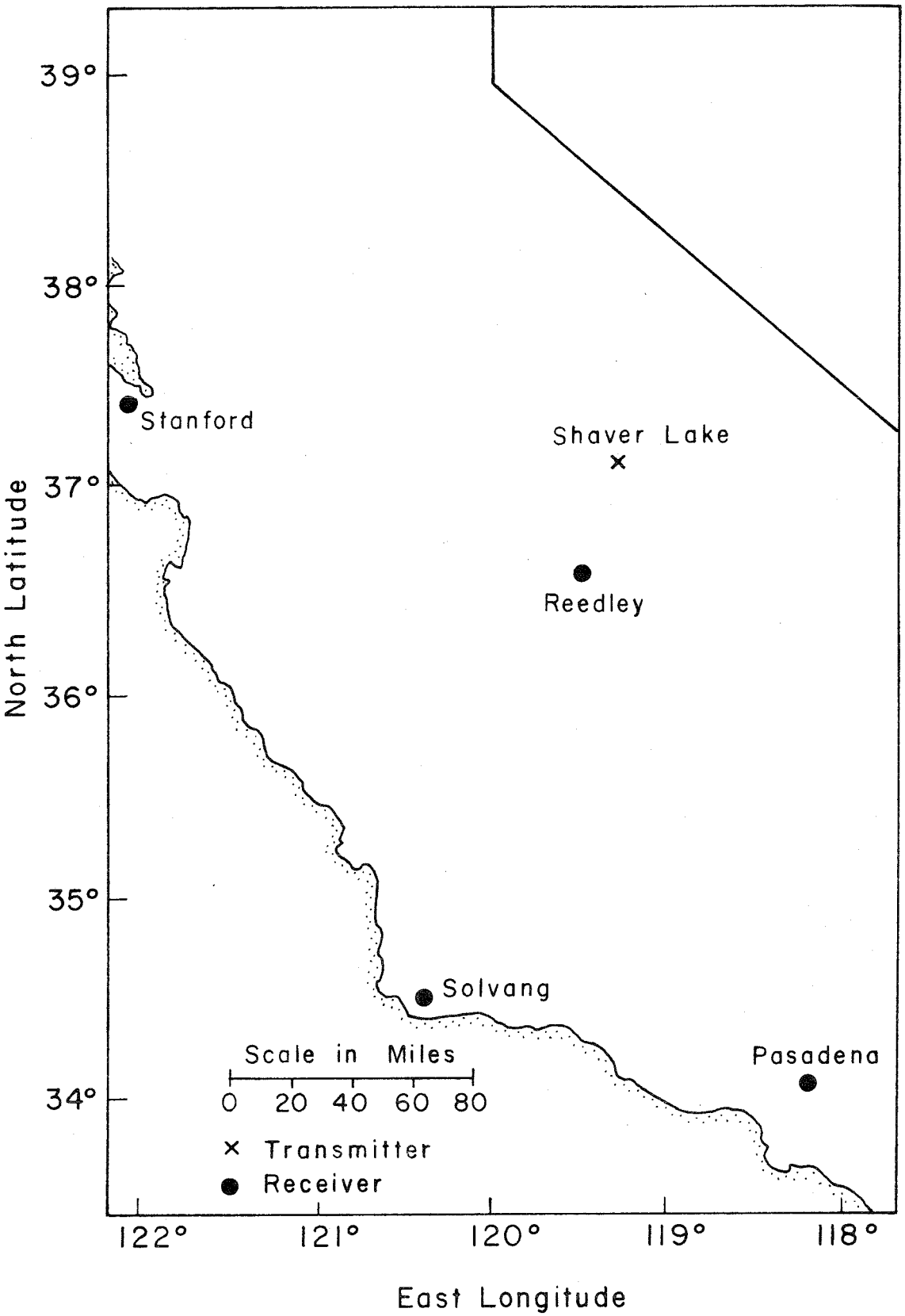

FIGURE VI-8. PORTION OF SOUTHERN CALIFORNIA SHOWING RELATIVE LOCATIONS OF REEDLEY, PASADENA, SOLVANG AND STANFORD.

may be possible to detect round trip echoes at this lower power level by using a receiver of narrower bandwidth and slightly more gain. This consideration, together with a description of the transmitting and receiving equipment, is given in the following section.

VII. TRANSMITTING AND RECEIVING EQUIPMENT

Transmitting System

Because the amount of effective power radiated by a horizontal antenna is an inverse function of the ground conductivity (19, 28, 34), it is necessary to locate such an antenna over an area having as low a value of ground conductivity as possible.

Extensive measurements made in Southern and Central California, revealed that the area around Shaver Lake, in the Sierra Nevada Mountains, was best suited for this purpose. (A detailed map of this area is shown in figure VII-1.) The ground conductivity in this region ranged from 2 to 5 x 10^{-4} mhos per meter. Coincidentally, the area contained an 11 kv power line (located along the Dinkey Creek road) which was approximately the correct length for a half-wave antenna at 8 kc (the original choice of frequency for the vlf experiments).

Permission was granted by the Southern California Edison Company (owners of the line) to use this line as an antenna, provided this use did not interfere with the flow of 60 cycle power or with the Edison Company's carrier current communication system. From a study of the frequencies used for the carrier current system, it was decided that operation at 8.4 kc, instead of 8 kc, would probably cause the least amount of interference with the carrier channels.

The conversion of the power line to a power line-antenna system was accomplished by the use of resonant tuned circuits as shown in figure VII-2. The ideal equivalent circuits of the antenna network system at 60 cycles and at 8.4 kc are shown in figures VII-3a and 3b respectively.

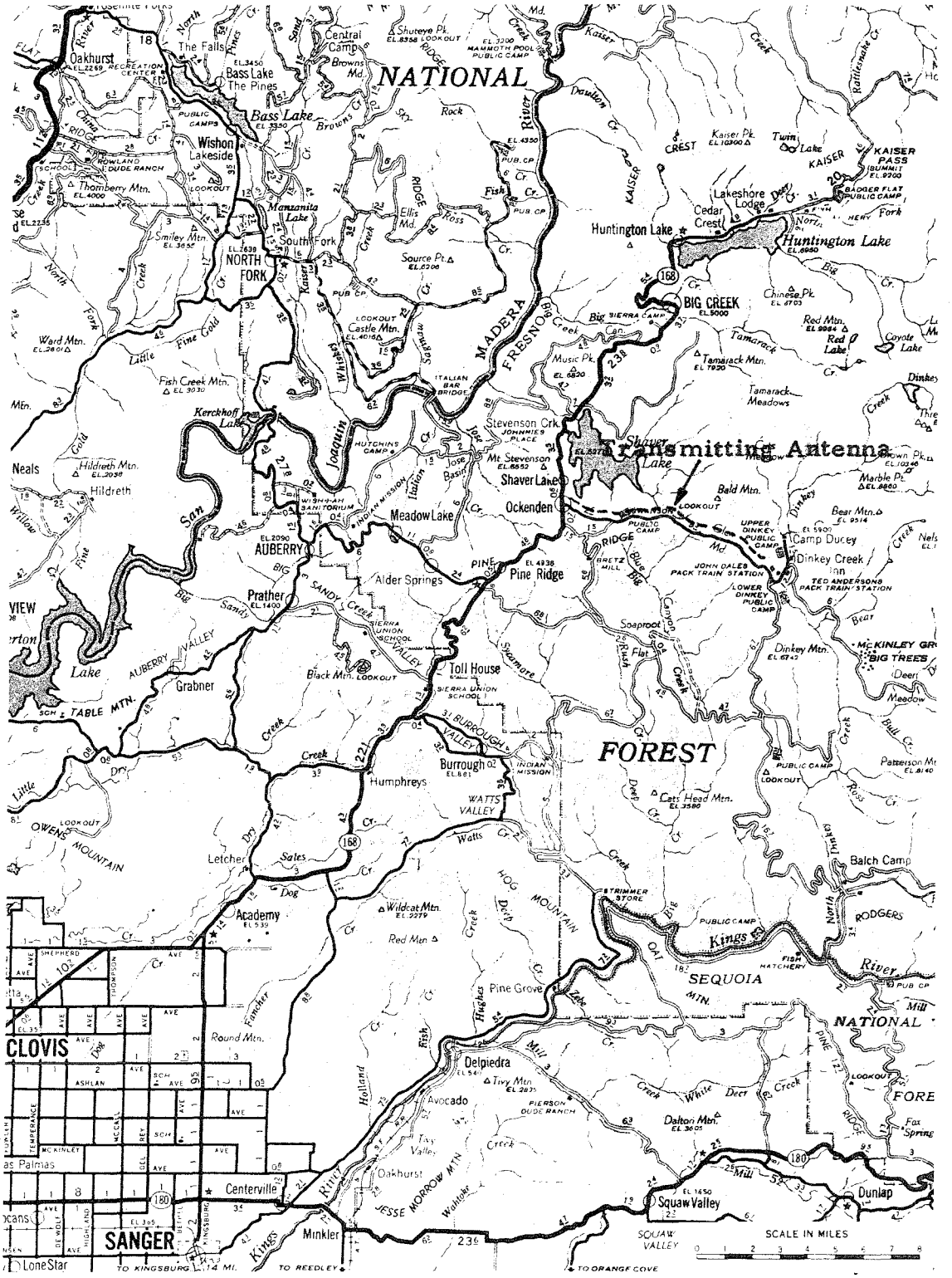

FIGURE VII-1. DETAILED MAP OF TRANSMITTING SITE.

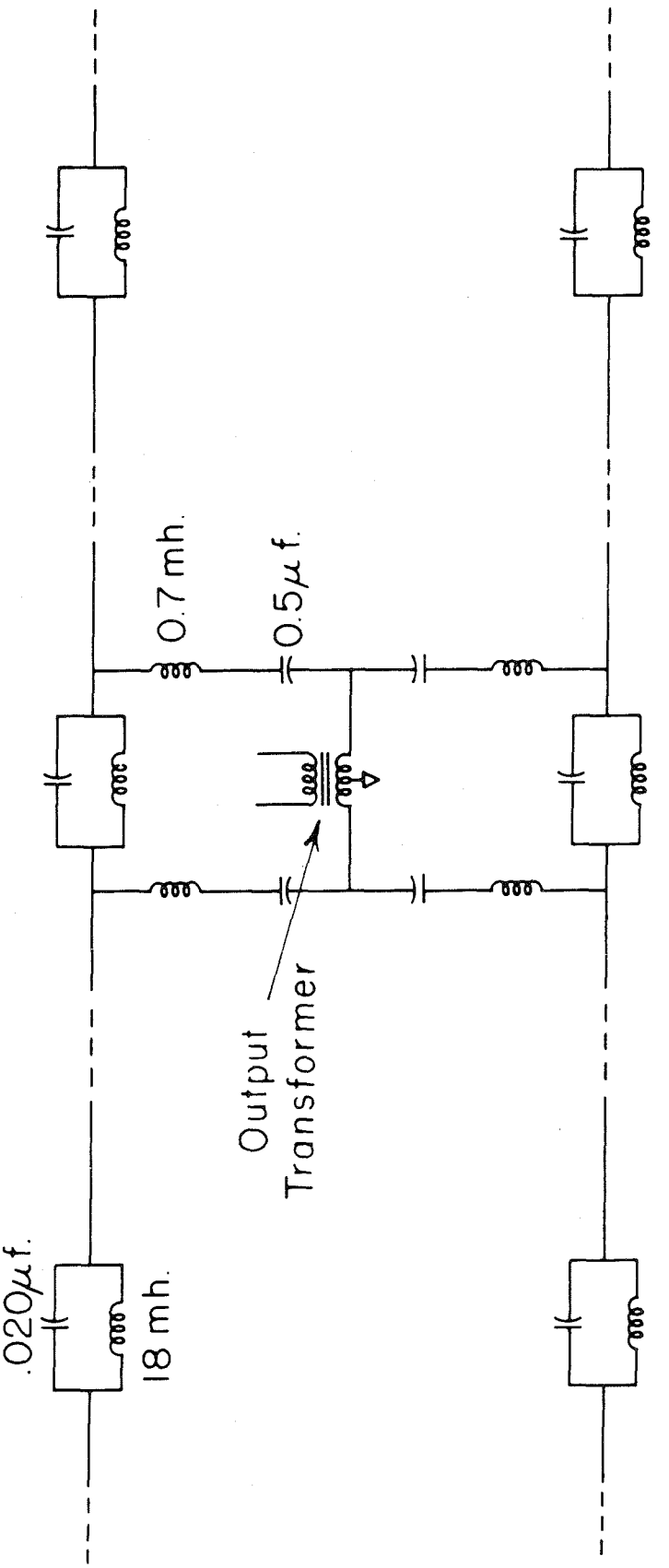

FIGURE VII-2. SCHEMATIC DIAGRAM OF ANTENNA SYSTEM.

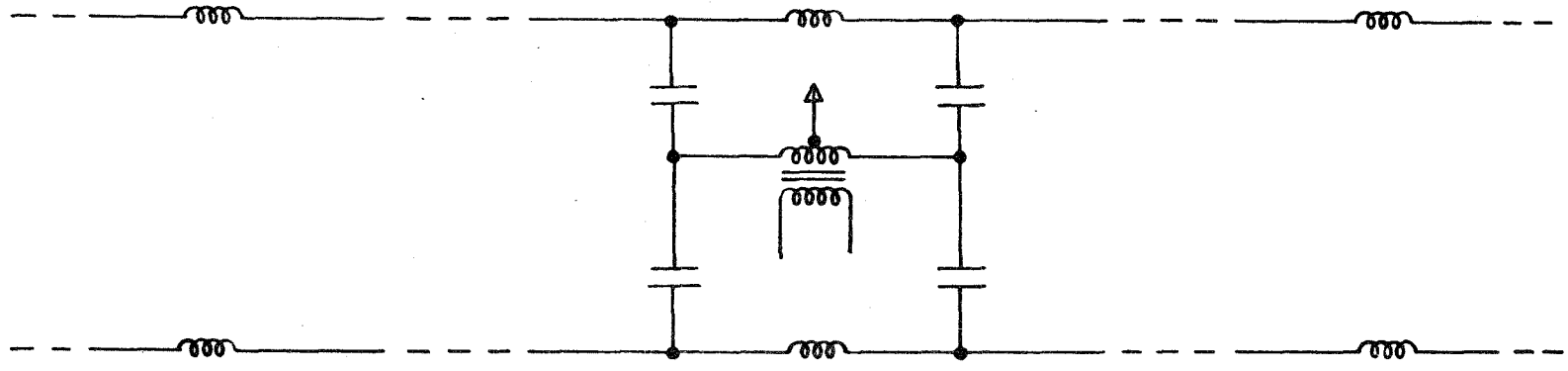

60 cps Equivalent Circuit

(a)

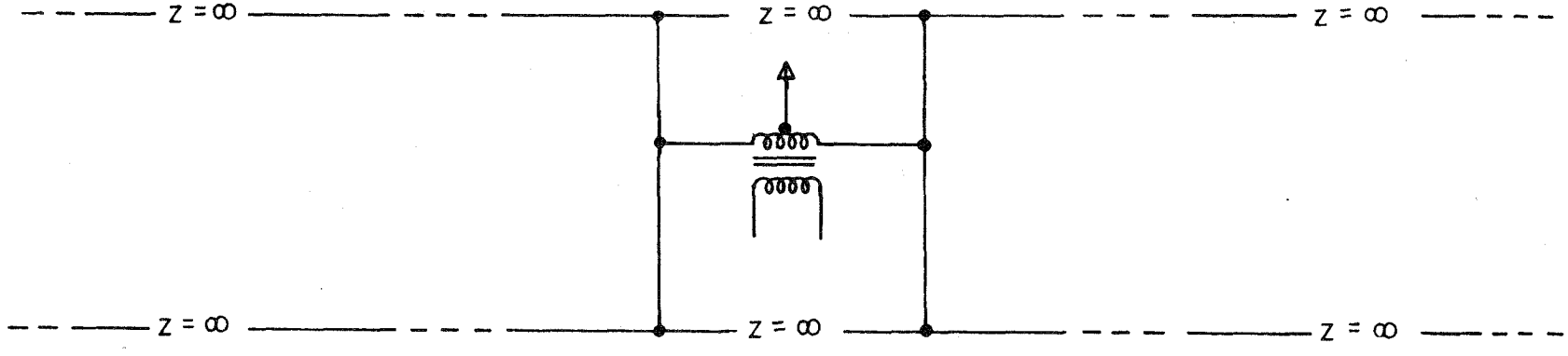

8.4 kc Equivalent Circuit

(b)

FIGURE VII-3. EQUIVALENT CIRCUIT OF ANTENNA SYSTEM.

The two wires present comprise one phase of a three phase distribution system. They are driven in phase (at the center of the line) so as to reduce possible parasitic effects.

Details of the construction and installation of the tuned circuits are given in (34). Appendix G contains photographs of the transmitter bungalow and the associated coupling and safety equipment required.

The transmitter (see appendix G) built by Ling Electronics, Inc. of Culver City, California, is a modified vibration power amplifier. It is designed to deliver 20 kw of power continuously into a matched load of 80 ohms over a frequency range between 4 and 40 kc. A functional block diagram of the transmitter is given in figure VII-4.

The signal source for the transmitter is an 8.4 kc crystal oscillator, the circuit diagram for which is also given in appendix G. The input to the transmitter is controlled by either a key or one of two synchronous timers. The timers are used to control the transmitter during the 3 minute - 1 minute and the .5 second - 4.5 second transmissions. The 3 minute-1 minute timer provided an easily recognizable pattern that verified the existence of the 8.4 kc signal.

During typical operation, the input power to the antenna was 6 kw. Higher levels of operation caused overloading of the resonant circuits at the ends of the antenna. Hence the maximum power capabilities of the transmitter could not be realized.

Receiving Equipment

The 8.4 kc receiver consists of a portable pre-selector unit, and a double-conversion vlf receiver. The receiving antennas are two

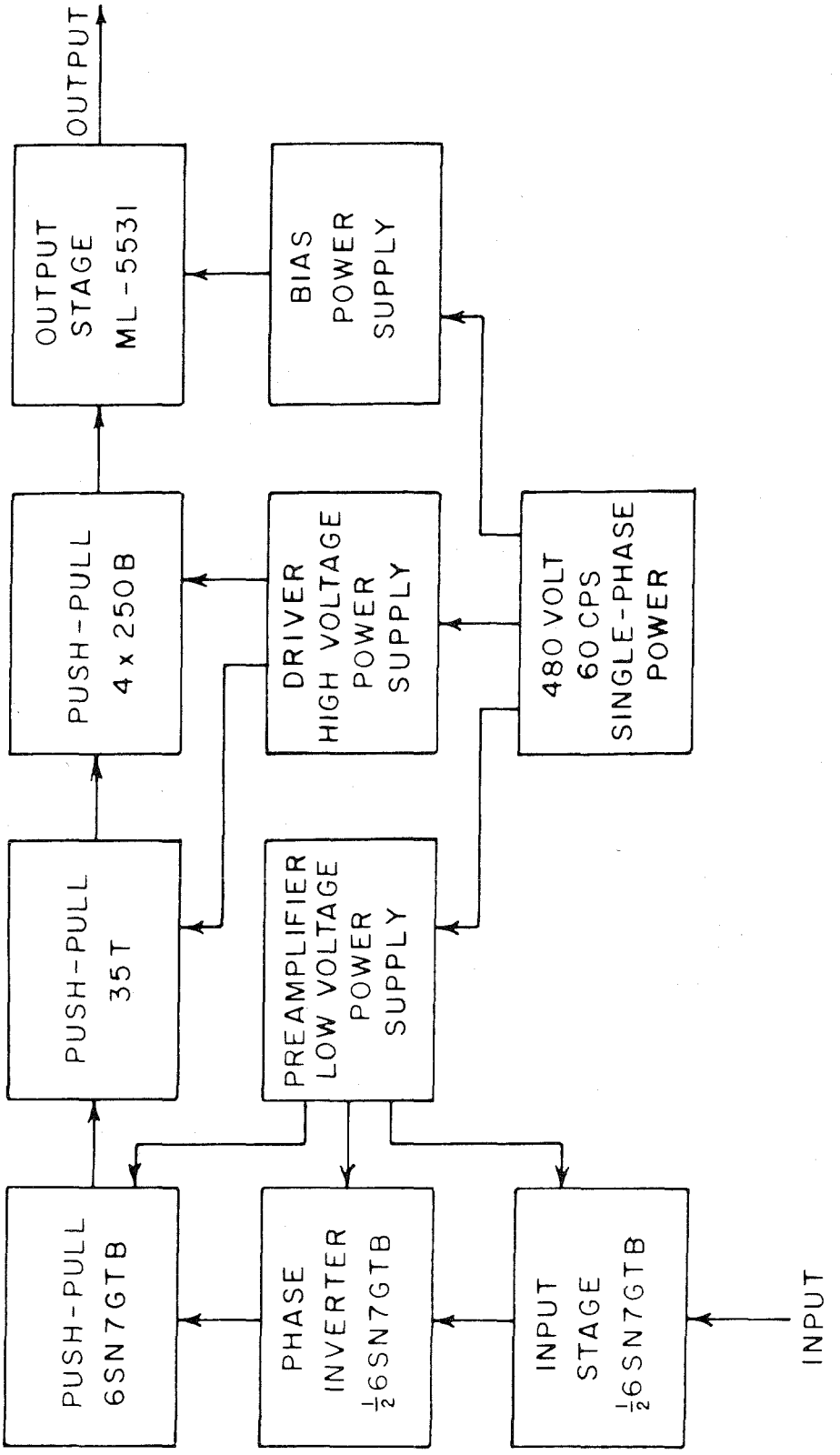

FIGURE VII-4. FUNCTIONAL BLOCK DIAGRAM OF TRANSMITTER.

identical loops, one meter square and oriented in mutually perpendicular directions. Each loop has a self-inductance of .99 mhy. The orientation of the loops was determined according to the directions corresponding to minimum and maximum signals received. By locating the loops in the perpendicular bisector plane of the transmitting antenna (ground wave minimum, see figure III-3) it was possible to obtain a measure of the magnitude of the reflection coefficients (see section V) of the sky wave.

The pre-selector is coupled to the receiving loops by a low impedance-to-grid input transformer which is connected to a tuned-grid differential amplifier. A functional block diagram of the pre-selector is given in figure VII-5.

The cathode follower output of the pre-selector drives a tuned-grid, tuned-plate amplifier which constitutes the first stage of the vlf receiver (a functional block diagram of which is given in figure VII-6). The 8.4 kc signal is then mixed in a balanced mixer pair with a 7.35 kc sine wave supplied by a crystal oscillator. A differential amplifier with tuned plate circuit, follows the mixer and precedes the second conversion stage. The second local oscillator frequency is derived from the crystal oscillator by the use of a frequency multiplying and dividing circuit. An R-C coupled stage follows the second mixer and is connected to a high-Q tuned-grid amplifier stage. The detailed circuitry of the pre-selector and receiver is given in appendix F.

Cathode follower outputs are provided at 8.4 kc, 1.05 kc, and 98.4 cycles. An additional tuned circuit and stage of amplification were later coupled to the 8.4 kc output in order to increase the sensitivity while attempting to detect gyroelectric-echoes.

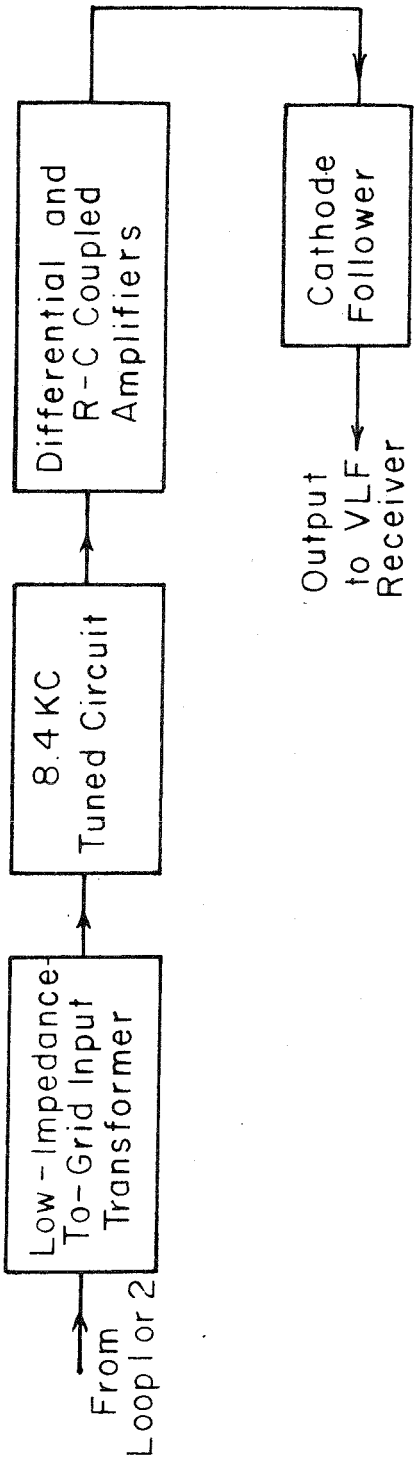

FIGURE VII-5. FUNCTIONAL BLOCK DIAGRAM OF 8.4 KC PRE-SELECTOR.

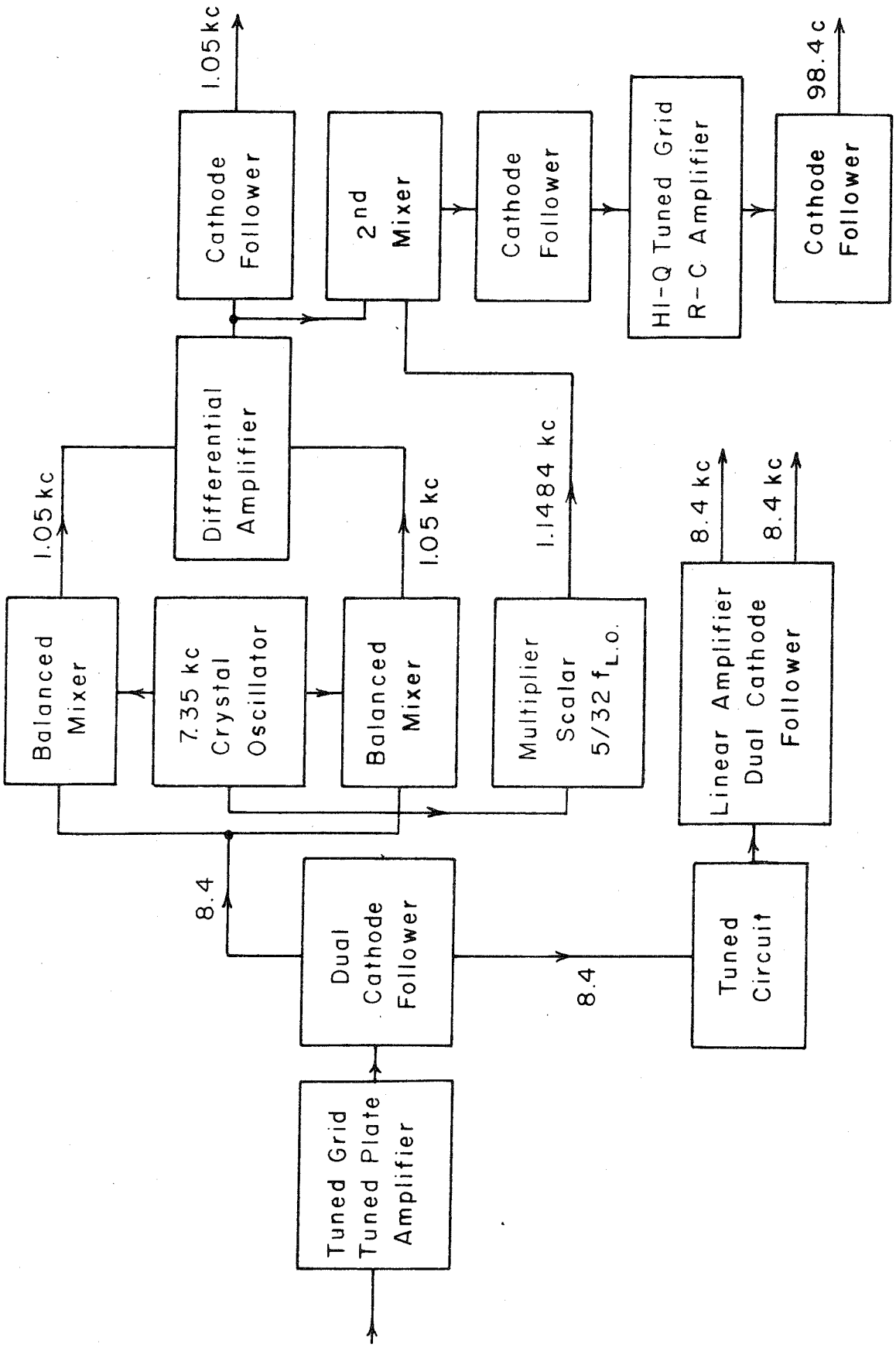

FIGURE VII-6. FUNCTIONAL BLOCK DIAGRAM OF VERY LOW-FREQUENCY RECEIVER.

Bandwidth measurements indicated a bandwidth of 135 cycles at 8.4 kc (115 cycles with the use of the additional circuit), 68 cycles at 1.05 kc and 1 cycle at 98.4 cycles. Because of the narrow bandwidth of the 98.4 cycle output, transients, excited in the receiver by atmospheric noise, persisted for an unduly long time. For this reason, the amplitude data was generally recorded from the 1.05 kc output.

In order to obtain measurements from the mutually perpendicular loops, a switching scheme was devised such that the receiver was alternately switched between the loops, the switching occurring during the middle of the off periods of the transmitter. (This circuitry is also shown in appendix F.)

The rms output of the receiver was measured by a vacuum tube voltmeter or by a pen chart recorder which utilized the VTVM circuitry. A tape recorder was used to record the output of the receiver during the .5 second - 4.5 second transmissions so that the tapes could later be studied for the possible existence of gyroelectric-echoes.

Receiver calibration was accomplished in the following manner: one of the loops normally used for receiving was used as a transmitting loop and placed at a fixed distance from the receiver. The output level of the receiver was then recorded as a function of the input current to the transmitting loop. This measurement was repeated for several distances between the loops and for two orientations - axes of the loops collinear and axes parallel. The field strength was then computed from the expressions for the radiation field of a magnetic dipole (21, 35). These are,

$$\underline{H} = \left\{ \underline{e}_r \left[\frac{1}{2\pi} \left(\frac{1}{R^3} - \frac{ik}{R^2} \right) \cos\theta \right] + \underline{e}_\theta \left[\frac{1}{4\pi} \left(\frac{1}{R^3} - \frac{ik}{R^2} - \frac{k^2}{R} \right) \sin\theta \right] \right\} AIe^{i(\underline{k} \cdot \underline{R} - \omega t)} \qquad \text{(VII-1)}$$

where

R is the distance from the center of the dipole

$k = \omega/c$

A is the area of the dipole

θ is the angle between $\underline{R}$ and the normal of the dipole

I is the current (rms or peak value) in the magnetic dipole

From a knowledge of the magnetic field strength, an equivalent electric field can be computed from $\left|\underline{E}_{equiv}\right| = 377 \left|\underline{H}\right|$.

The above measurements gave values of field strength per unit deflection on the pen recorder ranging between 375 and 700 micro-volts per meter per unit deflection. In the experimental data given, an average value of 500 was used in determining the amplitude of the received field strength. (A later adjustment of the receiver increased the gain by a factor of 9 db so that the scale factor was changed from 500 to 180.)

VIII. RESUME AND PROPOSALS FOR CONTINUED RESEARCH

With the increased use of very low frequencies by the armed services as a reliable communication channel and with the possibility of using vlf as a world-wide frequency standard, a need has arisen for extending experimental data concerning the radio properties of the ionosphere to these lower frequencies. A comparatively economical experimental transmitting and receiving system for doing this has been presented together with a number of theoretical and experimental results concerning vlf propagation.

In the theoretical investigations considered, the ionosphere has been treated as a homogeneous gyroelectric medium and curves have been given showing the dependence of the phase and group index of refraction as a function of the gyro- and plasma frequencies of the medium. These curves graphically illustrate the dispersion and anisotropic properties of the ionosphere.

It is seen that for incident waves in the vlf range, the phase index can assume large positive values which means that propagation can take place in the medium with relatively little attenuation. Therefore it is only in this frequency range that gyroelectric-echoes or the natural phenomenon of whistlers can be observed. (For waves such that $\omega >> \omega_g$, the ionosphere becomes a transparent medium.)

Also presented are reflection and transmission coefficients for the case of vertical incidence and $\omega < \omega_g$. All of the above results are for the lossless case when the effects of collisions between electrons can be neglected.

Experimental data at 8.4 kc shows the variation of the received signal amplitude as a function of time of day. In general, the near vertical incidence data shows rapid fading near sunrise and sunset. The data also shows that the signal level at night is subject to a greater fluctuation than the daytime signal.

Round trip gyroelectric-echoes have not been detected at present but may be detected with a narrower bandwidth receiver or by operating the transmitter at a higher power level. Data recorded at distances around 300 km from the transmitting antenna indicates that, except for locations in the ground wave minimum of the antenna, the received signal consists primarily of the ground or surface wave radiated by the antenna. The signal has also been detected at a distance of 4,200 km thereby giving much encouragement to the increased use of such a transmitting system.

The receiver used for the above experiments was originally intended for detecting gyroelectric-echoes and had no provision for simultaneously recording phase and amplitude of the received signal from the mutually perpendicular receiving loops. By the use of a more sophisticated receiving system (see figure VIII-1) it would be possible to make direct measurements of the reflection coefficients (amplitude and phase) of the ionosphere as well as virtual height measurements.

At the present writing, the crystal oscillator used to drive the transmitter is stable to about one part in 20,000 and therefore is not well suited for phase stability measurements. Construction of a

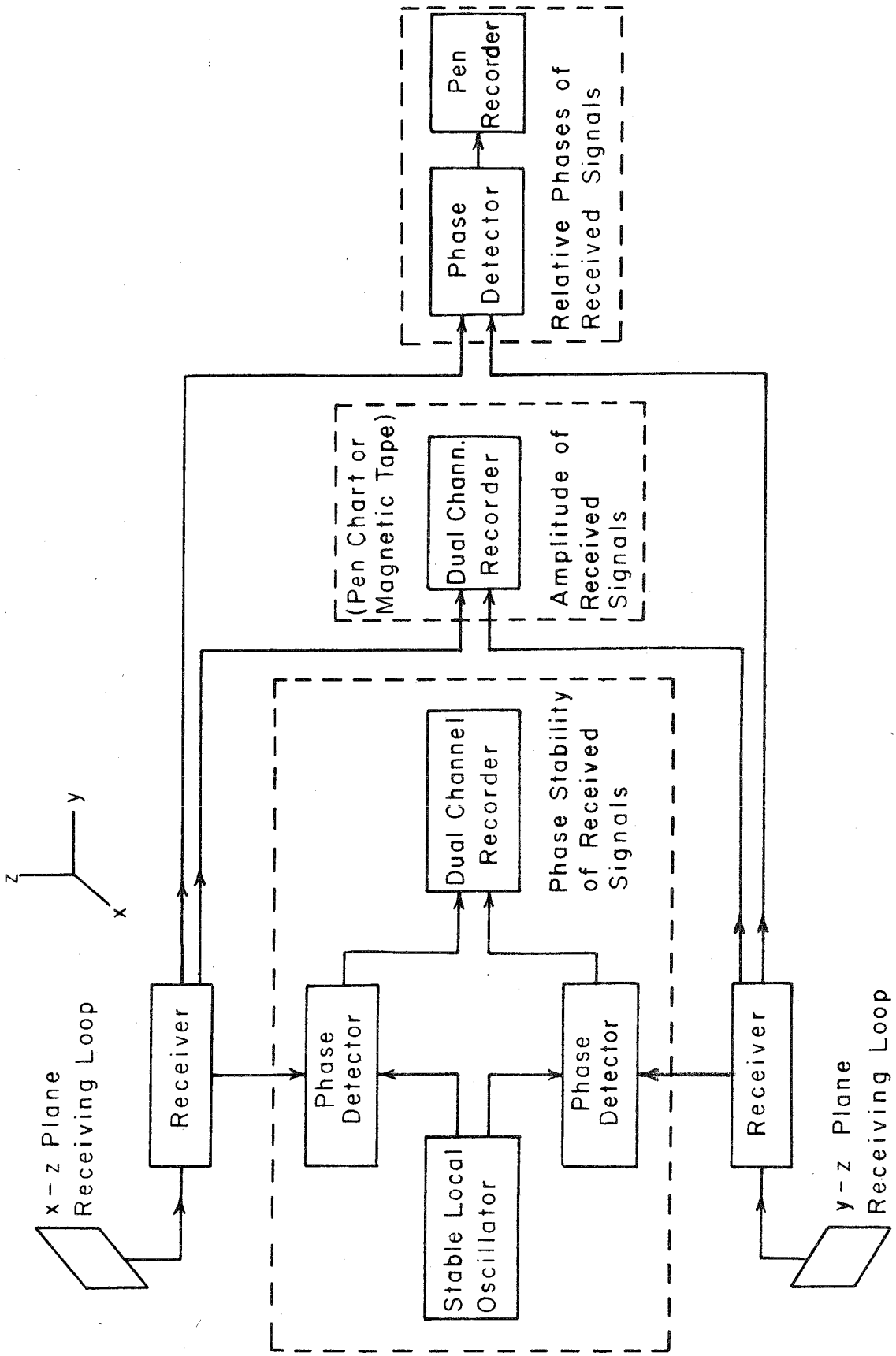

FIGURE VIII-1. FUNCTIONAL BLOCK DIAGRAM OF PROPOSED VERY LOW-FREQUENCY RECEIVING SYSTEM.

more stable source is under way so that phase stability measurements at 8.4 kc can be made in the near future. Phase stability measurements of the received signal can then be made at 8.4 kc by comparing the received signal with a local oscillator that is at least as stable as the transmitter oscillator.

By modifying the tuned circuits of the antenna, it should be possible to increase the power radiated by the antenna and thereby increase the probability of generating and detecting gyroelectric-echoes. At the same time, the sensitivity and selectivity of the receiver might be increased so that the 8.4 kc signal can be directly recorded without the use of a conversion stage in the receiver.

With increased power output of the transmitter and increased sensitivity of the receiver, it should then be possible to make vlf measurements on a transcontinental basis.

REFERENCES

1. Beynon, W. J. G.: "Radio Studies During the International Geophysical Year 1957-58," Journal of British Institute of Radio Engineers, July 1958, Vol. 18, p. 401.

2. Kennelly, A. E.: Electrical World and Engineering, 1902, Vol. 15, p. 473.

3. Heaviside, O: Encyclopaedia Britannica, 1902, Ninth Edition, Vol. 33, p. 215.

4. Eccles, W. H.: Proceedings of the Royal Society A, 1912, Vol. 87, p. 79.

5. Larmor, J.: Philosophy Magazine, 1924, Vol. 48, p. 1025.

6. Appleton, E. V.: Proceedings of the Physical Society (London), 1925, Vol. 37, p. 16D.

7. Appleton, E. V.: Journal of the Institute of Electrical Engineers, 1932, Vol. 71, p. 642.

8. Goldstein, S.: Proceedings of the Royal Society A, 1928, Vol. 121, p. 260.

9. Hartree, D. R.: Proceedings of the Cambridge Philosophical Society, 1929, Vol. 25, p. 47.

10. Waynick, A. H.: "Present State of Knowledge Concerning the Lower Ionosphere," Proceedings of the Institute of Radio Engineers, June 1957, Vol. 45, p. 746.

11. Smith-Rose, R. L.: "Electron-Density Profiles in the Ionosphere During the I. G. Y.," Proceedings of the Institute of Radio Engineers, November 1958, Vol. 46, p. 1874.

12. Chapman, S.: Proceedings of the Physical Society (London), 1931, Vol. 43, pp. 26, 483.

13. Manning, L. A., and V. R. Eshleman: "Meteors in the Ionosphere," Proceedings of the Institute of Radio Engineers, February 1959, Vol. 47, pp. 186 - 199.

14. Appleton, E. V., and M. A. F. Barnett: Electrician, 1925, Vol. 95, p. 678.

15. Appleton, E. V., and M. A. F. Barnett: Nature, 1925, Vol. 115, p. 333.

16. Hollingworth, J.: Proceedings of the Royal Society A, 1928, Vol. 119, p. 444.

17. Breit, E. V.: Journal of the Institute of Electrical Engineers, 1932, Vol. 71, p. 642.

18. Bergman, C. W., R. S. Macmillan, and W. H. Pickering: "A New Technique for Investigating the Ionosphere at Low and Very Low-Frequencies," Rocket Exploration of the Upper Atmosphere, 1954, Interscience Publishers, Inc., New York.

19. Macmillan, R. S., W. V. T. Rusch, and R. M. Golden: "A New Antenna to Eliminate Ground Wave Interference in Ionospheric Sounding Experiments," Journal of Atmospheric and Terrestrial Physics, 1958, Vol. 13, pp. 183 - 186.

20. Papas, C. H.: "A Note Concerning a Gyro-Electric Medium," Technical Report No. 4, May 1954, California Institute of Technology, Nonr 220 (14).

21. Stratton, J.: Electromagnetic Theory, 1941, McGraw-Hill Book Company, New York and London.

22. Sommerfeld, A.: Optics, 1954, Academic Press, New York.

23. Barkhausen, H.: "Whistling Tones From the Earth," Proceedings of the Institute of Radio Engineers, July 1930, Vol. 18, pp. 1155 - 1159.

24. Eckersley, T. S.: "Musical Atmospherics," Nature, January 1935, Vol. 139, pp. 104 - 105.

25. Storey, L. R. O.: "An Investigation of Whistling Atmospherics," Philosophical Transactions of the Royal Society of London, Series A, July 1953, Vol. 246, pp. 113 - 141.

26. Helliwell, R. A., J. H. Crary, J. H. Pope, and R. L. Smith: "The 'Nose' Whistler, a New High Latitude Phenomena," Journal of Geophysics Research, 1956, Vol. 61, pp. 139 - 142.

27. Helliwell, R. A., and M. G. Morgan: "Atmospheric Whistlers," Proceedings of the Institute of Radio Engineers, February 1959, Vol. 47, pp. 200 - 208.

28. Golden, R. M., R. S. Macmillan, R. Nathan, and W. V. T. Rusch: "A Calculation of the Radiation Fields of Whistling Atmospherics," Technical Report No. 1, July 1956, California Institute of Technology, ASTIA Document No. AD 115 042.

29. Helliwell, R. A., and E. Gehrels: "Observations of Magneto-Ionic Duct Propagation Using Man-Made Signals of Very Low Frequency," Proceedings of the Institute of Radio Engineers, April 1958, Vol. 46, pp. 785 - 787.

30. Bremmer, H.: Terrestrial Radio Waves, 1949, Elsevier Publishing Company, New York.

31. Booker, H.G.: "Propagation of Wave Packets Incident Obliquely Upon a Stratified Doubly-Refractory Ionosphere," Proceedings of the Royal Society, September 1938, Vol. 237, pp. 411 - 445.

32. Wait, J.R.: "Calculations of Ionospheric Reflection Coefficients at Very Low Radio Frequencies," Journal of Geophysical Research, March 1957, Vol. 62, pp. 43 - 56.

33. Yabroff, I.W.: "Reflection at a Sharply-Bounded Ionosphere," Proceedings of the Institute of Radio Engineers, June 1957, Vol. 45, pp. 750 - 753.

34. Golden, R.M., R.V. Langmuir, R.S. Macmillan, and W.V.T. Rusch: "Design and Construction of Equipment Used to Operate a Commercial Power Line as a Very Low Frequency Antenna," Technical Report No. 3, October 1958, California Institute of Technology, ASTIA Document No. AD 204 514.

35. Smythe, W.R.: Static and Dynamic Electricity, 1950, McGraw-Hill Book Company, Inc., New York, Toronto and London.

36. Mitra, S.K.: The Upper Atmosphere, 1952, The Asiatic Society, Calcutta, India.

37. Joos, Georg: Theoretical Physics, 1950, Hafner Publishing Company, New York.

APPENDIX A

DERIVATION OF THE FIELD EQUATIONS FOR A GYROELECTRIC MEDIUM

1. Electron Velocity and Convection Current

The approximate force on an electron is given by equation III-2 as:

$$\underline{F}_e = -i\omega m\underline{v} + m\omega_c\underline{v} = e\underline{E} + e\underline{v} \times \underline{B}_o \qquad \text{(A-1)}$$

Forming the vector and scalar product of equation A-1 with $\underline{B}_o$, yields respectively,

$$-i\omega m(\underline{v} \times \underline{B}_o) + m\omega_c(\underline{v} \times \underline{B}_o) = e(\underline{E} \times \underline{B}_o) + e(\underline{B}_o \cdot \underline{v})\underline{B}_o - eB_o^2\underline{v} \qquad \text{(A-2)}$$

and

$$-i\omega m(\underline{v} \cdot \underline{B}_o) + m\omega_c(\underline{v} \cdot \underline{B}_o) = e(\underline{E} \cdot \underline{B}_o) \qquad \text{(A-3)}$$

Substituting the value of $(\underline{v} \cdot \underline{B}_o)$ from equation A-3 into equation A-2, gives $(\underline{v} \times \underline{B}_o)$ as,

$$(\underline{v} \times \underline{B}_o) = \frac{e(\underline{E} \times \underline{B}_o) - eB_o^2\underline{v} + \dfrac{e^2(\underline{E} \cdot \underline{B}_o)\underline{B}_o}{m\omega_c - i\omega m}}{m\omega_c - i\omega m} \qquad \text{(A-4)}$$

This relation, when substituted into equation A-1, gives, upon rearranging terms, equation III-3.

The convection current, $Ne\underline{v}$, is therefore found to be:

$$Ne\underline{v} = \underline{j} = \frac{(\omega_c - i\omega)\omega_p^2 \varepsilon_v}{(\omega_c - i\omega)^2 + \omega_g^2}\underline{E} + \frac{1}{(\omega_c - i\omega)^2 + \omega_g^2}\frac{\omega_p^2 \omega_g \varepsilon_v}{B_o}(\underline{E} \times \underline{B}_o)$$

$$+ \frac{\varepsilon_v \omega_p^2 \omega_g^2}{(\omega_c - i\omega)\left[(\omega_c - i\omega)^2 + \omega_g^2\right]}\frac{(\underline{E} \cdot \underline{B}_o)\underline{B}_o}{B_o^2} \qquad (A\text{-}5)$$

By assuming $\underline{B}_o$ lies along the z axis, $\underline{E} \times \underline{B}_o = \underline{e}_x E_y B_o - \underline{e}_y E_x B_o$ and $\underline{E} \cdot \underline{B}_o = E_z B_o$, so that equation III-4 becomes,

$$\nabla \times \underline{H} = \begin{bmatrix} I_x \\ I_y \\ I_z \end{bmatrix} = -i\omega \begin{bmatrix} \varepsilon_{xx} & -i\varepsilon_{xy} & 0 \\ i\varepsilon_{yx} & \varepsilon_{yy} & 0 \\ 0 & 0 & \varepsilon_{zz} \end{bmatrix} \begin{bmatrix} E_{ox} \\ E_{oy} \\ E_{oz} \end{bmatrix} \qquad (A\text{-}6)$$

which is equation III-6.

The unit wave normal, $\underline{n}$, is given by,

$$\underline{n} = \underline{e}_y \sin\phi + \underline{e}_z \cos\phi \qquad (A\text{-}7)$$

so that equation III-10 can now be written in component form as:

$$E_{ox}\left[1 - \left(\frac{1}{M^2}\right)\left(\frac{\varepsilon_{xx}}{\varepsilon_v}\right)\right] + E_{oy}\left[i\left(\frac{1}{M^2}\right)\left(\frac{\varepsilon_{xy}}{\varepsilon_v}\right)\right] = 0$$

$$E_{ox}\left[-i\left(\frac{1}{M^2}\right)\left(\frac{\varepsilon_{yx}}{\varepsilon_v}\right)\right] + E_{oy}\left[\cos^2\phi - \left(\frac{1}{M^2}\right)\left(\frac{\varepsilon_{yy}}{\varepsilon_v}\right)\right] - E_{oz}\left[\cos\phi \sin\phi\right] = 0$$

$$- E_{oy}\left[\sin\phi \cos\phi\right] + E_{oz}\left[\sin^2\phi - \frac{1}{M^2}\frac{\varepsilon_{zz}}{\varepsilon_v}\right] = 0$$

(A-8)

The above equations are finally represented in matrix form in equation III-11.

2. Ratio of Field Components

The ratios of the field components can be determined from equation III-11 and are found to be:

$$\frac{E_{oz}}{E_{ox}} = i r_{ozx} \qquad (A\text{-}9)$$

$$r_{ozx} \equiv \frac{\sin\phi \cos\phi}{(\sin^2\phi - \frac{\varepsilon_3}{M^2})} \quad \frac{(\varepsilon_1 + \varepsilon_2 - 2M^2)}{(\varepsilon_1 - \varepsilon_2)}$$

and

$$\frac{E_{oy}}{E_{ox}} = i r_{oyx} \qquad (A\text{-}10)$$

$$r_{oyx} \equiv \frac{(\varepsilon_1 + \varepsilon_2 - 2M^2)}{(\varepsilon_1 - \varepsilon_2)}$$

3. Index of Refraction

For computational purposes, equation III-12 was put into the following form with the various coefficients defined below:

$$M^4 + \frac{\left[-a - b - (c+d)\tan^2\phi\right]}{cd\tan^2\phi + ab} M^2 + \frac{1 + \tan^2\phi}{cd\tan^2\phi + ab} = 0 \qquad (A\text{-}11)$$

$$a \equiv \frac{1}{\varepsilon_1} \qquad c \equiv \frac{1}{\varepsilon_3}$$

$$b \equiv \frac{1}{\varepsilon_2} \qquad d \equiv \frac{1}{2}(a + b)$$

The Burroughs Datatron 205 digital computer was used to compute the M^2 curves presented in figures III-2a through III-2f.

For the lossless case ($\omega_c = 0$), a, b, c, d are real constants and therefore M^2 is a real number as is shown by the following. Equation A-11 can be rewritten as,

$$M^4\left[(ab - cd)\sin^2\phi - ab\right] + M^2\left[(c-d)\sin^2\phi + (a+b)\right] - 1 = 0 \qquad \text{(A-12)}$$

The discriminant of this quadratic form is

$$\left[(c-d)\sin^2\phi + (a+b)\right]^2 + 4\left[(ab - cd)\sin^2\phi - ab\right]$$

This can be reduced to $(c-d)^2\sin^4\phi + (a-b)^2\cos^2\phi$. Since a, b, c, d are all real, the discriminant is real and greater than 0. Hence M^2 is always real for this case.

4. Polarization of Plane Waves in a Gyroelectric Medium

The polarization as defined by equation III-14.1 is,

$$P = \frac{E_{x'}}{E_{z'}} = \frac{1}{\left(\frac{E_{oz}}{E_{ox}}\right)\sin\phi - \left(\frac{E_{oy}}{E_{ox}}\right)\cos\phi} \qquad \text{(A-13)}$$

Substituting for the ratios E_{oz}/E_{ox} and E_{oy}/E_{ox} given in equations A-9 and A-10 respectively yields:

$$P = \frac{i(\epsilon_2 - \epsilon_1)}{\epsilon_3}\,\frac{\left[M^2\sin^2\phi - \epsilon_3\right]}{\left[\epsilon_1 + \epsilon_2 - 2M^2\right](\cos\phi)} = \frac{i(\epsilon_2 - \epsilon_1)}{\epsilon_3}\,\frac{\left[\tan^2\phi(M^2 - \epsilon_3) - \epsilon_3\right]}{\sqrt{1+\tan^2\phi}\left[\epsilon_1 + \epsilon_2 - 2M^2\right]} \qquad \text{(A-14)}$$

APPENDIX B

CONSTRUCTION OF THE DUAL EQUATION INVOLVING THE VECTORS $\underline{E}$, $\underline{D}$, $\underline{s}$

1. Relations Between $\underline{n}$ and $\underline{s}$

Because $\underline{D}$, $\underline{E}$, $\underline{s}$ are coplanar $\left[\underline{D} \cdot (\underline{E} \times \underline{s}) = 0\right]$, the following equation can be formed using the undetermined coefficients, a and b.

$$\underline{D} - a\underline{s} = b\underline{E} \tag{B-1}$$

This form is chosen so that it resembles the corresponding equation for $\underline{D}$, $\underline{E}$ and $\underline{n}$. Taking the scalar product of both sides with $\underline{s}$, gives:

$$\underline{s} \cdot \underline{D} - a\underbrace{s^2}_{\Longrightarrow 1} = b\underline{s} \cdot \underbrace{\underline{E}}_{\Longrightarrow 0} \tag{B-2}$$

so

$$a = (\underline{s} \cdot \underline{D}) \tag{B-3}$$

The coefficient b is found by taking the scalar product of $\underline{s}$ and $\underline{E} - \underline{n}(\underline{n} \cdot \underline{E}) = \mu_v u^2 \underline{D}$ and the scalar product of $\underline{n}$ and $\underline{D} - a\underline{s} = b\underline{E}$,

$$\underline{s} \cdot \underbrace{\underline{E}}_{\Longrightarrow 0} - \underline{n} \cdot \underline{s}(\underline{n} \cdot \underline{E}) = \mu_v u^2 (\underline{D} \cdot \underline{s}) \tag{B-4}$$

$$(\underline{n} \cdot \underbrace{\underline{D}}_{\Longrightarrow 0}) - (\underline{n} \cdot \underline{s})(\underline{s} \cdot \underline{D}) = b(\underline{E} \cdot \underline{n}) \tag{B-5}$$

so

$$(\underline{n} \cdot \underline{E}) = -\frac{(\underline{n} \cdot \underline{s})(\underline{s} \cdot \underline{D})}{b} \tag{B-6}$$

therefore,

$$(\underline{n} \cdot \underline{s})^2 \frac{(\underline{s} \cdot \underline{D})}{b} = \mu_v u^2 (\underline{D} \cdot \underline{s}) \qquad (B-7)$$

and,

$$b = \frac{(\underline{n} \cdot \underline{s})^2}{\mu_v u^2} \qquad (B-8)$$

Equation B-1 now becomes,

$$\underline{D} - (\underline{s} \cdot \underline{D})\underline{s} = \frac{(\underline{n} \cdot \underline{s})^2}{\mu_v u^2} \underline{E} \qquad (B-9)$$

The quantity $(\underline{n} \cdot \underline{s})^2$ can be eliminated in the following manner, remembering that,

$$(\underline{n} \cdot \underline{s}) = \frac{\underline{n} \cdot (\underline{E} \times \underline{H})}{|\underline{E}||\underline{H}|} \qquad (B-10)$$

Equations III-4 and III-5 reduce to,

$$\underline{k} \times \underline{H} = -\omega \underline{D} \qquad (B-11)$$

$$\underline{k} \times \underline{E} = \omega \mu_v \underline{H} \qquad (B-12)$$

Taking the scalar product of equation B-12 with itself gives,

$$\omega^2 \mu_v^2 H^2 = (\underline{k} \times \underline{E}) \cdot (\underline{k} \times \underline{E}) = k^2 E - (\underline{k} \cdot \underline{E})^2 \qquad (B-13)$$

so

$$H = \frac{k}{\omega\mu_v}\left[E^2 - (\underline{n}\cdot\underline{E})^2\right]^{1/2} \qquad (B-14)$$

This permits writing $\underline{S}$, as,

$$\underline{S} = \underline{E}\times\underline{H} = \frac{1}{\omega\mu_v}\underline{E}\times(\underline{k}\times\underline{E}) = \frac{1}{\omega\mu_v}\left[E^2\underline{k} - (\underline{E}\cdot\underline{k})\underline{E}\right] \qquad (B-15)$$

Therefore, $\underline{n}\cdot(\underline{E}\times\underline{H})$ in equation B-10 becomes,

$$\underline{n}\cdot(\underline{E}\times\underline{H}) = \frac{k}{\omega\mu_v}\left[E^2 - (\underline{E}\cdot\underline{n})^2\right] \qquad (B-16)$$

Combining equations B-14 and B-16 with equation B-10 gives $(\underline{n}\cdot\underline{s})$ as,

$$(\underline{n}\cdot\underline{s}) = \left[1 - \frac{(\underline{E}\cdot\underline{n})^2}{E^2}\right]^{1/2} \qquad (B-17)$$

The ray velocity is defined as the velocity of energy propagation in the $\underline{s}$ direction. This is related to the phase velocity u, and the wave normal $\underline{n}$, by

$$v = \frac{u}{\cos\sigma} = \frac{u}{(\underline{n}\cdot\underline{s})} \qquad (B-18)$$

where $(\underline{n}\cdot\underline{s})$ is given by equation B-17. Hence equation B-9 finally reduces to,

$$\underline{D} - (\underline{s}\cdot\underline{D})\underline{s} = \frac{1}{\mu_v v^2}\underline{E} \qquad (B-19)$$

For the special case that $\underline{E}\cdot\underline{n} = 0$, $\underline{u} = \underline{v}$ so that the two velocities coincide.

It should be noted that the following relation for $(\underline{n} \cdot \underline{s})$ is also true, namely,

$$(\underline{n} \cdot \underline{s}) = \frac{(\underline{E} \cdot \underline{D})}{|\underline{E}|\,|\underline{D}|} \qquad \text{(B-20)}$$

This is readily shown by forming the right hand side of equation B-20 and then substituting for $\underline{D}$ from equation B-11.

2. The Ray Index of Refraction

The ray index of refraction, M', can be determined from the above equation and in terms of the phase index of refraction. The ray index is defined as,

$$M' = c/v \qquad \text{(B-21)}$$

From equation B-18 and B-17,

$$\frac{u^2}{v^2} = (\underline{n} \cdot \underline{s})^2 = 1 - \frac{(\underline{E} \cdot \underline{n})^2}{E^2} = \frac{M'^2}{M^2} \qquad \text{(B-22)}$$

Using equations A-7 and A-9 gives $(\underline{E} \cdot \underline{n})$ as,

$$(\underline{E} \cdot \underline{n}) = E_{ox}\left[\, i r_{oyx} \sin\phi + i r_{ozx} \cos\phi\right] \qquad \text{(B-23)}$$

Substituting equation B-23 into equation B-22 finally yields

$$\frac{M'^2}{M^2} = \frac{(\sin^2\phi - \frac{\epsilon_3^2}{M^2}) + (\frac{\epsilon_1 + \epsilon_2 - 2M^2}{\epsilon_2 - \epsilon_1})^2 \left\{(\sin^2\phi - \frac{\epsilon_3^2}{M^2}) + \sin^2\phi\left[\cos^2\phi + (1 - \frac{\epsilon_3^2}{M^2})\right]\right\}}{(\sin^2\phi - \frac{\epsilon_3^2}{M^2}) + (\frac{\epsilon_1 + \epsilon_2 - 2M^2}{\epsilon_2 - \epsilon_1})^2 \left[(\sin^2\phi - \frac{\epsilon_3^2}{M^2}) + \sin^2\phi\cos^2\phi\right]} \qquad \text{(B-24)}$$

APPENDIX C

DISPERSION LAW OF WHISTLERS

An elementary derivation of the frequency-time law of whistlers is as follows.

For a plane wave propagating in a homogeneous gyroelectric medium and in a direction parallel to the constant magnetic field, $\phi = 0$, equation III-12 reduces to:

$$\left(\frac{1}{M^2} - \frac{1}{\varepsilon_1}\right)\left(\frac{1}{M^2} - \frac{1}{\varepsilon_2}\right) = 0 \qquad \text{(C-1)}$$

Therefore,

$$M^2 = \varepsilon_1 \quad \text{or} \quad \varepsilon_2 \qquad \text{(C-2)}$$

and

$$\varepsilon_1 = 1 - \frac{\omega_p^2}{\omega(\omega - \omega_g)} \qquad \text{(C-2.1)}$$

$$\varepsilon_2 = 1 - \frac{\omega_p^2}{\omega(\omega + \omega_g)} \qquad \text{(C-2.2)}$$

for the case of negligible losses. Examination of the curves for M^2 (figures III-2a through III-2f) shows that the so-called longitudinal mode occurs for $M^2 = \varepsilon_1$ and $\omega < \omega_g$. With this in mind, it is now possible to determine the time delay of whistlers.

The time of arrival of a whistler can be determined from

$$T = \int_{\text{path}} \frac{ds}{v_g} \qquad \text{(C-3)}$$

Hence it is necessary to evaluate v_g, the group velocity of the whistler. The group velocity is given by,

$$v_g = \frac{1}{(dk/d\omega)} \qquad \text{(C-4)}$$

where

$$k = \frac{\omega}{u} = \frac{\omega}{c} M \qquad \text{(C-4.1)}$$

This is related to the phase refractive index by

$$v_g = \frac{c}{M + \omega \frac{dM}{d\omega}} \qquad \text{(C-5)}$$

Combining this with $M = \sqrt{\varepsilon_1}$ from equation C-2 above, yields,

$$v_g = \frac{2c\sqrt{\varepsilon_1}}{2\varepsilon_1 + \omega \frac{d\varepsilon_1}{d\omega}} \qquad \text{(C-6)}$$

Substituting for ε_1 and $\frac{d\varepsilon_1}{d\omega}$, then gives,

$$v_g = \frac{2c(\omega_g - \omega)^{3/2}\left[\omega^2(\omega_g - \omega) + \omega\omega_p^2\right]^{1/2}}{2\omega^3 - 4\omega^2\omega_g + 2\omega\omega_g^2 + \omega_g\omega_p^2} \qquad \text{(C-7)}$$

This can be further simplified if only the case $\omega \ll \omega_g \ll \omega_p$ is considered. With this simplification, v_g reduces to:

$$v_g = \frac{2c\sqrt{\omega\,\omega_g}}{\omega_p} \qquad \text{(C-8)}$$

Substituting equation C-8 into equation C-3 yields,

$$T = \int_{\text{path}} \frac{\omega_p \, ds}{2c\sqrt{\omega \omega_g}} = \frac{D}{\sqrt{f}} \qquad \text{(C-9)}$$

where

$$D = \frac{1}{2c} \int_{\text{path}} \frac{f_p \, ds}{\sqrt{f_g}} \qquad \text{(C-10)}$$

and is called the dispersion path. Applying these same restrictions to ε_1 shows that

$$\varepsilon_1 = 1 - \frac{\frac{\omega_p^2}{\omega_g^2}}{\frac{\omega}{\omega_g}\left(\frac{\omega}{\omega_g} - 1\right)} \simeq 1 + \frac{\omega_p^2}{\omega_g^2} \frac{\omega_g}{\omega} \simeq \frac{\omega_p^2}{\omega_g^2} \frac{\omega_g}{\omega} \qquad \text{(C-11)}$$

Therefore,

$$M = \sqrt{\varepsilon_1} \simeq \frac{\omega_p}{\sqrt{\omega \omega_g}} = \frac{c}{u} \qquad \text{(C-12)}$$

so that,

$$u \simeq \frac{c\sqrt{\omega \omega_g}}{\omega_p} = \frac{v_g}{2} \qquad \text{(C-13)}$$

Hence the group velocity is twice the phase velocity for this approximation.

APPENDIX D

REFLECTION AND TRANSMISSION COEFFICIENTS FOR WAVES OF THE ELECTRIC TYPE

The incident electric field is represented by,

$$\underline{H} = \underline{e}_x \sqrt{\frac{\epsilon_v}{\mu_v}}\, E_e\, e^{i(\underline{k}_o \cdot \underline{r} - \omega t)} \qquad \text{(D-1)}$$

$$\underline{E} = \left[- \underline{e}_y \cos\theta + \underline{e}_z \sin\theta \right] E_e\, e^{i(\underline{k}_o \cdot \underline{r} - \omega t)} \qquad \text{(D-1.1)}$$

The reflected fields consist of electric-type waves and magnetic-type waves, and are represented by the subscripts ee and em respectively.

$$\underline{H}_{ee} = \underline{e}_x R_{ee} \sqrt{\frac{\epsilon_v}{\mu_v}}\, E_e\, e^{i(\underline{k}_o \cdot \underline{r} - \omega t)} \qquad \text{(D-2)}$$

$$\underline{E}_{ee} = \left[\underline{e}_y \cos\theta + \underline{e}_z \sin\theta \right] R_{ee}\, E_e\, e^{i(\underline{k}_o \cdot \underline{r} - \omega t)} \qquad \text{(D-2.1)}$$

and

$$\underline{H}_{em} = \left[- \underline{e}_y \cos\theta - \underline{e}_z \sin\theta \right] R_{em} \sqrt{\frac{\epsilon_v}{\mu_v}}\, E_e\, e^{i(\underline{k}_o \cdot \underline{r} - \omega t)} \qquad \text{(D-3)}$$

$$\underline{E}_{em} = \underline{e}_x R_{em}\, E_e\, e^{i(\underline{k}_o \cdot \underline{r} - \omega t)} \qquad \text{(D-3.1)}$$

(R_{ee} and R_{em} are the reflection coefficients of the reflected waves and are sometimes given as ${}_{\perp}R_{\perp}$ and ${}_{\perp}R_{\parallel}$, respectively.)

The refracted field can be represented in the same form as given for waves of the magnetic type. Using equation V-8 and letting

$$E_{x_{1,2}} = T_{e_{1,2}} E_m \tag{D-4}$$

results in the following relations:

$$\frac{\underline{E}_{1,2}}{E_e} = T_{e_{1,2}} \underline{e}_x + T_{e_{1,2}} \underline{e}_y \left[i r_{yx_{1,2}} \right] + \underline{e}_z T_{e_{1,2}} \left[i r_{zx_{1,2}} \right] \tag{D-5}$$

$$\frac{\underline{H}_{1,2}}{E_e} = \sqrt{\frac{\varepsilon_v}{\mu_v}} M_{1,2} \left\{ \underline{e}_x T_{e_{1,2}} \left[i r_{zx_{1,2}} \sin(\beta+\phi_{1,2}) - i r_{yx_{1,2}} \cos(\beta+\phi_{1,2}) \right] + \underline{e}_y T_{e_{1,2}} \cos(\beta+\phi_{1,2}) + \underline{e}_z \left[- T_{e_{1,2}} \sin(\beta+\phi_{1,2}) \right] \right\} \tag{D-5.1}$$

The boundary conditions require that,

$$H_x: \quad 1 + R_{ee} = i T_{e_1} M_1 \left[\rho_1(M_1,\phi_1) \right] + i T_{e_2} M_2 \left[\rho_2(M_2,\phi_2) \right] \tag{D-6}$$

$$H_y: \quad -R_{em} \cos\theta = T_{e_1} M_1 \cos(\beta+\phi_1) + T_{e_2} M_2 \cos(\beta+\phi_2) \tag{D-6.1}$$

$$E_x: \quad R_{em} = T_{e_1} + T_{e_2} \tag{D-6.2}$$

$$E_y: \quad -\cos\theta + R_{ee} \cos\theta = T_{e_1} i r_{yx_1} + T_{e_2} i r_{yx_2} \tag{D-6.3}$$

The quantities r_{yx}, r_{zx} and ρ are defined by equations V-9, V-10 and V-13 respectively.

APPENDIX E

EQUIVALENCE BETWEEN THE GYROELECTRIC FORMULATION OF SECTION III AND THE APPLETON-HARTREE FORMULATION

The coordinate system used in the Appleton-Hartree formulation is shown below:

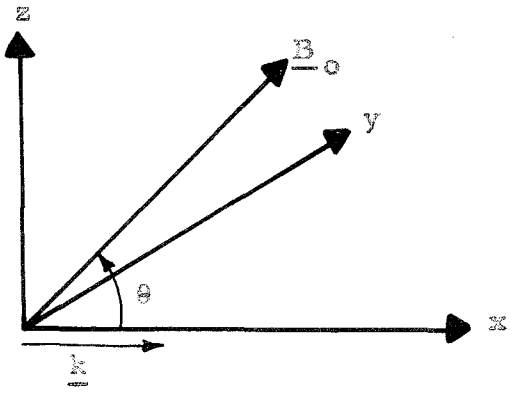

The complex index of refraction is given by:

$$M^2 = 1 + \frac{2}{2(a+j\beta) - \frac{\gamma_T^2}{1+a+j\beta} \pm \sqrt{\frac{\gamma_T^4}{(1+a+j\beta)^2} + 4\gamma_L^2}} \qquad (E-1)$$

where:

$$a = -\omega^2/\omega_p^2$$

$$\beta = \omega\omega_c/\omega_p^2$$

$$\gamma = \omega\omega_g/\omega_p^2$$

$$\gamma_L = \gamma\cos\theta$$

$$\gamma_T = \gamma\sin\theta$$

This coordinate system is related to the coordinate system of figure III-4 by,

$$\begin{bmatrix} x \\ y \\ z \end{bmatrix} = \begin{bmatrix} 0 & \sin\theta & \cos\theta \\ -1 & 0 & 0 \\ 0 & -\cos\theta & \sin\theta \end{bmatrix} \begin{bmatrix} ox \\ oy \\ oz \end{bmatrix} \qquad (E\text{-}2)$$

The equivalence between the above expression for M^2, and equation III-12 can be shown by making the following substitutions:

1. $\theta \longrightarrow \phi$
2. $1 + \alpha + j\beta = \left[\dfrac{\varepsilon_3}{\varepsilon_3 - 1}\right]$
3. $\gamma = \dfrac{1}{2}\left[\dfrac{1}{1 - \varepsilon_1} - \dfrac{1}{1 - \varepsilon_2}\right]$
4. $\omega \longrightarrow -\omega$
5. $\alpha + j\beta = \dfrac{1}{\varepsilon_3 - 1}$
6. $\gamma_L = \gamma\cos\phi$
7. $\gamma_T = \gamma\sin\phi$

The polarization, as given in the Appleton-Hartree formulation, is defined as:

$$R = \frac{h_z}{h_y} = -\frac{j}{\gamma_L}\left[\frac{1}{M^2 - 1} - (\alpha + j\beta)\right] \qquad (E\text{-}3)$$

In terms of the primed coordinate system of figure III-4, this is $-\dfrac{h_z'}{h_x'}$. From $\underline{k} \times \underline{E} = \omega\mu\underline{H}$, one determines,

$$\omega\mu\underline{H} = \underline{e}_x'\left[kE_z'\right] - \underline{e}_z'\left[kE_x'\right] \qquad (E\text{-}4)$$

Therefore

$$\omega\mu H_x' = kE_z'$$

$$\omega\mu H_z' = kE_x'$$

Hence

$$R = -\frac{h_z'}{h_x'} = \frac{E_x'}{E_z'}$$

as defined by equation III-14.

APPENDIX F

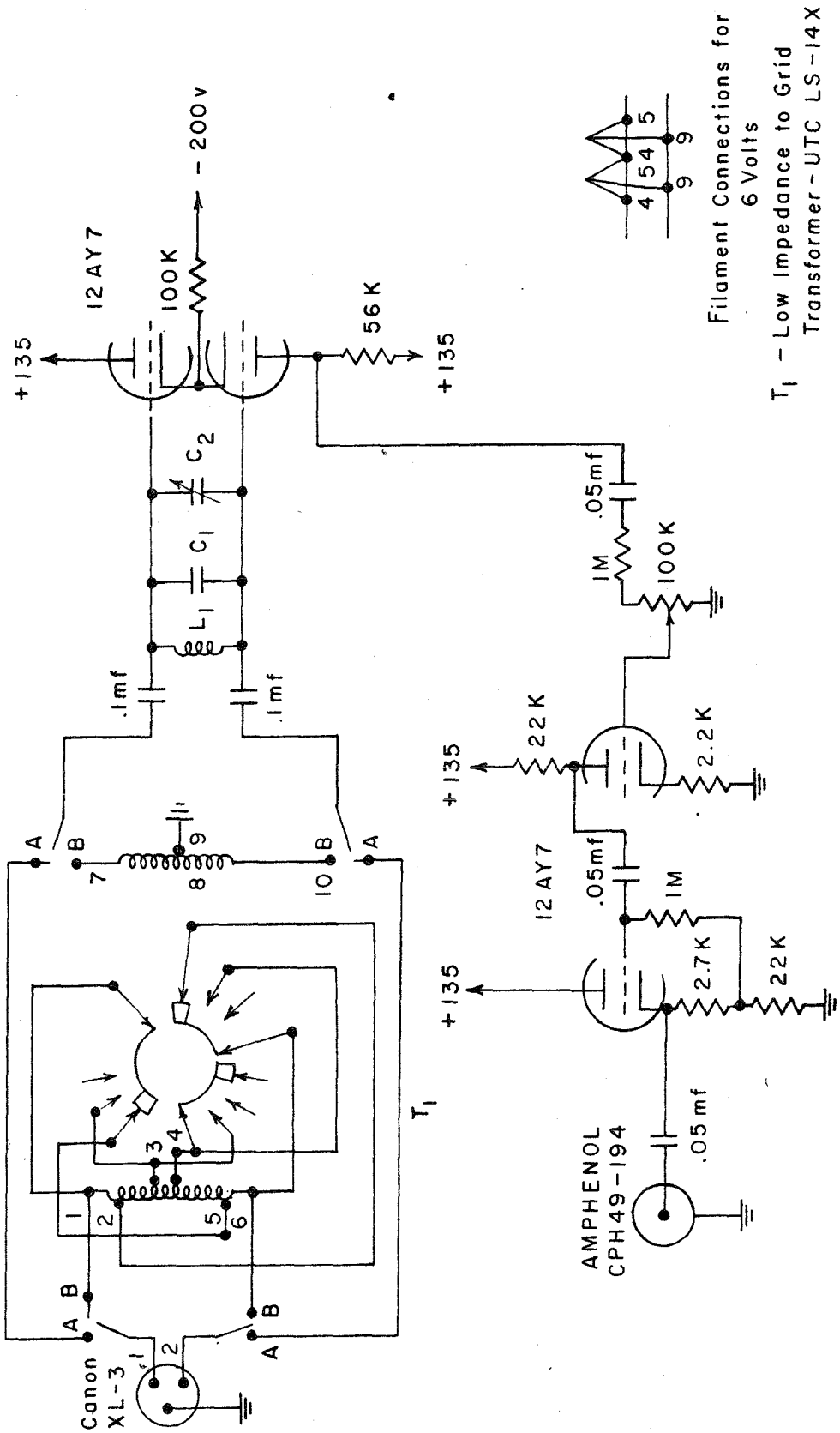

FIGURE F-1. CIRCUIT DIAGRAM OF PORTABLE 8.4 KC PRE-SELECTOR.

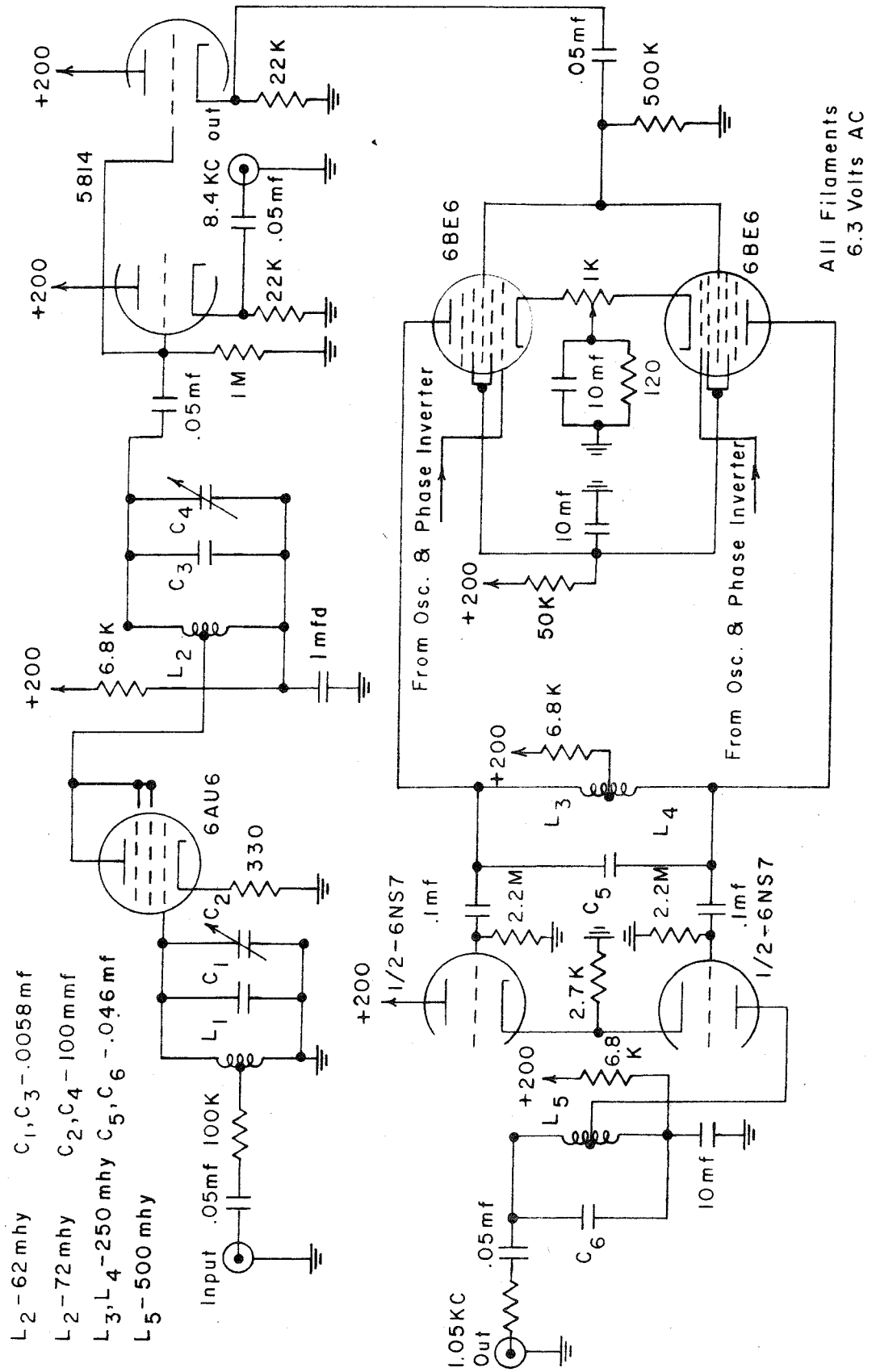

FIGURE F-2. CIRCUIT DIAGRAM OF VERY LOW-FREQUENCY RECEIVER: 8.4 KC AMPLIFIER AND FIRST INTERMEDIATE FREQUENCY STAGE.

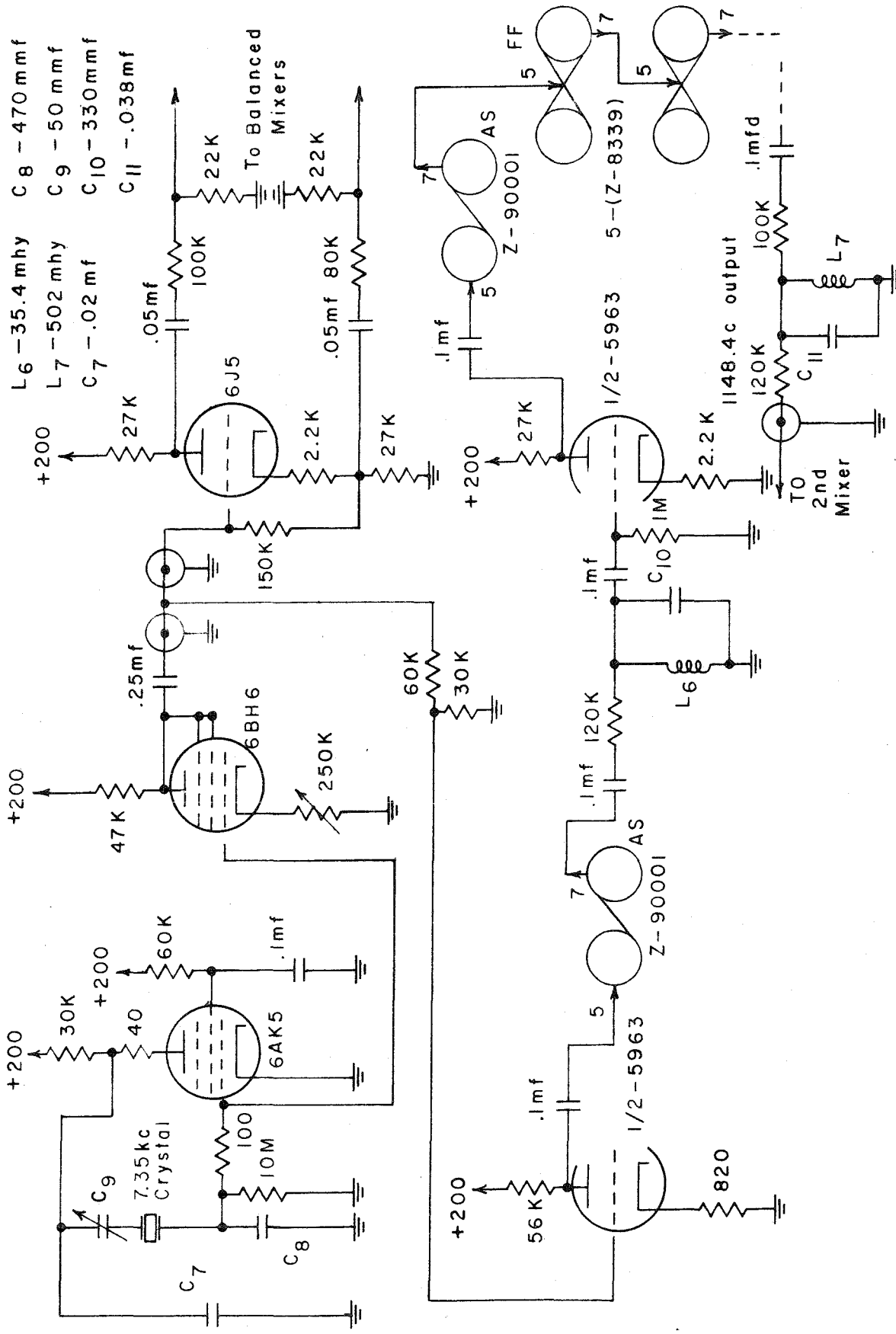

FIGURE F-3. CIRCUIT DIAGRAM OF VERY LOW-FREQUENCY RECEIVER: CRYSTAL OSCILLATOR, PHASE INVERTER AND SCALING CIRCUITS.

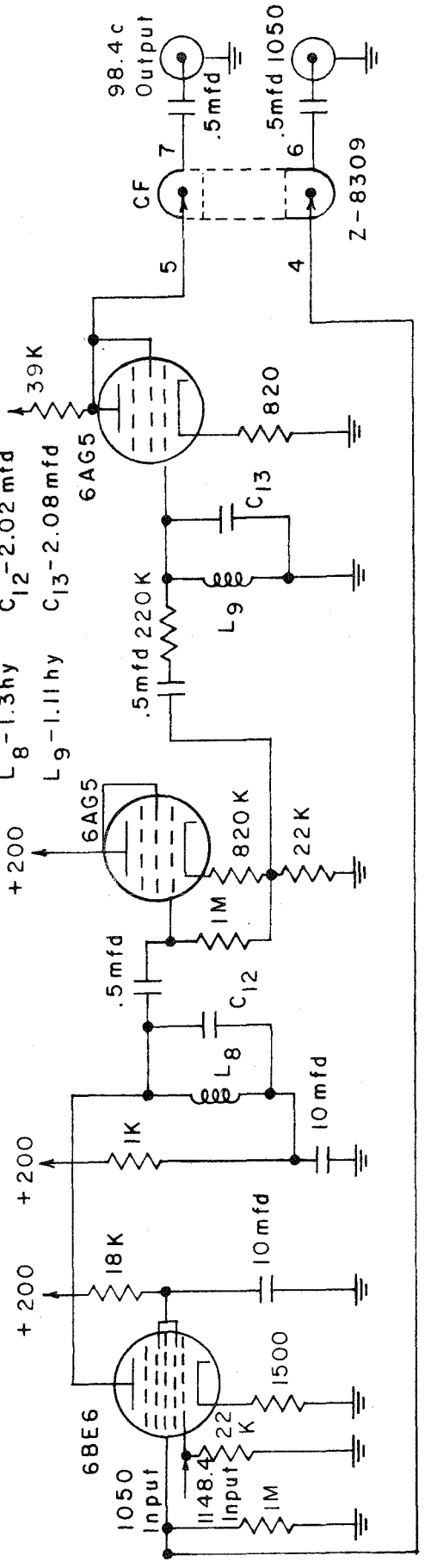

FIGURE F-4. CIRCUIT DIAGRAM OF VERY LOW-FREQUENCY RECEIVER: SECOND INTERMEDIATE FREQUENCY AND CATHODE FOLLOWER OUTPUTS.

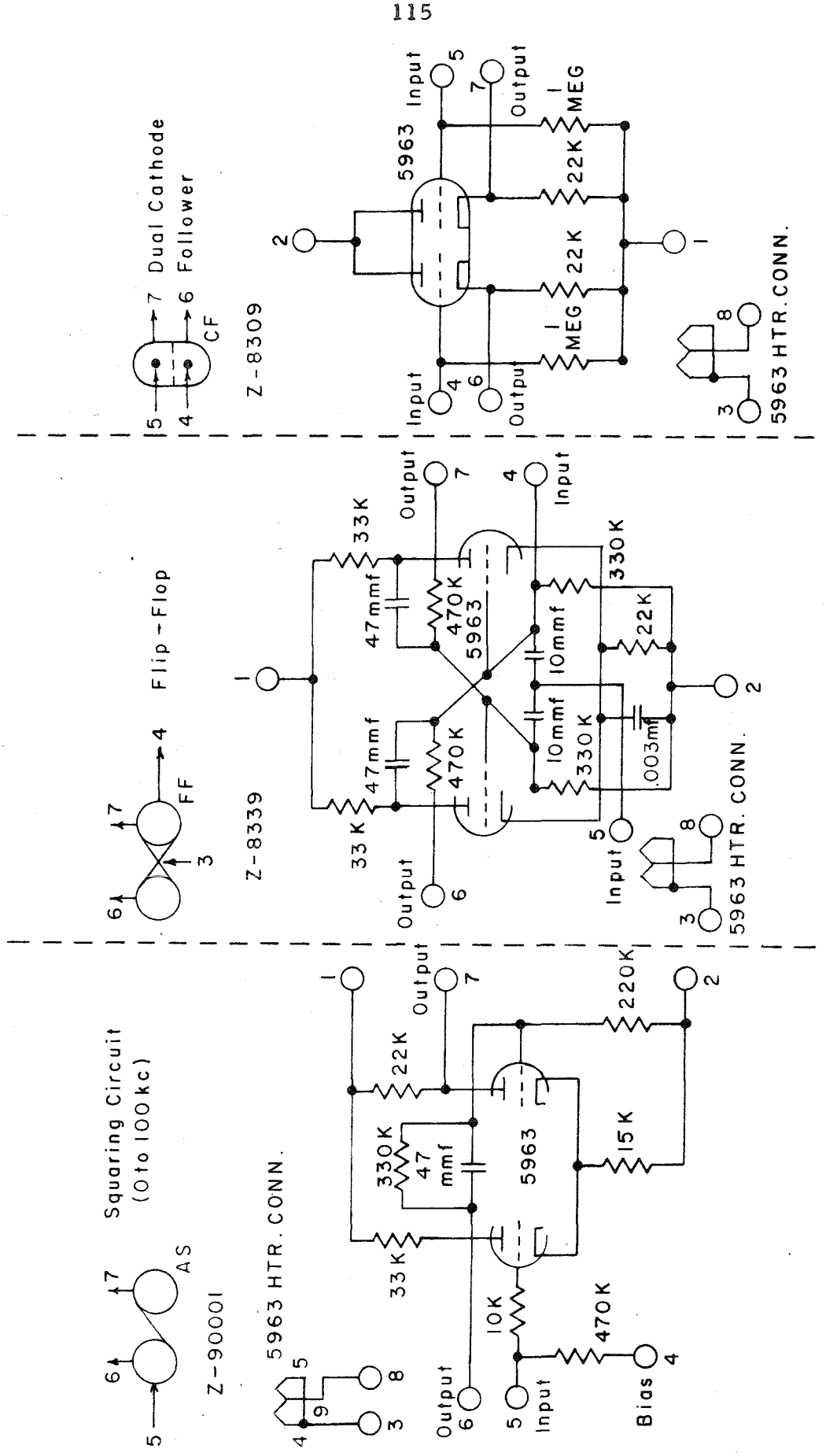

FIGURE F-5. CIRCUIT DIAGRAMS OF EECO PLUG-IN UNITS FOR FREQUENCY SCALING CIRCUITS IN VERY LOW-FREQUENCY RECEIVER.

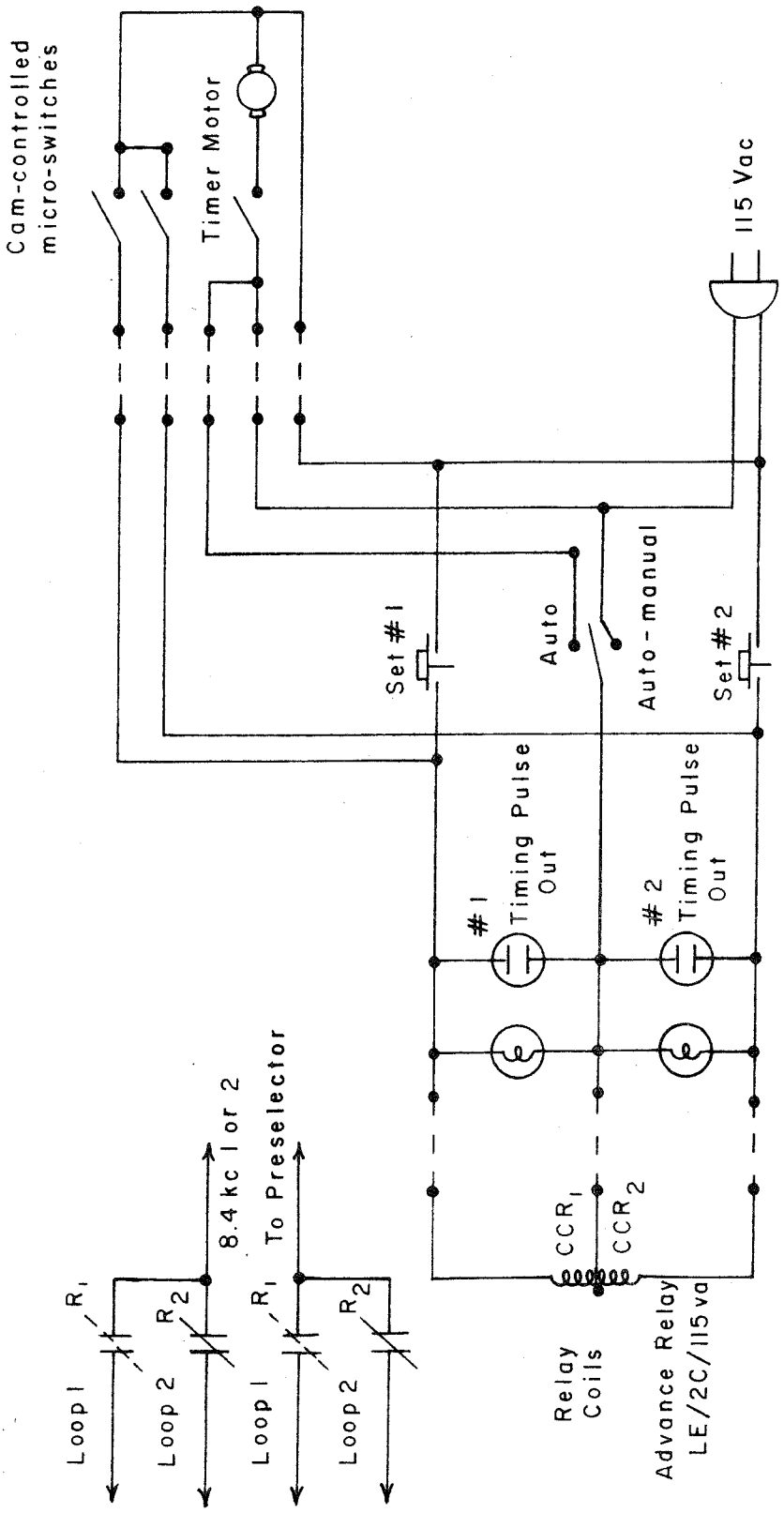

FIGURE F-7. CIRCUIT DIAGRAM OF RECEIVING LOOP SWITCHING RELAY AND TIMER.

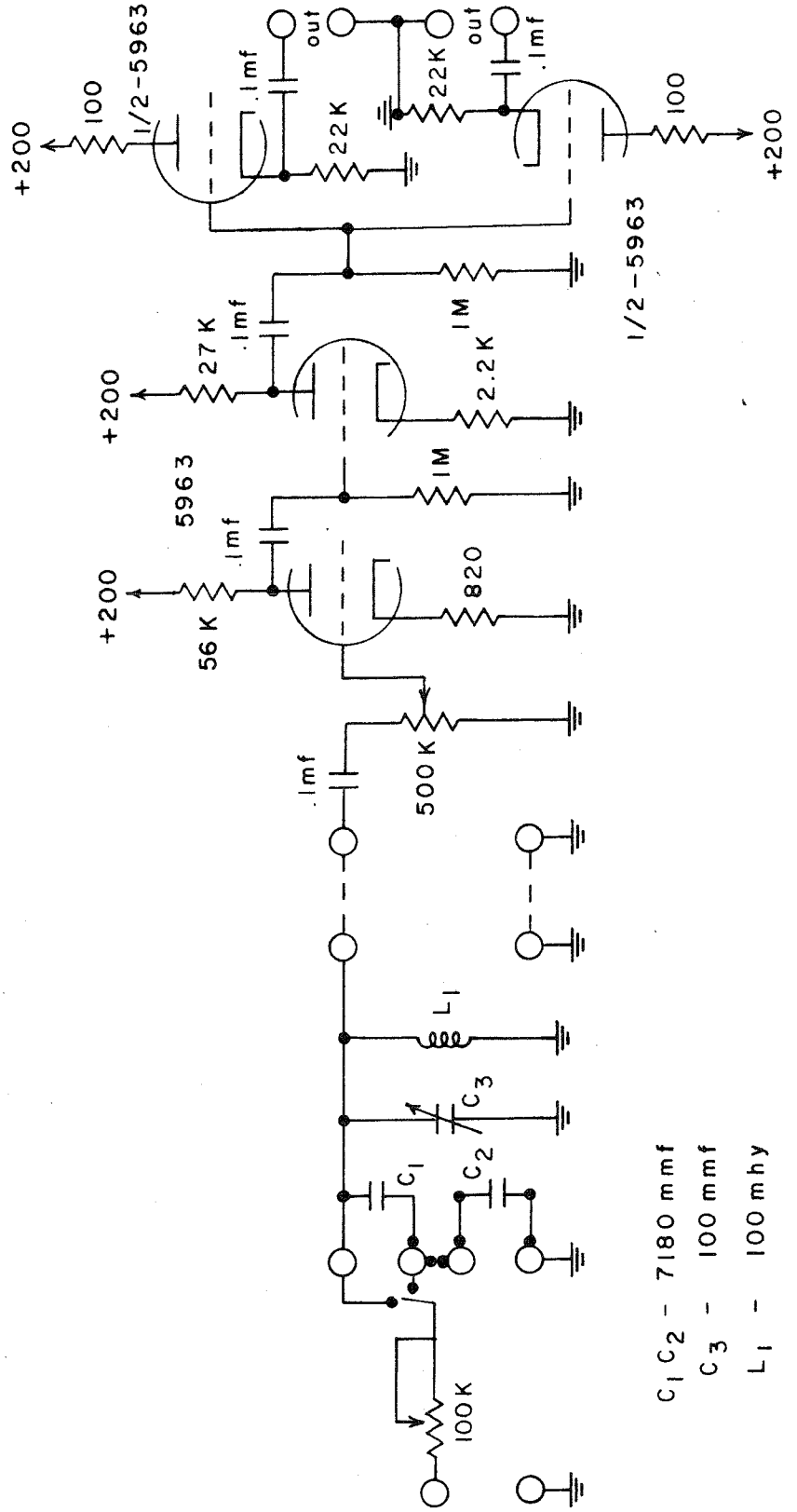

$C_1 C_2$ - 7180 mmf
C_3 - 100 mmf
L_1 - 100 mhy

FIGURE F-6. CIRCUIT DIAGRAM OF EXTERNAL 8.4 KC TUNED CIRCUIT AND AMPLIFIER.

APPENDIX G

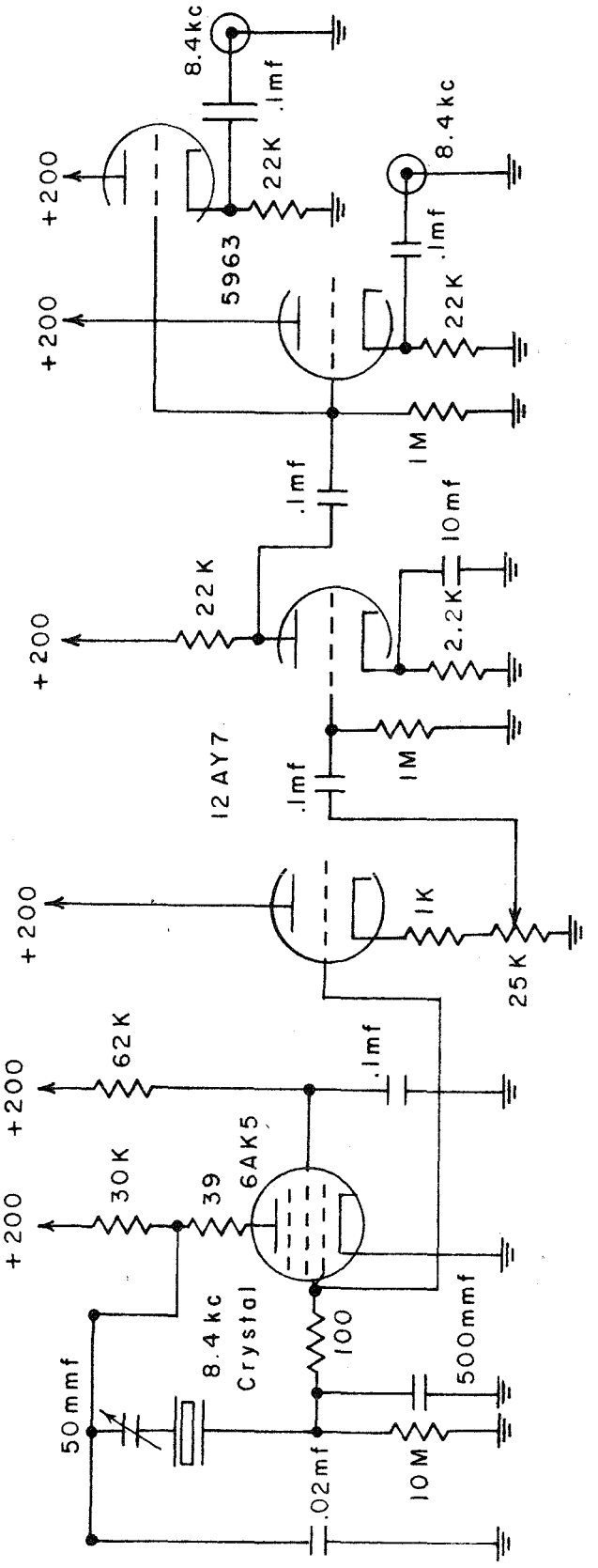

FIGURE G-1. CIRCUIT DIAGRAM OF 8.4 KC TRANSMITTER CRYSTAL OSCILLATOR.

FIGURE G-2. LING ELECTRONICS 20 KW TRANSMITTER.

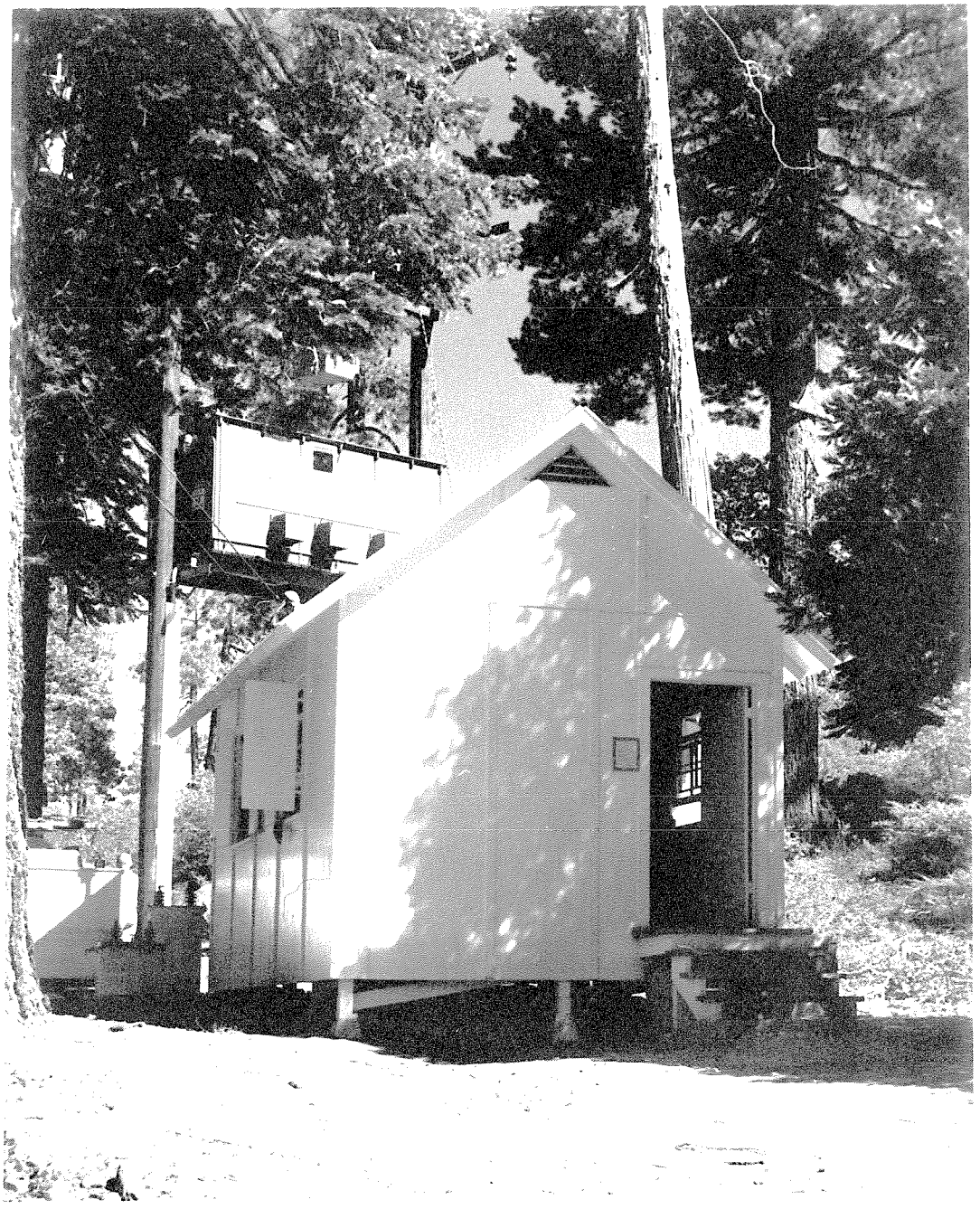

FIGURE G-3. TRANSMITTER BUNGALOW.

FIGURE G-4. TRANSMITTER BUNGALOW AND ASSOCIATED COUPLING EQUIPMENT.

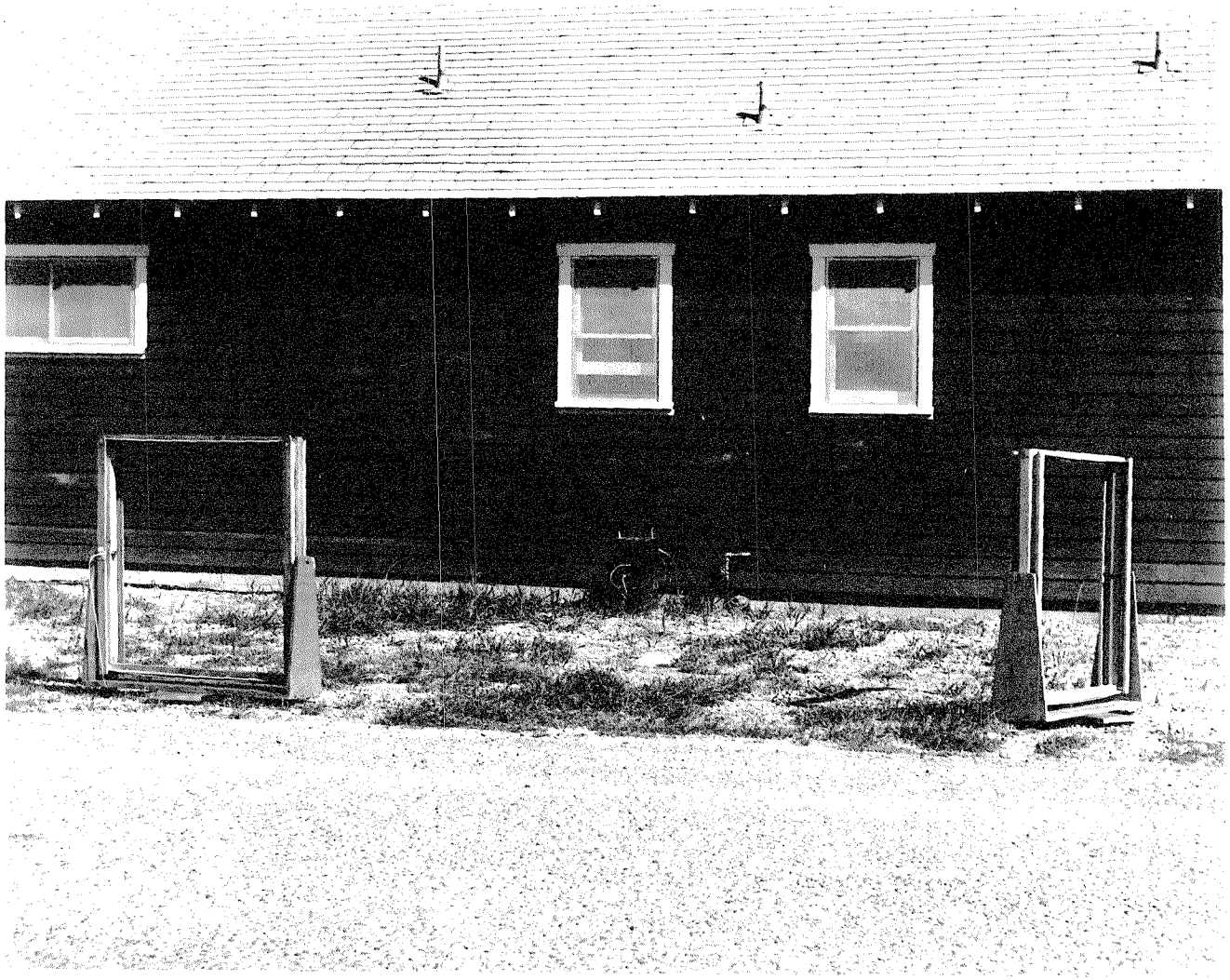

FIGURE G-5. RECEIVING LOOPS (FOREGROUND) AND 8.4 KC PRE-SELECTOR (BACKGROUND).

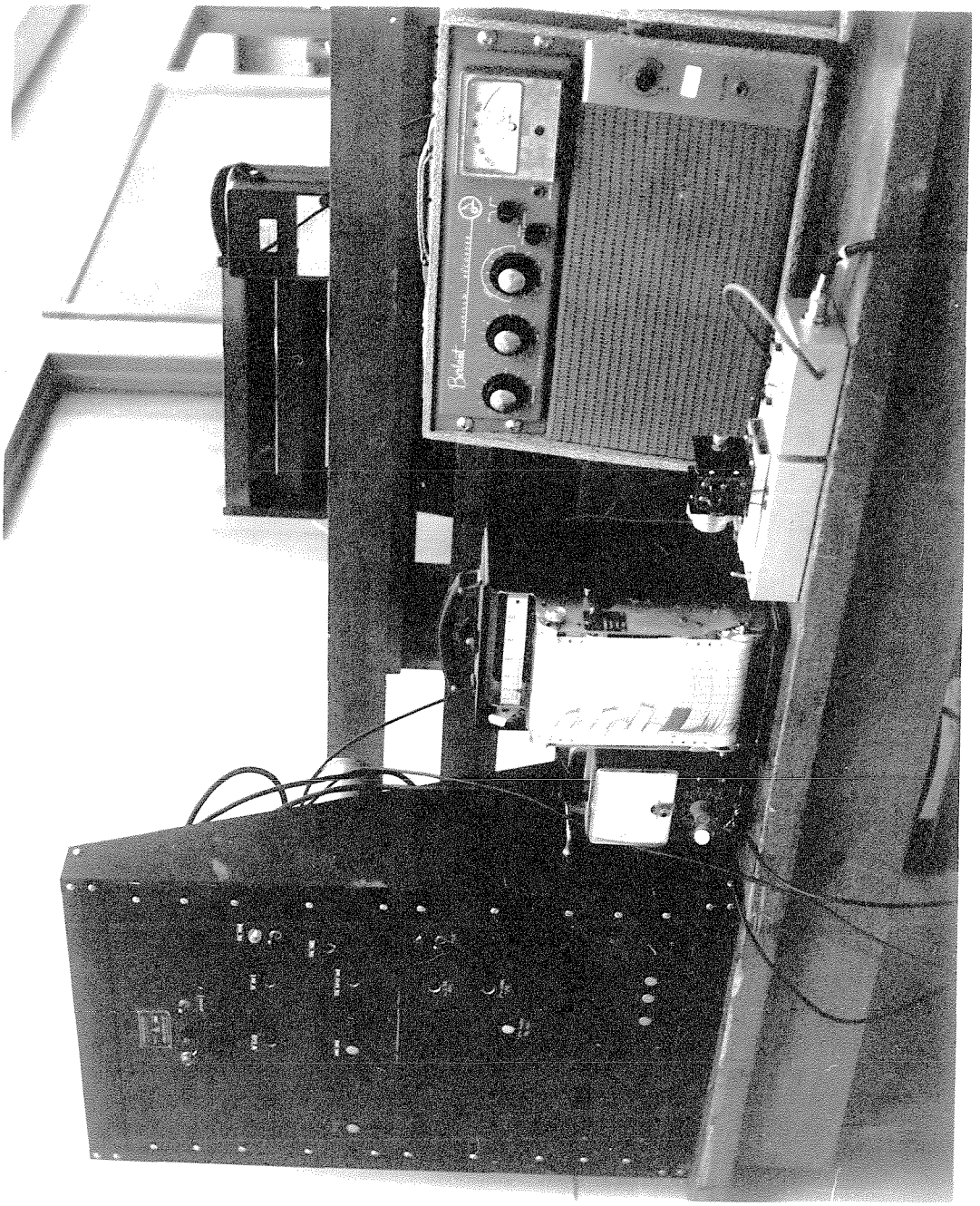

FIGURE G-6. VERY LOW-FREQUENCY RECEIVER AND PEN RECORDER.

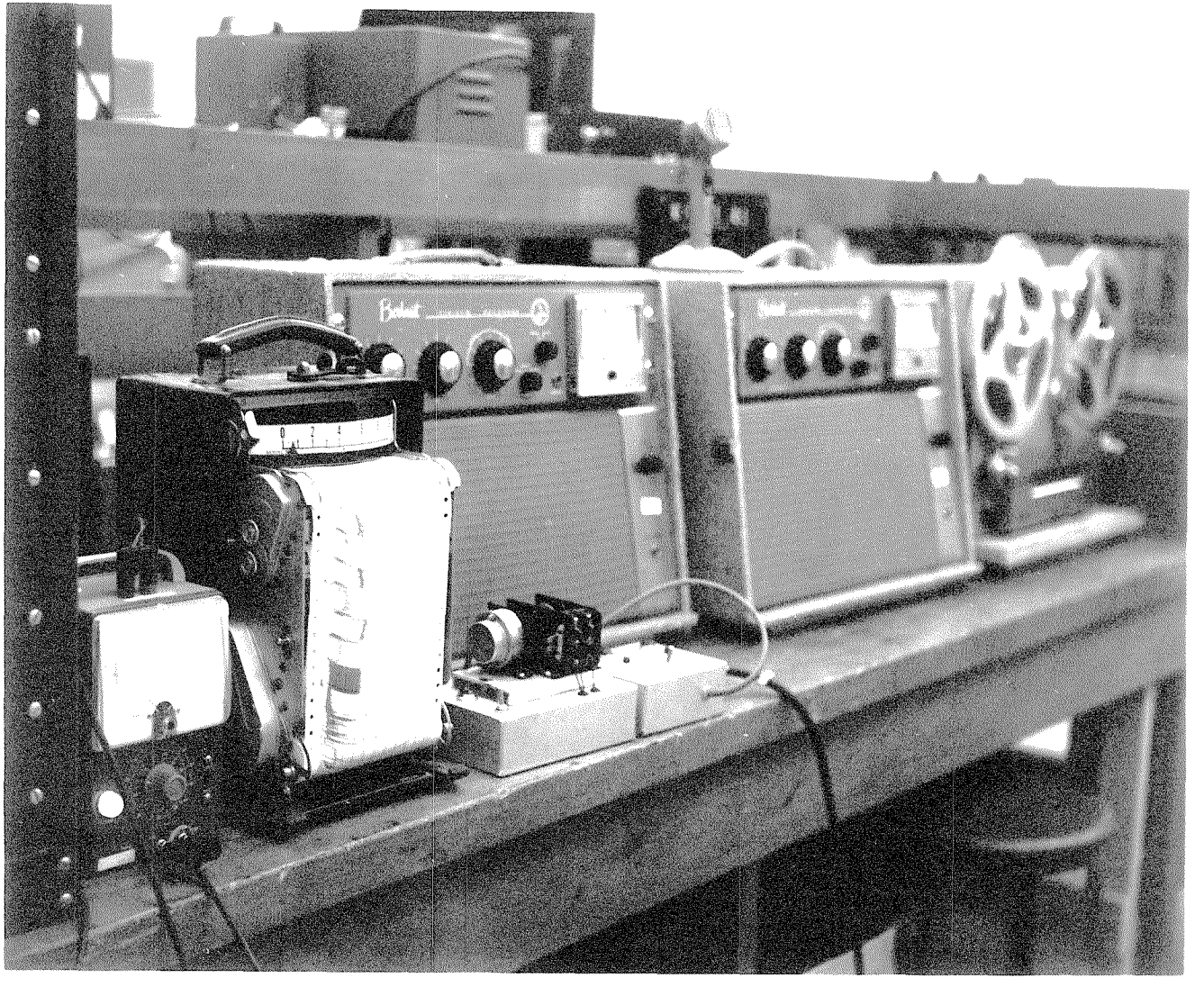

FIGURE G-7. PEN RECORDER AND MAGNETIC TAPE RECORDER USED FOR RECORDING AMPLITUDE DATA.